SENS4ICE

SENSORS AND CERTIFIABLE HYBRID ARCHITECTURES
FOR SAFER AVIATION IN ICING ENVIRONMENT

Final report on airborne demonstration and atmospheric characterisation

SENS4ICE Deliverable D4.3

Submission date: 06/02/2024

Authors: Johannes Lucke, Alessandra Lucia Zollo, Ben Bernstein, Tina Jurkat-Witschas,

Dissemination level: Public

Grant Agreement number:	824253
Project acronym:	SENS4ICE
Project title:	SENSors and certifiable hybrid architectures FOR safer aviation in ICing Environment
Funding scheme:	Research and Innovation Action
Project coordinator:	DLR (German Aerospace Center)
Project website:	www.sens4ice-project.eu

This project has received funding from the European Union's Horizon 2020 research and innovation programme under grant agreement No 824253.

File name	SENS4ICE_D4.3_Final_report_on_airborne_demonstration_and_atmosphere_characterisation_DLR_20240209.docx

APPROVALS

Role	Name	Organisation	Date
Coordinator	Schwarz	DLR	10 JAN 2024
WP leader	Deiler	DLR	13 DEC 2023
Task leader	Jurkat-Witschas	DLR	09 JAN 2024
Other (quality)	Behrendt	L-up	12 JAN 2024

DOCUMENT HISTORY

Version	Date	Modification	Author
1	02 OCT 2023	Creation	Jurkat-Witschas, Lucke, Zollo, Bernstein
2	17 NOV 2023	Review by coordinator	Schwarz
3	12 JAN 2024	Quality review	Behrendt

LIST OF AUTHORS

Name	Organisation
Tina Jurkat-Witschas	DLR
Johannes Lucke	DLR
Alessandra Lucia Zollo	CIRA
Ben Bernstein	LEA

DISTRIBUTION LIST

This deliverable report is public.

TABLE OF CONTENTS

LIST OF FIGURES

LIST OF TABLES

GLOSSARY

Acronym	Signification
ATR	Avions de transport régional
CCP	Cloud Combination Probe
CDP	Cloud Droplet Probe
CER	Contrôle Essais Réception / Dedicated ATC for tests & acceptance
CIP	Cloud Imaging Probe
CIRA	Centro Italiano Ricerche Aerospaziali (Italian Aerospace Research Centre)
DLR	Deutsches Zentrum für Luft- und Raumfahrt e.V. (German Aerospace Center)
FZDZ	Freezing Drizzle
IA	Iowa
ICD	Ice crystal detector
IL	Illinois
IN	Indiana
IWC	Ice water content
LAS	Large aspherical particles
LWC	Liquid water content
MED	Median effective diameter
MI	Michigan
MN	Minnesota
MSG	Meteosat Second Generation
MVD	Median volume diameter
NAM	North American Model
OF	Observational flight
OH	Ohio
SAFIRE	Service des Avions Français Instrumentés pour la Recherche en Environnement (French facility for airborne research)
SAT	Static air temperature
SCRAIN	Supercooled rain water
SEA	Science Engineering Associates
SLD	Supercooled large droplet
TAS	True airspeed
TWC	Total water content
UTC	Coordinated Universal Time
WI	Wisconsin

If not acknowledged otherwise, images courtesy of the SENS4ICE consortium partners.

This document reflects only the consortium's view. The European Commission and the European Climate, Infrastructure and Environment Executive Agency (CINEA) are not responsible for any use that may be made of the information it contains.

This document is one of the four final public deliverables for the EU-funded project SENS4ICE (Grant Agreement No 824253, 2019-2023):

D4.1 Sensor evaluation results and final roadmaps for future technology development and exploitation

D4.2 Final report on hybrid ice detection development

D4.3 Final report on airborne demonstration and atmospheric characterisation

D4.4 Final report on evaluation of technologies developed in SENS4ICE and technical project results

1. Overview of the report

This report gives an overview of the flights performed and the microphysical properties of the clouds encountered during the two airborne campaigns for technology testing within the SENS4ICE project. The first SENS4ICE flight test campaign took place between February 23 and March 10, 2023, based out of Alton, Illinois, USA. The second flight test campaign took place between April 3 and April 27, 2023, based out of Toulouse, France. The campaigns are therefore referred to as the (North) American and the European flight test campaign, respectively.

This report first describes the measurement platform and the reference instrumentation that were used to characterize the atmospheric conditions during the campaigns. Subsequently, the evaluation strategy of the instruments is explained. Thereafter, the campaign flights are briefly summarized and an overview of the icing conditions that were encountered is given.

Individual flights with interesting icing conditions are discussed in detail and compared to satellite remote sensing products developed within the project.

Prior to the campaigns, different models and satellite observations on icing occurrence in Europe and the North America were analyzed to find the best region with the highest occurrence rate of icing in general and SLD in particular, given the different safety constraints on the flight maneuvers. The overview and conclusions of the weather statistics analysis are summarized in [1].

2. Measurement platforms and reference instrumentation

This section describes the aircraft and the instruments for the characterization of microphysical properties of the clouds encountered. The North American flight test campaign used an Embraer Phenom 300 aircraft as the measurement platform (see Figure 1). The Phenom carried a Cloud Combination Probe (CCP) [2, 3, 4], owned by Embraer and manufactured by Droplet Measurement Technologies for the measurement of particle size distributions. For the measurement of liquid water content (LWC) and total water content (TWC), the Phenom 300 also carried a SEA ice crystal detector (ICD) manufactured and operated by Science Engineering Associates (SEA) [5].

Figure 1: The Embraer Phenom 300 aircraft, which was used for the American flight campaign. (Copyright Embraer/ SENS4ICE project)

For the European flight test campaign, an ATR-42 aircraft of the French facility for airborne research (SAFIRE) was used (see Figure 2). A large suite of reference instruments was installed on the plane, which is listed in Table 1 and shown in Figure 3. To maintain consistency with the North American

flight test campaign data, only measurements of the CCP and the Nevzorov probe were used for the European campaign data. In the future, more detailed microphysical analysis and instrument comparisons will also take into account the data from the other instruments.

Figure 2: The SAFIRE ATR-42 aircraft. (Copyright DLR with SAFIRE permission/ SENS4ICE project)

Table 1: Instruments used during the European flight campaign.

Instrument	Owner	Parameter(s) measured
CCP	DLR	Particle size and shape (2-960 µm diameter)
CIP	SAFIRE	Particle size and shape (15-960 µm diameter)
CDP	SAFIRE	Particle size (2-50 µm diameter)
BCPD [6]	DLR	Particle size and shape (2-42 µm diameter)
PIP	DLR	Particle size and shape (100 – 6400 µm diameter)
HSI	DLR	Particle size and shape (20 – 2000 µm diameter)
Nevzorov probe [7, 8]	DLR	LWC and TWC
Robust probe	SAFIRE	TWC
Gerber	SAFIRE	LWC
LiCOR	SAFIRE	Water vapor
UHSAS	SAFIRE	Particle size (0.06 – 1 µm diameter)

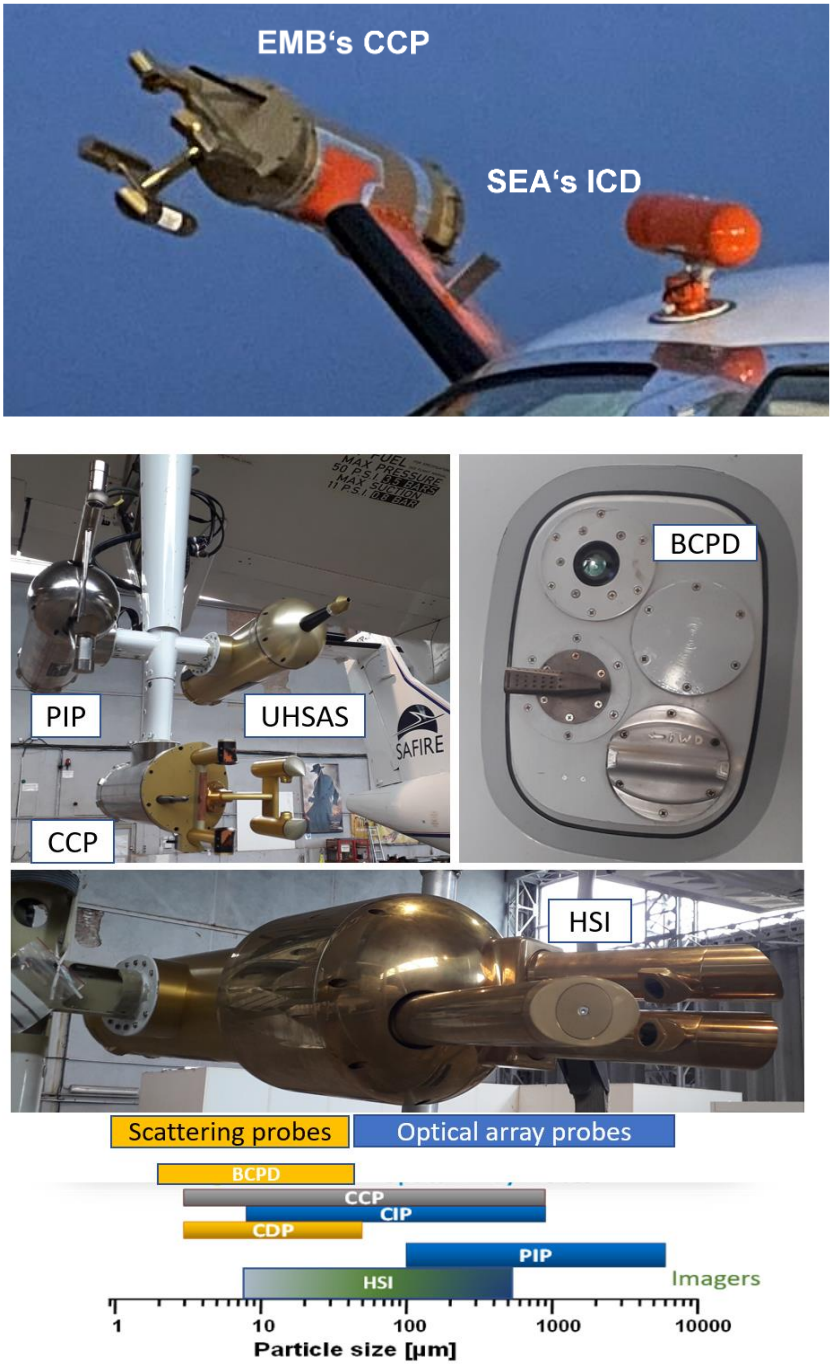

Figure 3: Overview of reference instrumentation. Left panel shows DLR reference instrumentation for the European campaign and right panels shows the Embraer CCP and SEA ICD for the American campaign. Plots taken from [1] © SAE.

3. Evaluation strategy

The reference measurements of both campaigns can be grouped into particle size measurements and bulk LWC and TWC measurements. This section details the evaluation steps necessary for both types of instruments.

3.1 Measurements of particle size with the Cloud Combination Probe

The particle size measurements of both campaigns were performed with a CCP (Cloud Combination Probe). The CCP is a combination probe, that consists of a Cloud Droplet Probe (CDP) [9, 4], for measuring particles between 2 and 50 µm diameter, and the Cloud Imaging Probe (CIP), which measures particles with sizes between 15 and 960 µm diameter.

The CDP is a scattering probe that derives the particle size from the intensity of forward scattered light that is measured at a photo diode. The CDP measurement does not yield any information on the particle shape. For the data evaluation it is assumed that all measured particles are spherical.

The CIP is an optical array probe [10, 11, 12] with a resolution of 15 µm. Particles that pass through its sample volume shadow its photo diode array and their size and shape is recorded. The shape identification is only applicable for larger particles. The minimum size that can be measured with the CIP corresponds to one pixel of the diode array and naturally no shape information can be retrieved from a single pixel measurement. The sample volume of the CIP is size dependent, small particles are only imaged if they are close to the focal plane, while larger particles are recorded at any position between the CIP arms. Furthermore, the CIPs used in the flight campaigns were grayscale probes, meaning that they can differentiate between different degrees of shadowing. A pixel can be measured to be un-shadowed, more than 25% shadowed, more than 50% shadowed and more than 75% shadowed, depending on the voltage measured at the individual photo diode. The degree of shadowing allows to deduce at what distance from the focal plane a particle passed [11]. For the assessment of atmospheric conditions, a joint size distribution of CDP and CIP is needed. In this work, CDP data were used up to a particle diameter of 43 µm, for larger particles CIP measurements were used. The 15 µm-resolution of the CIP means, that only particles with a size of minimum three pixels (equivalent to 45 µm) are used in the evaluation. Only particles which were completely imaged were considered for the analysis. Additionally, the data were corrected for stuck bits and shattering artefacts.

The combined size distributions of CDP and CIP were then divided into 1 µm-bins and a cumulative mass distribution was derived from these high - resolution size distributions. The cumulative mass distribution allows to derive the median volume diameter as well as the VD90 and VD99 (the diameters which mark the 90^{th} and 99^{th} percentiles of the cumulative volume distribution). An example of a cumulative mass distribution can be seen in Figure 4.

To obtain an accurate estimate of the icing risk, it is important that the size distribution contains only liquid particles. As mentioned before, the CDP data does not allow to distinguish the shape or phase of particles. All particles measured by the CDP are assumed to be liquid. For the identification of liquid droplets from the CIP measurements an in-house python code of DLR that identifies droplets based on their roundness was used and developed further [13, 14]. It is important to understand, that while this code characterizes most particles correctly, ambiguities between relatively round ice crystals and droplets may exist. The differentiation is therefore associated with some uncertainty. An example that shows particles detected as liquid and not liquid can be seen in Figure 6.

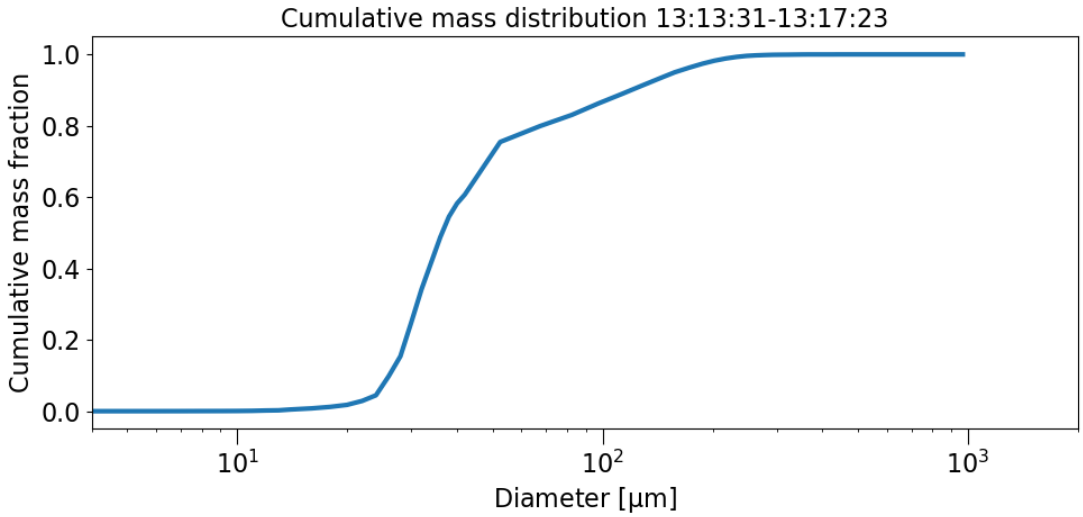

Figure 4: Cumulative mass distribution observed on 23rd February 2023 during F1475-1 of the American flight campaign. The MVD, VD90 and VD99 are those diameters where the cumulative mass distribution attains 0.5, 0.9 and 0.99, respectively.

3.2 Measurements of liquid and total water content

LWC and TWC measurements were performed with the ICD and the Nevzorov probe for the North American and European flight test campaign, respectively. Both instruments are hotwire probes [7], which mostly differ through the shape of their collector sensors [8] and the power that they are able to provide.

For hotwire probes, corrections for convective heat losses need to be made [7]. For the Nevzorov probe, dry air measurements were distinguished from measurements in clouds by the standard observation of the measurement, which is significantly smaller outside of a cloud. The measurements in dry air were then binned according to temperature, pressure and airspeed in the ambient atmosphere at the measurement point. Convective heat losses were derived for each of these bins and could then be subtracted from the Nevzorov measurements. The exact procedure is described in [15]. Small errors remain in the LWC and TWC data after the removal of the dry air term, which may lead to non-zero (slightly positive) LWCs and TWCs in cloud free segments. The threshold sensitivity of both hotwire probes (lower detection limit) is assumed to be 0.025 g/m³ for this work, i.e. smaller LWCs and TWCs cannot be detected and segments that show such values are considered to be cloud free. For the ICD, corrections for convective heat losses were made by the instrument manufacturer and operator SEA.

The measurements of the hotwire probes were compared to those of the optical instruments. In pure-liquid conditions, the LWC measured by the optical instruments should correspond to the TWC measured by the hotwire probes (the TWC sensors of the hotwire probes is used instead of the LWC sensors because the TWC sensors are more effective at collecting large droplets [16]). Good agreement between the LWC measurements of the CCP and the TWC measurements of the ICD were found for the North American flight test campaign, where the LWC measured by the CCP on average amounted to 90% of the TWC measured by the ICD (see right panel of Figure 5). For the European flight test campaign, there exists a significant mismatch between the measurements of the CCP and those of the Nevzorov probe 8 mm TWC sensor. The CCP LWC amounts on average to about 50%% of the Nevzorov TWC (Slope of the scatter plot, left panel on Figure 5). The cause for this discrepancy is still under investigation. A potential reason for this discrepancy may be the different positions of the sensors on the aircraft. Note that the LWC measurements were installed at

the fuselage of the ATR-42 and the size resolved water content measurement at the wing of the aircraft while for the North American campaign the two sensors were installed on the pylon on the roof of the Phenom 300.

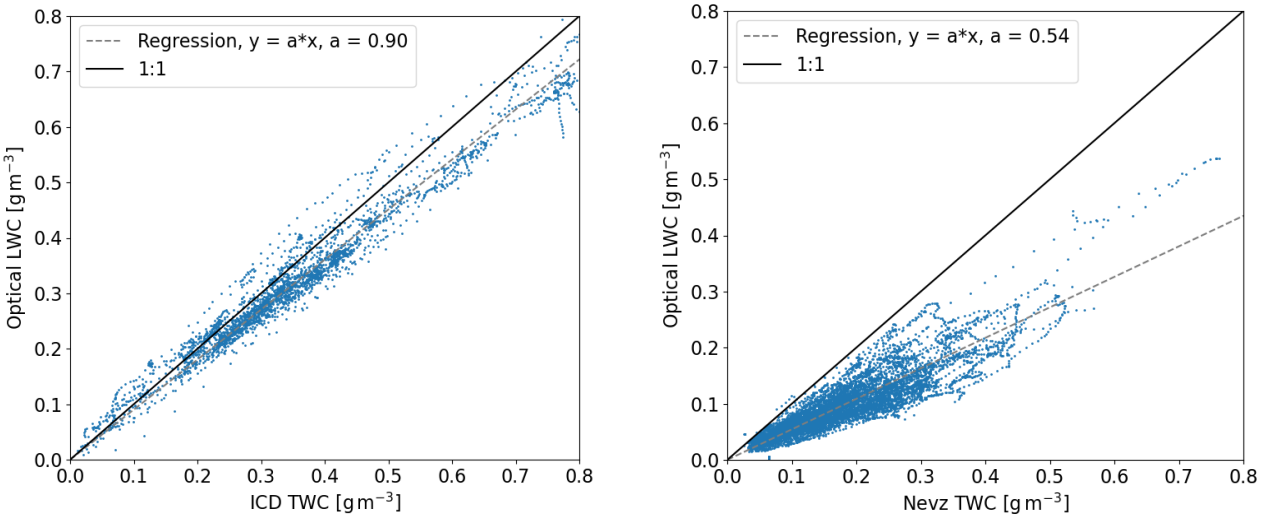

Figure 5: Comparison of TWC from Hotwire instruments with CCP based TWC. The left plot shows a comparison of the CCP LWC (Optical LWC) and the ICD LWC for one flight for the North American flight test campaign. The right plot provides a comparison of the Nevzorov LWC and CCP LWC for the European flight test campaign. Both flights show encounters of pure liquid clouds, hence TWC equals LWC.

3.3 Detection and classification of icing and Appendix O conditions

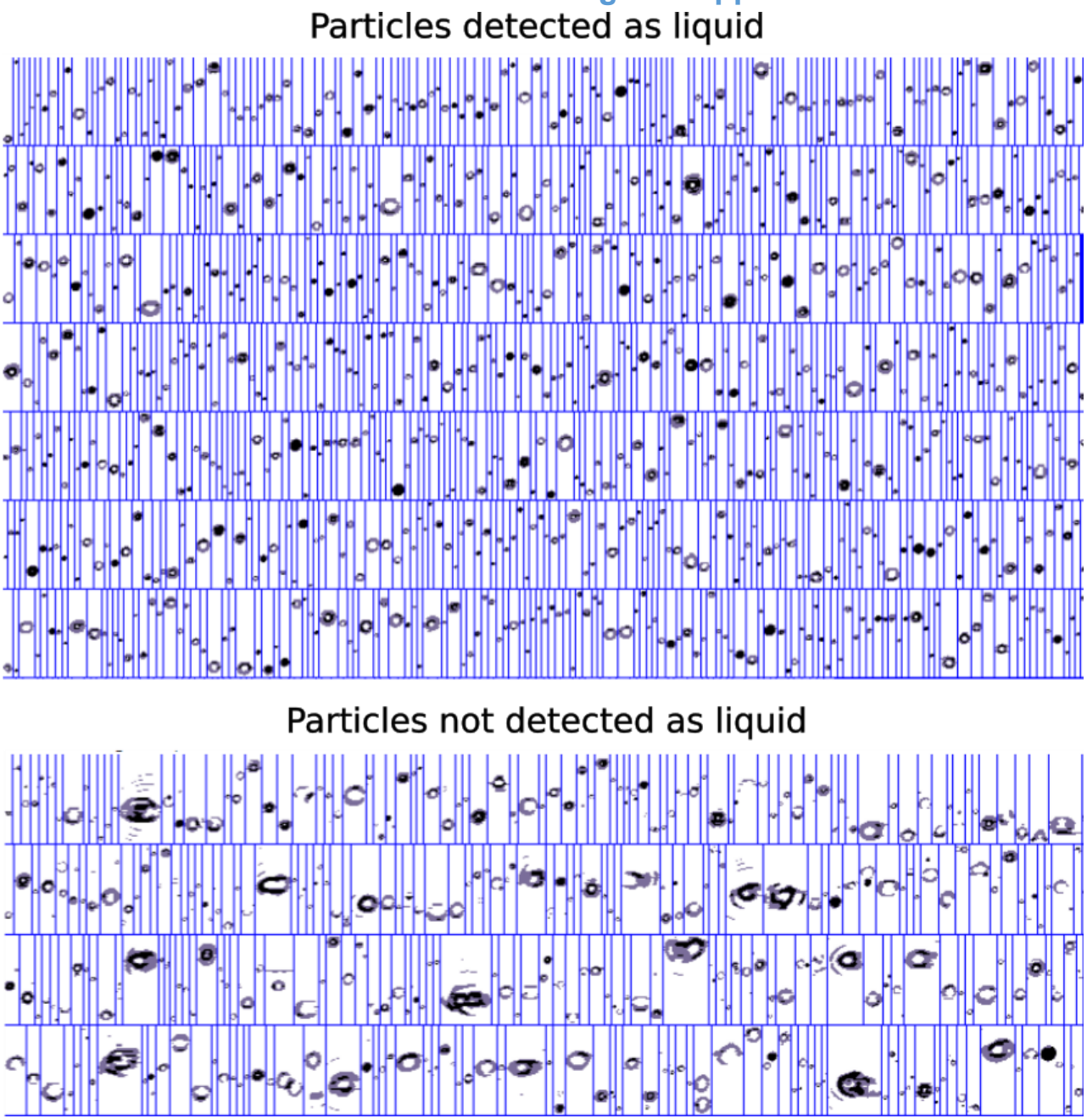

Figure 6: Example of particles detected as liquid (upper panel) and particles detected as non-liquid (lower panel) for one minute of a flight of the North American flight test campaign. Not all particles measured during the segment are shown.

In-situ cloud conditions are classified as “icing conditions” when the LWC from the hotwire instrument exceeds the sensitivity threshold of 0.025 g/m³ and the static air temperature (SAT) of the ambient air is less than 0°C. It is important to note, that the icing classification (a.k.a. flag) does not consider the ram air temperature rise at the fuselage due to the pressure increase, which can prevent ice accretion on surfaces when SAT is just slightly less than 0°C. In the data files containing the results of the microphysics analyses, the presence of icing conditions is marked through an icing flag, which takes a value of 1 when icing conditions are detected.

The assessment of the presence of Appendix O conditions is more complex. For SENS4ICE, Appendix O conditions were considered to be present when the following conditions were met:

1. Hotwire LWC > 0.025 g/m^3 to avoid cloud false detections.
2. Static Air Temperature < 0 °C.
3. More than one percent of total LWC need to be contained in SLD (equivalent to a VD99 > 100 µm).
4. Hotwire LWC / Hotwire TWC > 0.4.
5. SLD number concentration > 100 m^{-3}.
6. Ice crystal number concentration < 1000 m^{-3}
7. SLD number concentration > 10 * ice crystal number concentration.

The above requirements have in part also been used in previous evaluation of SLD flight campaigns, as described in [17]. Requirement 3 ensures, that only conditions with a significant portion of liquid water contained in SLD are identified as Appendix O. Requirement 4 has to be interpreted knowing that large droplets splash on the LWC sensors of the hotwire probes [16, 18]. In SLD conditions, the Hotwire TWC should therefore be larger than the LWC, but the Hotwire LWC should still at least amount to 40% of TWC, otherwise it is likely that ice crystals are present. Requirement 5 is included to eliminate situations where only small amounts of large droplets are present, which could for example occur outside of clouds in weak drizzle. Finally, requirements 6 and 7 are important to reduce the error rate of detecting ice crystals as SLD. By excluding conditions with a high number concentration of ice particles and limiting the number of ice crystals that can be present in comparison to the number of SLD, we avoid interpreting glaciated or mixed-phase conditions as SLD conditions. This however also means, that Appendix O conditions were large ice crystals and SLD coexist cannot be differentiated with this approach. Effectively, this current data evaluation represents a lower limit of the icing encounters and exceptionally those encounters with pure liquid clouds.

4. Data description

The main purpose of the dataset that was produced is to allow ice detection technology sensor developers to verify their technologies. This section describes the individual parameters of the dataset. As the SENS4ICE project focused on airframe icing, the dataset has been generated to provide high accuracy for the parameters of the liquid portion of clouds. Information on ice particles carries much larger uncertainties and should only be used after coordination with the authors of this work.

The data can be separated into averaged and non-averaged data (time resolution of 1 Hz). Averaging helps to provide more stable results, especially of parameters that can be influenced strongly by the detection / lack of detection of single particles, such as VD90 and VD99. Averaging times of 15 seconds and 30 seconds were used for the North American and European flight test campaigns, respectively. This reflects the higher airspeed of the Embraer Phenom over the SAFIRE ATR-42 and makes the data sets more comparable in terms of sampling distance. In general, all parameters that were considered to be stable without averaging are provided as 1Hz instantaneous values and as 1Hz rolling averages over the respective averaging period. Parameters that were considered to be unstable are provided only as rolling averages. A list of parameters output for the North American flight test campaign and the European flight test campaign can be seen in Table 2 and Table 3, respectively.

Table 2: Parameters provided in the dataset of the North American flight test campaign.

Parameter	Unit	Description
Time Start	s	UTC seconds of day
Datetime	YYYY-MM-DD hh:mm:ss	Date and Time, UTC
SAT	°C	Static air temperature measured by the aircraft
TAS	m/s	True airspeed measured by the aircraft
Altitude	m	Aircraft altitude
Latitude	degree	Latitude
Longitude	degree	Longitude
ICD LWC	kg/m³	LWC measured by the ICD LWC sensor
ICD TWC	kg/m³	TWC measured by the ICD TWC sensor
N 15s	1/m³	Number concentration all particles, from a rolling 15s mean.
SLD N 15s	1/m³	Number concentration of SLD, from a rolling 15s mean.
LAS N 15s	1/m³	Number concentration of large, aspherical ice particles, from a rolling 15s mean.
MVD 15s	m	MVD liquid particles only, from a rolling 15s mean.
VD99 15s	m	99th percentile volume diameter, from a rolling 15s mean.
VD90 15s	m	90th percentile volume diameter, from a rolling 15s mean.
LWC 15s	kg/m³	LWC computed from the CDP-CIP combination. Only particles classified as liquid are considered for this value. From a 15 s rolling mean.
SLD LWC 15s	kg/m³	LWC of the particles classified as SLD from CIP images. From a 15 s rolling mean.
ICD LWC 15s	kg/m³	LWC from the LWC sensor of the ICD. From a 15s rolling mean.
ICD TWC 15s	kg/m³	TWC from the TWC sensor of the ICD. From a 15s rolling mean.
Icing Flag	Boolean	1 if ICD LWC exceeds 0.025e-3 kg/m³ and SAT < 0°C. Else 0.
Icing Encounter Flag	Boolean	1 during icing encounters, else 0. (For encounter definition see section 4.4)
Appendix O Flag	Boolean	1 during Appendix O encounters, else 0. (For encounter definition see section 4.4)

Some of the parameters require a detailed explanation, which is provided in the following.

4.1 Measurements of LWC and TWC with the Ice Crystal Detector

As Appendix O conditions by definition (for this data) do not contain a significant number of ice crystals, the ICD TWC sensor value was used instead of the LWC in Appendix O conditions. The ICD LWC sensor is not accurate in conditions with large droplets, especially SLD, due to splashing of large droplets. In Appendix O conditions, it is therefore not recommended to use the ICD LWC value. The ICD TWC value is considered to be more accurate than the LWC value from the CDP and CIP, because CDP-CIP TWC is derived indirectly from the droplet diameters and thus contains significantly larger uncertainties.

4.2 Measurements of LWC and TWC with the Nevzorov probe

The Nevzorov probe data was not available for all flights of the European campaign due to an instrument malfunction. For flights, where no Nevzorov data was available, the LWC from the CDP and CIP is used as the LWC value. It is important, that for the flights where Nevzorov data was available, significant discrepancies exist between the LWC measurements of the CDP and CIP and those of the Nevzorov probe (see discussion in Section 3.2) The current assessment is that the Nevzorov probe data are more accurate than the CCP LWC measurements and should therefore be used for analysis purposes wherever available. As for the ICD, the Nevzorov probe TWC should be used in conditions were large droplets were present, as it is not affected by splashing effects [16].

Table 3: Parameters provided in the dataset of the European flight test campaign.

Parameter	Unit	Description
Time Start	s	UTC seconds of day
Datetime	YYYY-MM-DD hh:mm:ss	Date and Time, UTC
SAT	°C	Static air temperature measured by the aircraft
TAS	m/s	True airspeed measured by the aircraft
Altitude	m	Aircraft altitude
Latitude	degree	Latitude
Longitude	degree	Longitude
LWC	kg/m³	LWC computed from the CDP-CIP combination. Only particles classified as liquid are considered for this value.
Nevzorov LWC	kg/m³	LWC measured by the Nevzorov LWC sensor
Nevzorov TWC	kg/m³	TWC measured by the Nevzorov 8 mm TWC sensor
N 30s	1/m³	Number concentration all particles, from a rolling 30s mean.
SLD N 30s	1/m³	Number concentration of SLD, from a rolling 30s mean.
LAS N 30s	1/m³	Number concentration of large, aspherical ice particles, from a rolling 30 s mean.
MVD 30s	m	MVD liquid particles only, from a rolling 30 s mean.
VD99 30s	m	99th percentile volume diameter, from a rolling 30 s mean.
VD90 30s	m	90th percentile volume diameter, from a rolling 30 s mean.

LWC 30s	kg/m³	LWC computed from the CDP-CIP combination. Only particles classified as liquid are considered for this value. From a 30 s rolling mean.
SLD LWC 30s	kg/m³	LWC of the particles classified as SLD from CIP images. From a 30 s rolling mean.
Nevzorov LWC 30s	kg/m³	LWC from the LWC sensor of the Nevzorov probe. From a 30 s rolling mean.
Nevzorov TWC 30s	kg/m³	TWC from the 8 mm TWC sensor of the Nevzorov probe. From a 30 s rolling mean.
Icing Flag	Boolean	1 if Nevzorov LWC exceeds 0.025e-3 kg/m³ and SAT < 0°C. Else 0. For flights where the Nevzorov data was not available, the 1Hz LWC data from the optical instruments is used.
Icing Encounter Flag	Boolean	1 during icing encounters, else 0. (For encounter definition see section 4.4)
Appendix O Flag	Boolean	1 during Appendix O encounters, else 0. (For encounter definition see section 4.4)

4.3 Differentiation of droplets and LAS (Large aspherical ice particles)

The purpose of the LAS parameter is to provide information on the presence of ice crystals. Large aspherical ice particles are identified from the CIP images with a filter. The filter selects particles that are aspherical which are counted and then converted into a concentration. Particles are counted as clearly aspherical if their circular surface ratio [13] is smaller than 0.6, their surface at 50% grayscale level is larger than 100 pixels and the ratio of pixels at 75% grayscale level to pixels that are at least at 50% grayscale level is larger than 0.6. Alternatively, also particles for which the difference between the extents of the grayscale levels differs by more than 3 pixels in the x and y direction and whose surface is larger than 300 pixels are classified as large aspherical ice particles.

A concentration of LAS larger than zero is a clear indication of the presence of ice crystals. Conversely, a concentration of LAS equal to zero does not exclude the presence of ice particles. LAS is therefore not an accurate measure of the concentration of ice particles. The LAS parameter is however useful, for example for description and classification of Appendix C conditions. While for Appendix O conditions, it is ensured that LAS is below 1/L (see Section 3.3), no such requirement exists for Appendix C conditions, and ice crystals may therefore be present in significant numbers in Appendix C conditions. We know, that the filters for SLD are not perfect, and that a certain portion of ice particles can be detected as SLD. In the presence of ice crystals, parameters derived from the CCP data may therefore have a higher uncertainty (especially LWC 15s, MVD 15s, VD99 15s and VD90 15s). If measurements of Appendix C conditions are evaluated, it is therefore encouraged to check the LAS value. Microphysical parameters of Appendix C conditions can be considered correct when LAS is below 1000 per cubic meter.

4.4 Definition of Icing and Appendix O encounters

The data define Icing and Appendix O encounters. Unlike the icing flag, which is simply based on threshold values, certain requirements have been incorporated into the encounter flags to prevent the flag values from changing rapidly in highly variable clouds. The following requirements are implemented for the encounter flags:

1. An encounter needs to be at least 5 seconds long.
2. An encounter is terminated, after the required conditions (Icing or Appendix O conditions) is not detected for more than five seconds.

5. North American flight test campaign

This section details the individual flights of the North American flight test campaigns. Section 6 describes the European flight test campaign.

5.1 Description of measurement flights

Nine measurement flights were performed as part of the North American flight test campaign, which are listed in Table 4 and shown in the map in Figure 7. A total of 4 hours and 23 minutes were spent in icing conditions, 50 minutes of which were in Appendix O icing conditions, based on the definitions in Section 3. The following section gives a short overview of the individual flights. A detailed meteorological analysis of selected flights is available in [19].

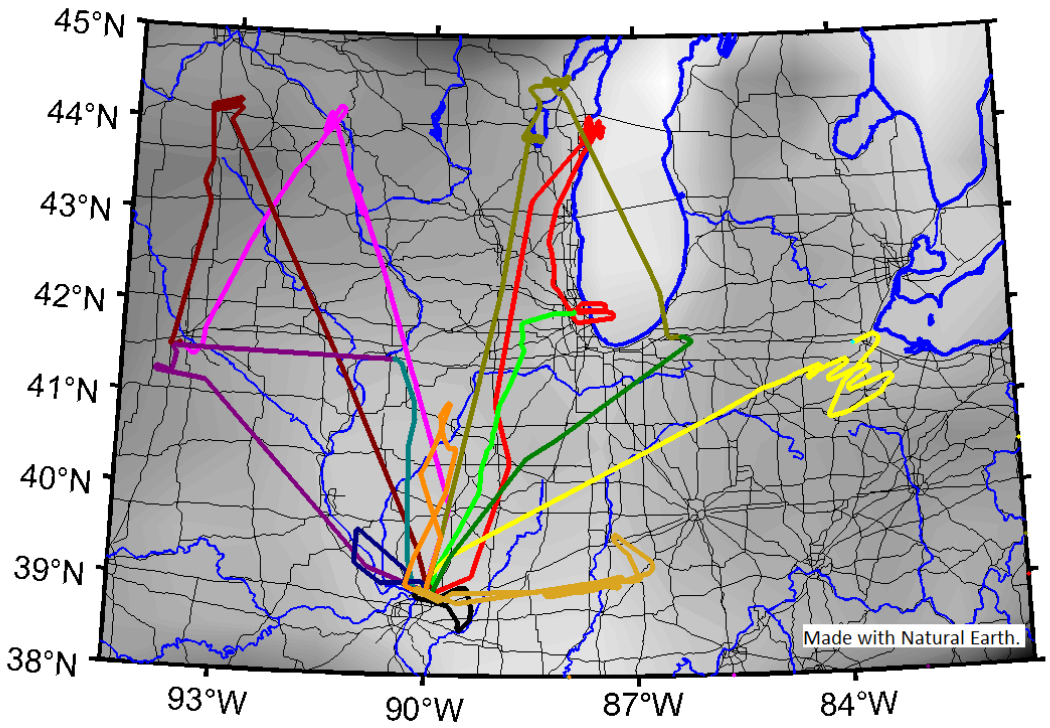

Figure 7: Ground tracks of the flights of the North American flight test campaign.

Table 4: Flights of the North American SENS4ICE flight test campaign.

Flight	Day	Flight time UTC	Time in Icing conditions [mm:ss]	Time in Appendix O conditions [mm:ss]	Comments
F1475-1	23/02/2023	11:43-14:29	20:18	9:03	
F1475-2	23/02/2023	17:18-18:33	19:59	0:00	
F1476	25/02/2023	11:38-13:43	38:47	22:24	Two flights in one datafile
F1477-1	01/03/2023	11:38-13:48	31:03	3:55	
F1477-2	01/03/2023	16:56-18:34	14:30	7:31	
F1478	06/03/2023	11:46-14:18	43:24	4:03	Two flights in one datafile
F1479	08/03/2023				Instrument failure
F1481	09/03/2023	12:01-13:13	15:51	2:46	
F1482	10/03/2023	12:08-17:40	79:59	0:00	Two flights in one datafile

5.1.1 F1475-1 - 23 February 2023

The first flight of the campaign sampled icing conditions over eastern Wisconsin, near the western shore of Lake Michigan, and was concluded by landing at the Chicago O'Hare International Airport (KORD; Figure 8). The area of sampling was located to the north of a slowly-moving, occluded, surface low-pressure system. Unstable, cool surface air was being overrun by moist, very stable air from ~1.3 km up to cloud tops at ~1.9 km. Temperatures increased from approximately -8°C to -3°C through this inversion layer. The aircraft sampled both the inversion, near 1.6 km, and at the top of the lower unstable layer, closer to 1 km (Figures 9 and 10). Clouds were widespread across the region, with large drops prevalent within a pocket of warm clouds over southeastern Wisconsin. Higher-altitude, cooler clouds moved into the area of sampling from the northwest, causing some snow to seed some of the lower clouds (see green features in longwave infrared imagery and green and blue patches on the radar mosaic; Figure 9). The combination of this seeding of the lower clouds, more significant snow to the north, overly warm temperatures to the south, the lake to the east, and normally-heavy air traffic around Milwaukee severely limited the workable SLD areas to a small swath over the land. Drizzly, low reflectivity was observed there and is indicated as a patch of grey echoes on the radar mosaic.

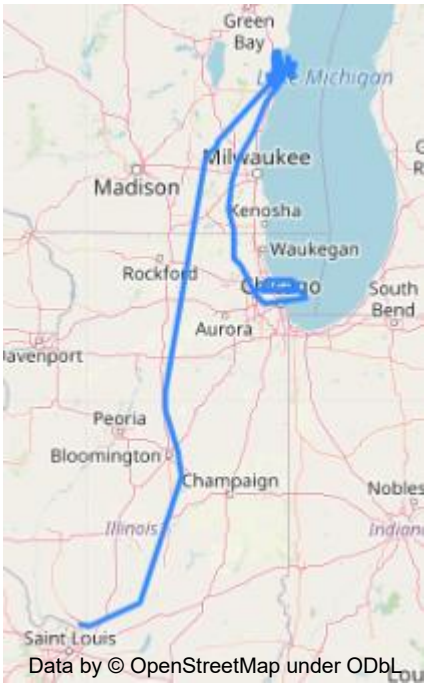

Figure 8: Flight track of F1475 – 1.

Appendix O conditions were observed during many of the targeted cloud encounters. MVDs in these conditions were between 30 and 40 µm, while LWCs ranged from 0.25 g/m³ to 0.5 g/m³ (Figure 10). Few ice crystals were detected in the clouds, the number concentration was at almost always less than 1 L^{-1}. An example of one Appendix O encounter of the flight can be seen in Figure 10. While the LWC of the presented encounter averaged 0.4 g/m³, the LWC contained in SLDs during this encounter was one of the largest observed during the campaign, with an average value of 0.05 g/m³. The VD90 and VD99 were 140 and 180 µm, respectively.

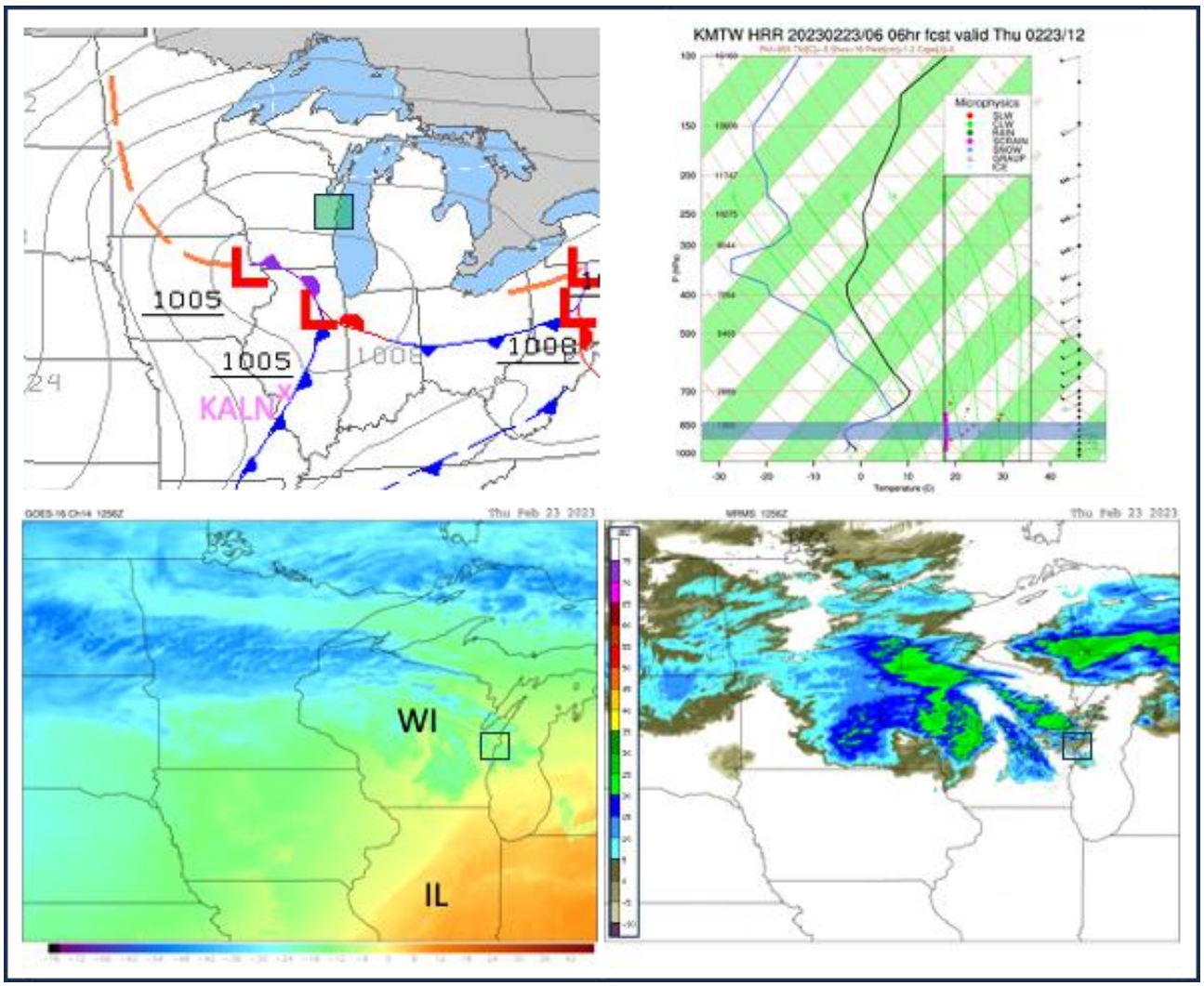

Figure 9: Meteorological environment present during the period of sampling for Flight F1475-1. 12 UTC surface chart (upper-left; from NOAA's AviationWeather.gov website) with the location of the aircraft base (KALN; Alton, IL) marked with a magenta "x" and the area of sampling enclosed with a light green box. HRRR model forecast skew-T valid at 12UTC at KMTW (Manitowoc, Wisconsin; upper right), located in the area of sampling, with output from the Thompson-Eidhammer microphysics indicated with colored dots. Red and magenta dots indicate forecast SLW (supercooled liquid water) and SCRAIN (supercooled rain water; supercooled drizzle in this case). A blue bar indicates the approximate altitudes of sampling. Long-wave infrared satellite imagery (lower-left) and MRMS mosaic of composite radar reflectivity (lower-right) for 13 UTC with boxes encompassing the area of sampling. For orientation, "WI" and "IL" mark the states of Wisconsin and Illinois. Locations of surface stations are approximate.

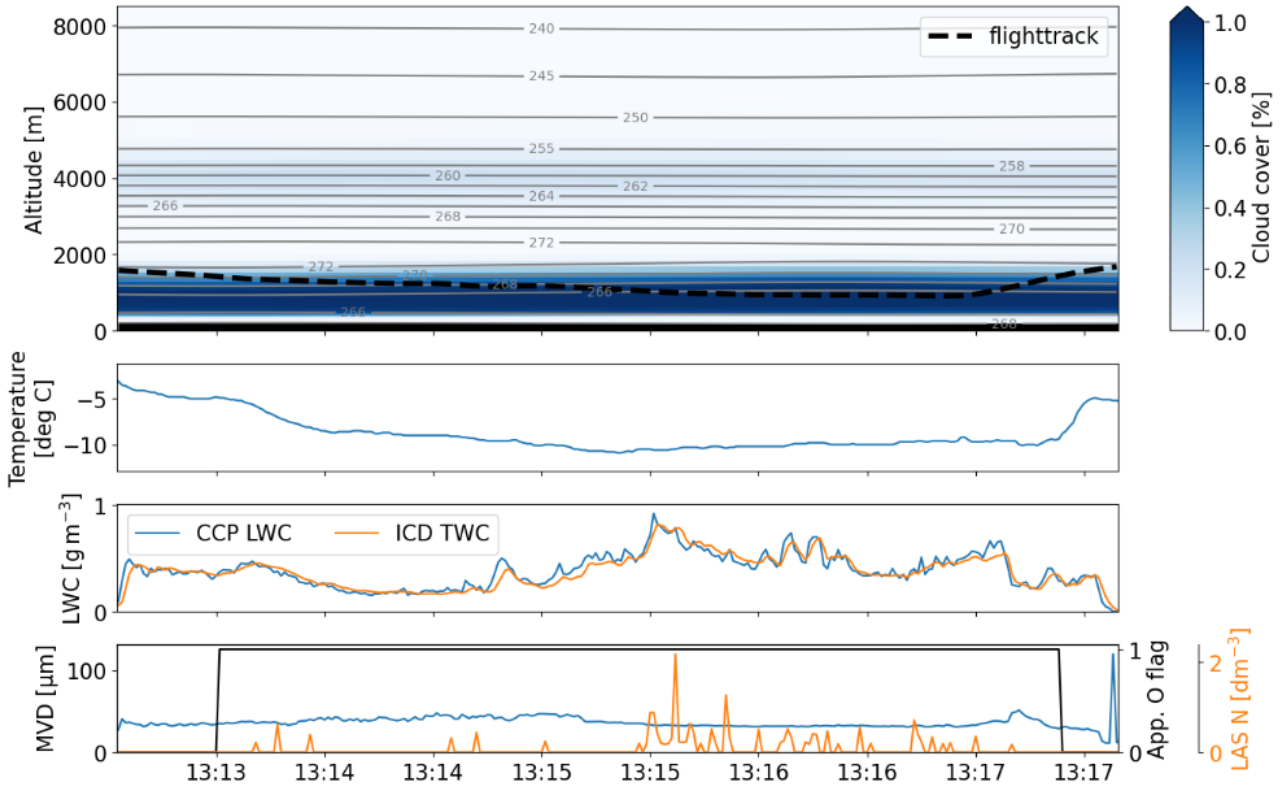

Figure 10: Example of an Appendix O encounter during F1475-1. Cloud cover and temperature data in the uppermost panel originate from ERA5 reanalysis data [19]. This is a reanalysis product which combines the forecast of numerical weather prediction products with observations from the ground. It therefore does not represent a direct measurement but just the likely position of the cloud cover.

5.1.2 F1475-2 - 23 February 2023

F1475-2 was the return flight from Chicago O'Hare (KORD) to Alton, Illinois (KALN), using a relatively direct route, and passing through Appendix C clouds over Central Illinois. These clouds formed within moist boundary layer air that trailed a cold front that was advancing across Illinois and Indiana between 12 and 18 UTC (Figure 11). The atmosphere behind the cold front was well-mixed, with a strong capping inversion from cloud top (~1.2 km) up to ~2.2 km MSL. LWCs were expected to exceed 0.5 g/m³ in this layer, with CCN concentrations simultaneously expected to be high, so drop sizes were expected to be relatively small. Infrared satellite imagery indicated that cloud tops were on the order of -5 to -8°C. No precipitation was indicated as falling from these warm, small drop clouds, and the total lack of echoes present in the radar reflectivity mosaic supports that.

The aircraft sampled icing conditions during certain portions of the flight, sampling clouds that were exclusively located beneath the inversion in an approximately 200-400 m thick layer at an altitude of ~1 km and temperatures between -4 and -7.5°C. As predicted, only Appendix C conditions were encountered. The clouds consisted almost exclusively comprised of supercooled droplets, with almost no ice crystals. LWCs were greater than during the morning flight, as expected, typically between 0.6 and 0.7 g/m³. MVDs were relatively small at 16-20 µm. An example of one of the Appendix C encounters can be seen in Figure 12.

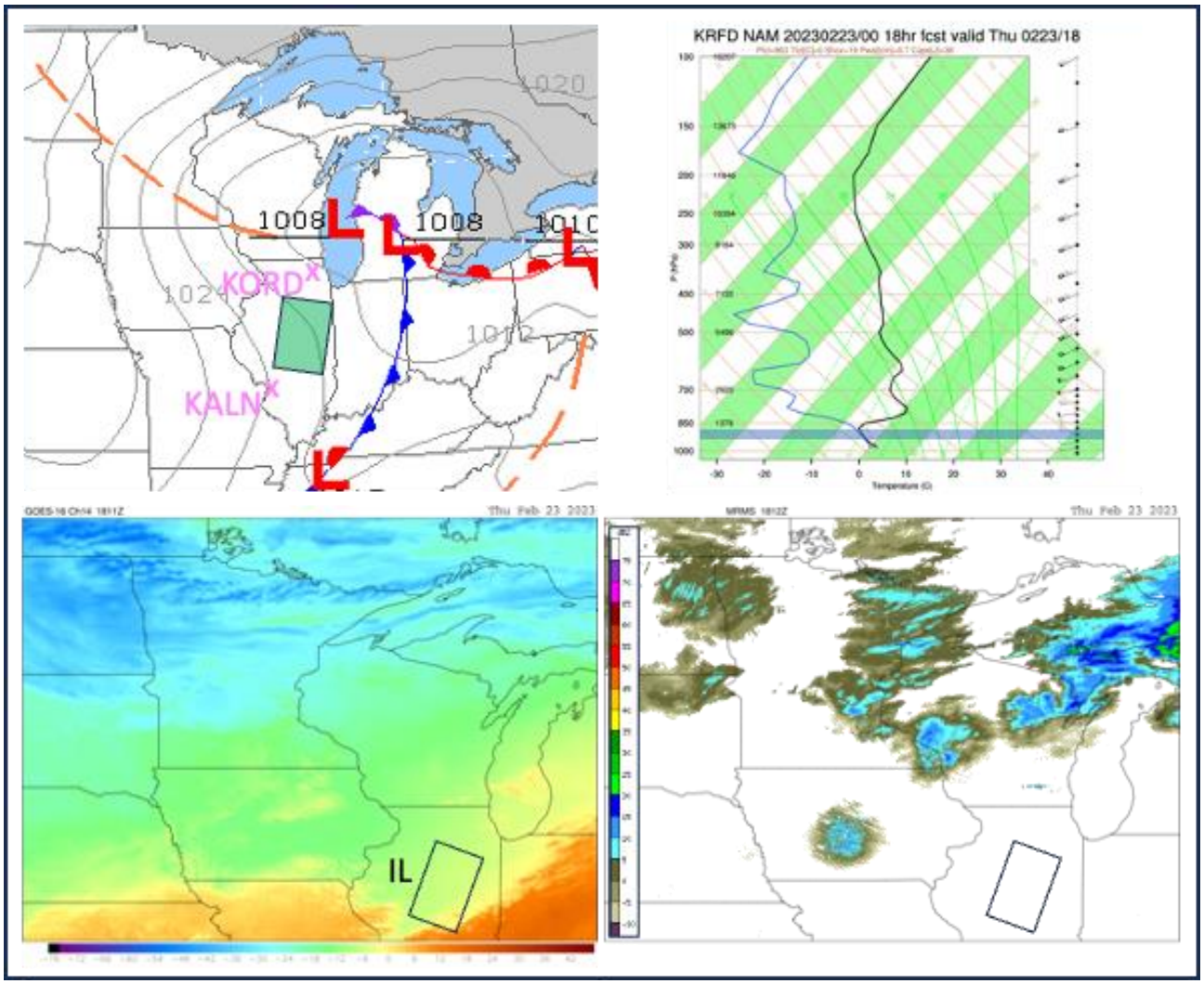

Figure 11: Same as Figure 9, but for Flight F1475-2, showing charts valid at ~18 UTC. The forecast sounding is from the North American Model (NAM), rather than the HRRR, and the location of the sounding was just to the north of the boxed area of flight, at KRFD = Rockford, IL. Microphysics output from the NAM model are not shown.

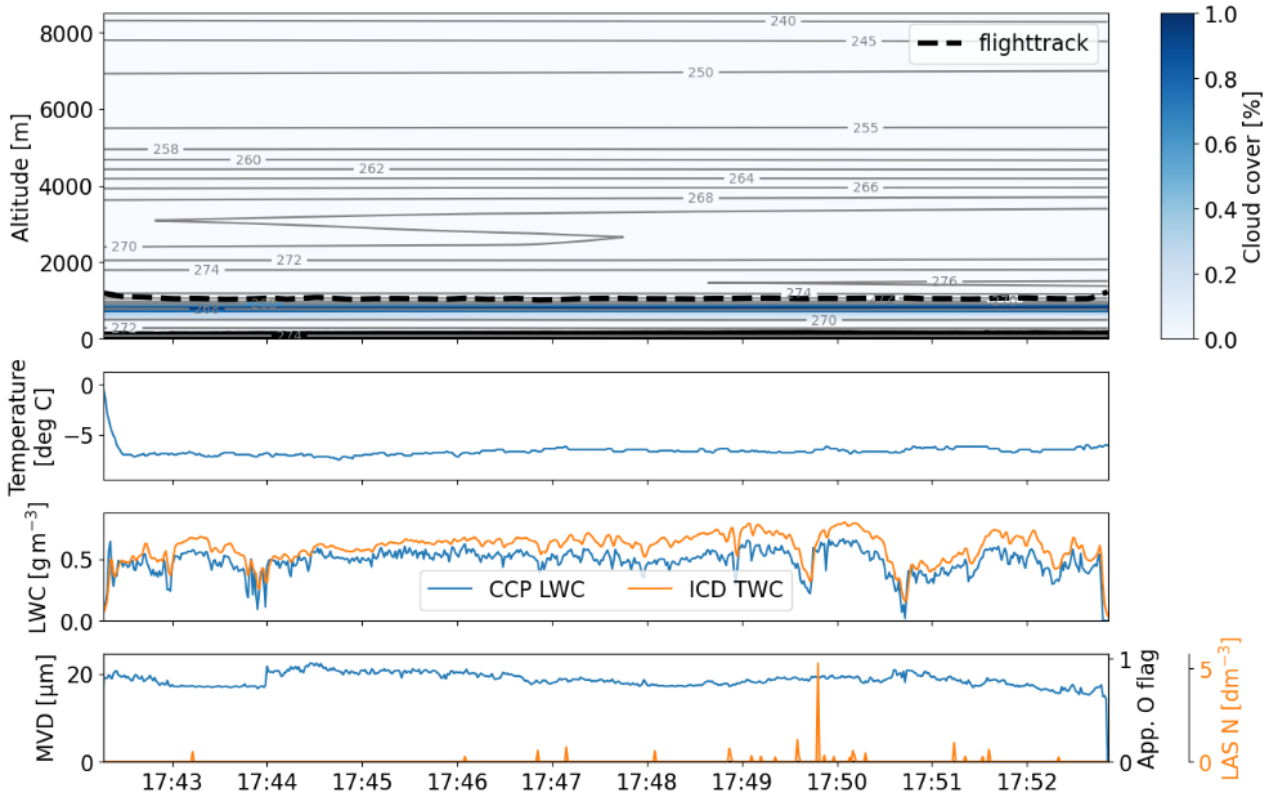

Figure 12: Example of an Appendix C encounter during F1475-2.

5.1.3 F1476 - 25 February 2023

Flight F1476, consisted of two flight segments, F1476-1 and F1476-2, with a refueling stop in Toledo, Ohio (KTOL). As only one data file exists for the flight, the two segments are not distinguished here. Clouds were sampled over northeastern Indiana and northwestern Ohio, between Fort Wayne, Indiana (KFWA) and KTOL (Figure 13). A broad swath of icing clouds focused between 2.1 and 2.5 km covered this area. They were located to the north of very weak low pressure, which the clouds did not appear to be associated with. Rather, they were more closely associated with weak warm air advection ahead of a subtle, elevated trough axis (not shown). The atmosphere was rather stable within this layer, with temperatures only falling slightly between cloud base and cloud top (Figure 14). Gradual lifting of the layer seemed to be present ahead of the trough axis. The air was mostly dry above this cloud layer, with some slightly sub-saturated conditions around 500 mb, thanks to some cooler icing clouds that had recently moved to the east of the target area. Infrared satellite imagery show the cooler, mid-level clouds to the east, while clouds over the target area were relatively warm (-5 to -10 °C). The radar mosaic shows that precipitation had also moved to the east with the cooler clouds, while the area of interest was essentially free of precipitation.

The aircraft found that the cloud layer extended from about 2.2 to 2.8 km. As for the previous flights, the cloud was approached from the top. Aircraft data showed a decrease in temperature by 3-5°C, depending on the encounter, as the aircraft descended into the cloud. This temperature inversion is not apparent from the ERA 5 data or the NAM forecast sounding (Figure 14, Figure 15). It is not unusual for models and thus, re-analysis grids to miss such fine-scale details. According to ERA5 and the NAM, a weak temperature inversion was present at around 800 m, well below the cloud base. Appendix O conditions were encountered multiple times during the flight. In Appendix O

conditions, MVDs were around 30 μm and LWCs ranged from 0.28 to 0.42 g/m³ at temperatures between -10 and -11.5ºC.

The return flight briefly sampled some remnant clouds over south-central Michigan, but they were too weak to be of interest. Temperatures were near -9˚C, LWCs were reported to be on the order of 0.15-0.20 g/m³, with MVDs on the order of 14 microns (to the left of Appendix C). The clouds were quickly abandoned and the aircraft returned to KALN.

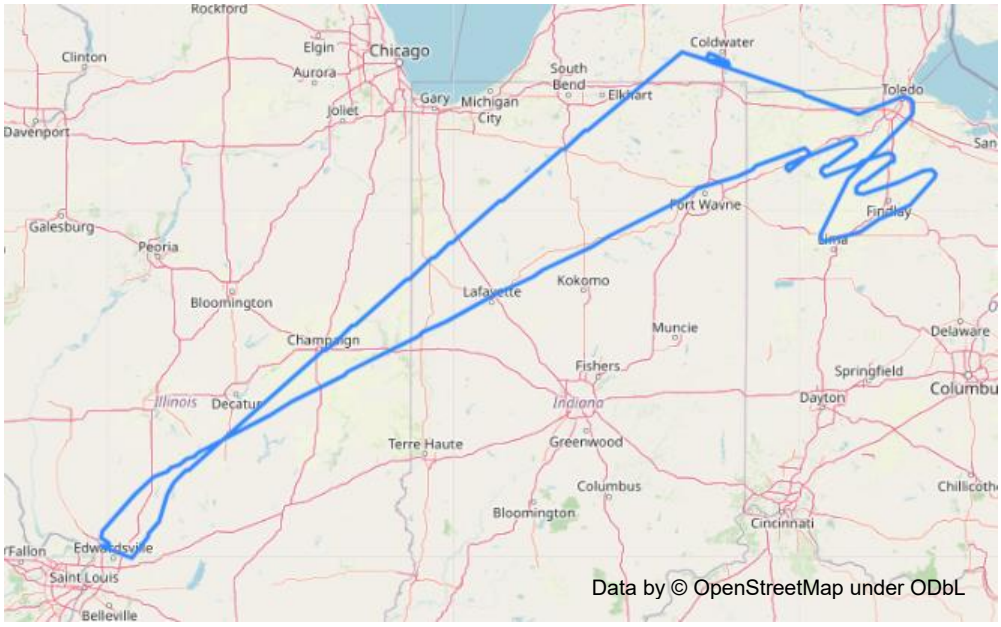

Figure 13: Flight track of F1476.

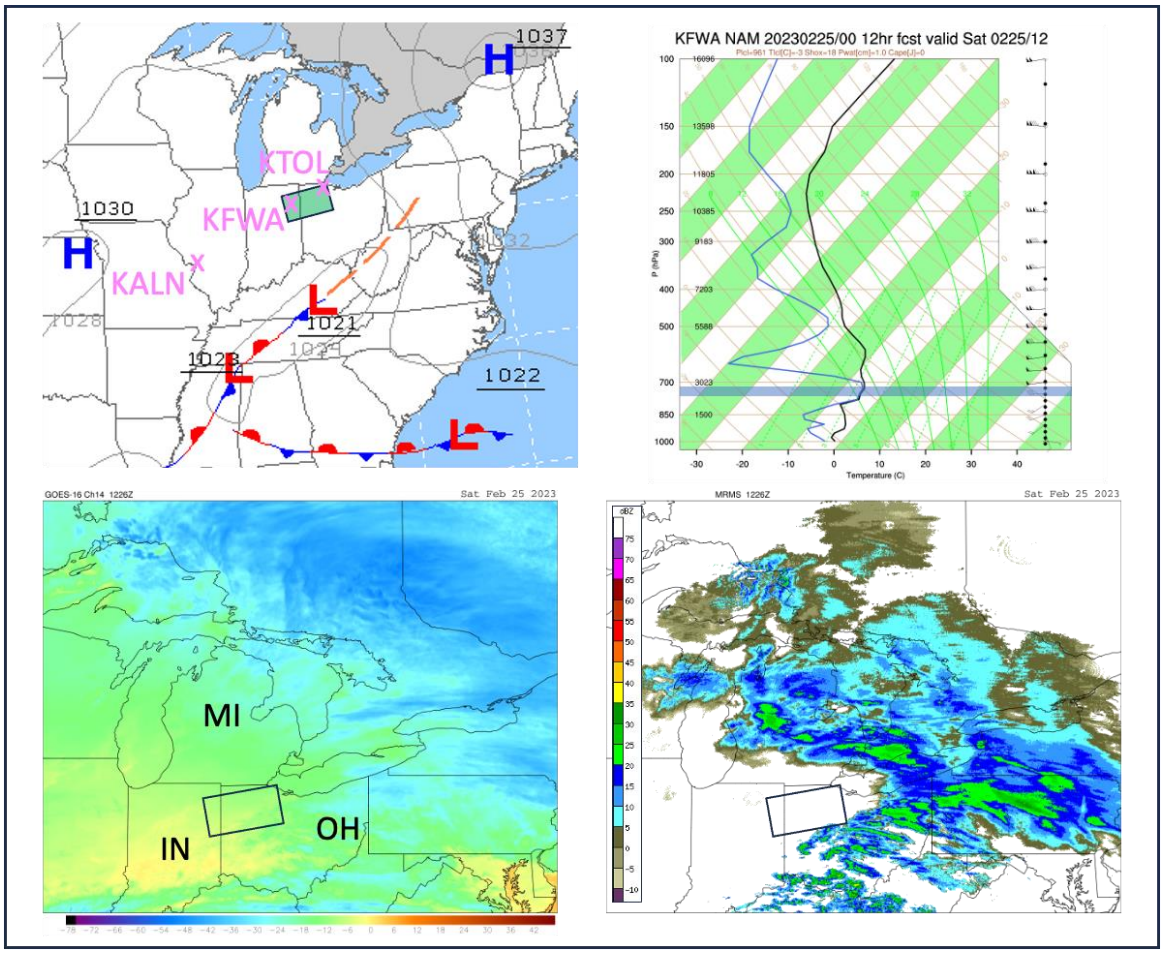

Figure 14: Same as Figure 9, but for Flight F1476, showing charts valid at ~12 UTC. MI=Michigan, IN=Indiana, OH=Ohio.

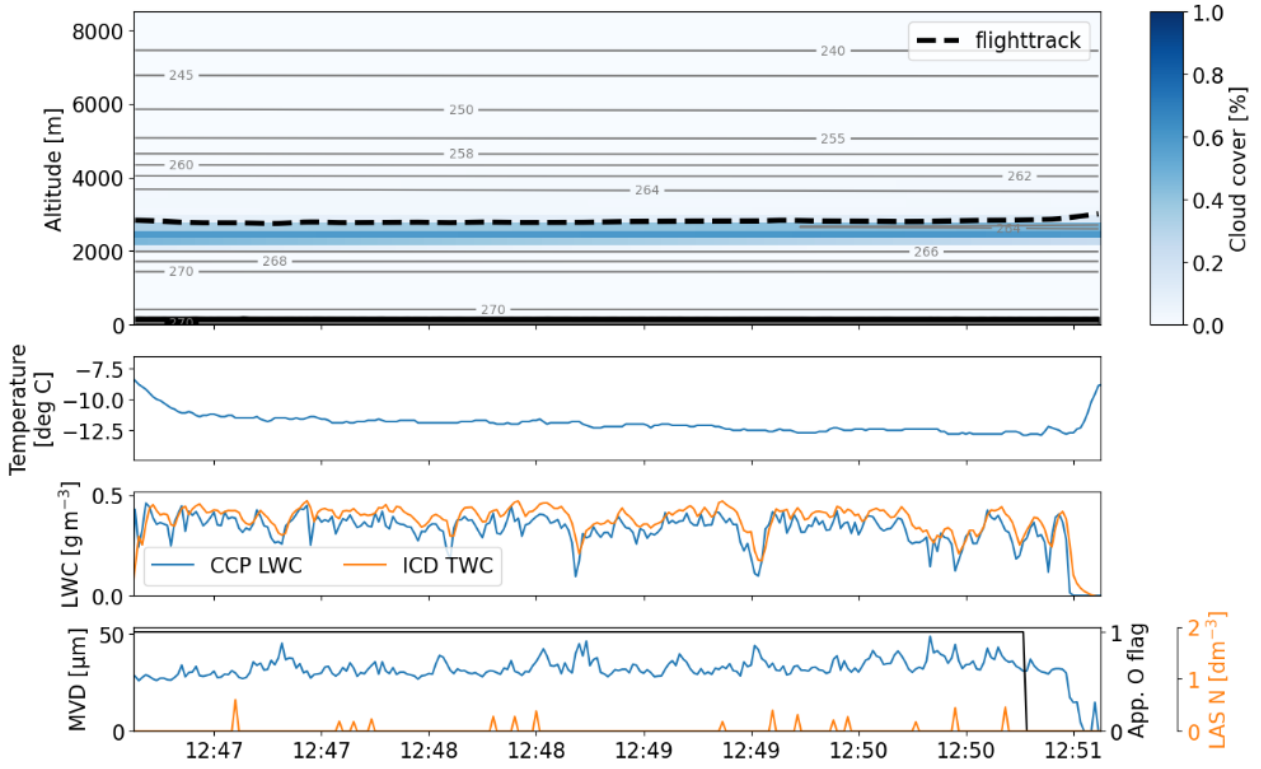

Figure 15: Example of an Appendix O encounter during F1476.

5.1.4 F1477-1 – 1 March 2023

Flight 1477-1 sampled clouds within a very complex storm system over the northern part of the Mississippi River valley, along the Minnesota-Wisconsin border. It occurred in a swath of icing clouds that were moving toward the northeast in advance of a progressive, occluded front located over central Iowa at 12 UTC. This front joined two low pressure systems, with one located over eastern South Dakota and the other located over central Missouri (Figure 16, Figure 17). The clouds of interest were located where Minnesota, Iowa and Wisconsin meet. They were not producing any precipitation on their own, but some cooler, higher clouds were causing some ice crystals that were seeding parts of the icing clouds, with evidence of this in satellite imagery and the radar reflectivity mosaic. The liquid clouds of interest were located between Dubuque, Iowa (KDBQ) and Rochester, Minnesota (KRST), sandwiched between two areas of ice-crystal seeding. Forecast soundings for this area provided further indication of the two-layer situation, with the ice-producing clouds found between 500 and 600 mb, and the lower liquid clouds located between 850 and 750 mb, with a dry layer in-between. The lower clouds were moist adiabatic in character and expected to have temperatures near -1 and -8°C at their bases and tops, respectively, with potential to develop substantial amounts of SLW toward cloud top. Temperatures were cooling within the cloud layer over time. The layer was expected to be isolated from the boundary layer by the isothermal layer that extended from cloud base to the surface, enhancing the chances for SLD to be present.

A plot of the flight track can be seen in Figure 16. Due to a problem with the data, the last portion of the flight track does not show the last stages of the flight, when the aircraft was approaching Des Moines, Iowa (KDSM) to refuel. For this flight, the ERA5 re-analysis data does not match the flight data or the HRRR forecast sounding well, with ERA5 having sub-saturated conditions at the altitudes where the Phenom sampled the icing clouds (~2.0-2.5 km; Figure 18). From the flight data it can be shown, that the clouds were at least 500 m thick at times. Two Appendix O and several Appendix C

encounters occurred. MVDs in Appendix O conditions were 20-25 μm, while they were 13-20 μm in the Appendix C condition. The LWC in one of the Appendix O encounters was 0.8 g/m³ over a period of approximately 2.5 minutes and a horizontal distance of 15 km (see Figure 18). The LWC contained in SLDs was lower than the maximum observed during F1475-1, only 0.017 g/m³, with a VD90 value of 49 μm and a VD99 of 140 μm. The Appendix C clouds contained also relatively high LWCs, with values in excess of 1 g/m³ observed.

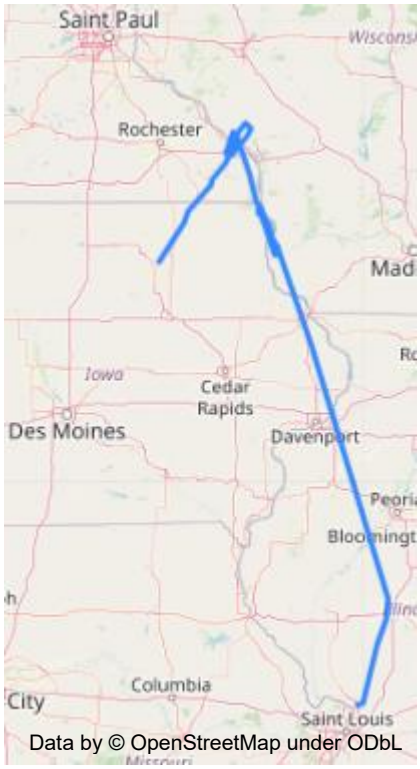

Figure 16: Flight track of F1477-1. The flight landed in Des Moines, but due to a problem with the data, the last portion of the flight cannot be portrayed here.

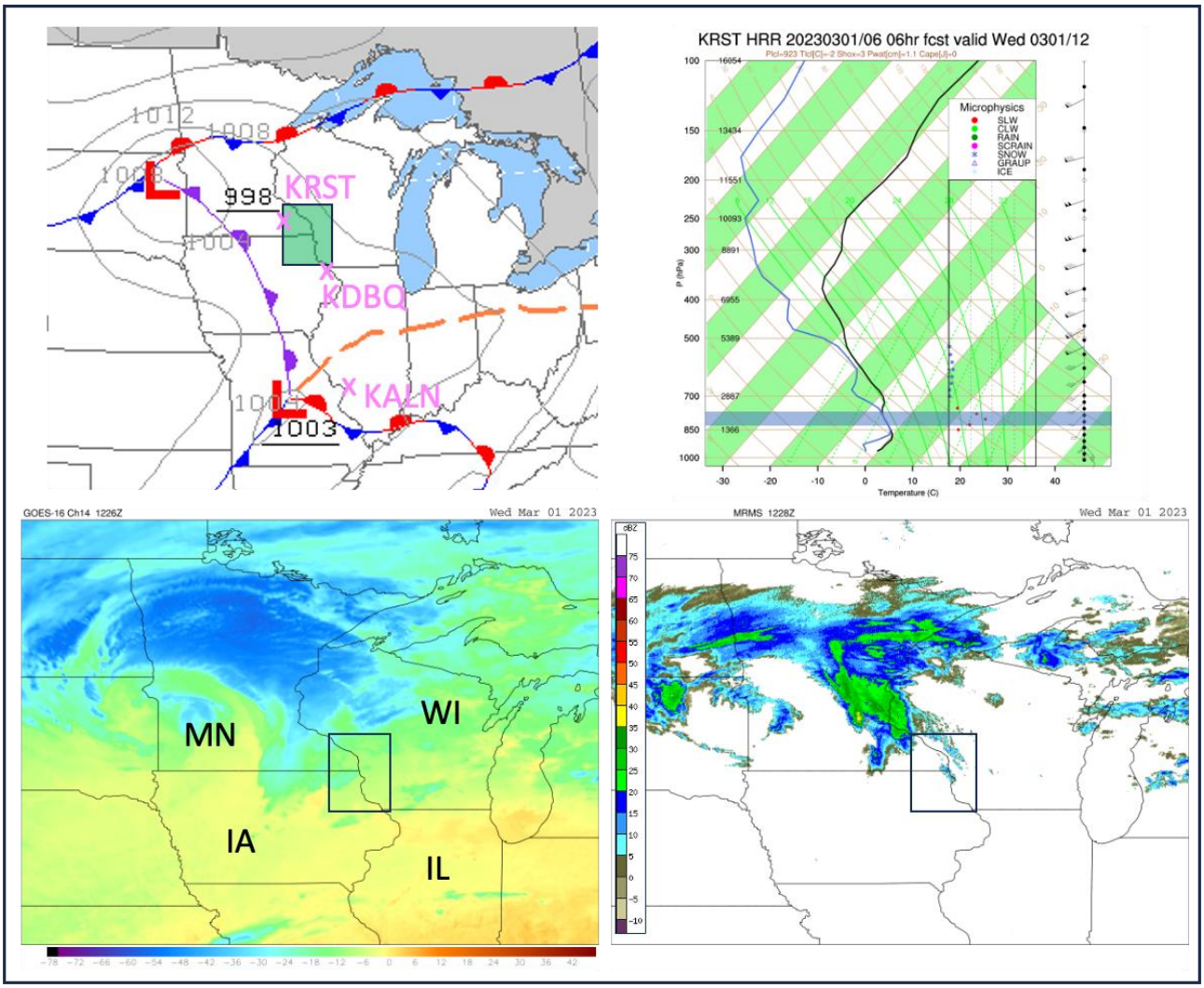

Figure 17: Same as Figure 9, but for Flight F1477-1, showing charts valid at ~12 UTC. MN=Minnesota, WI=Wisconsin, IA=Iowa, IL=Illinois. The forecast sounding is for Rochester, Minnesota (KRST).

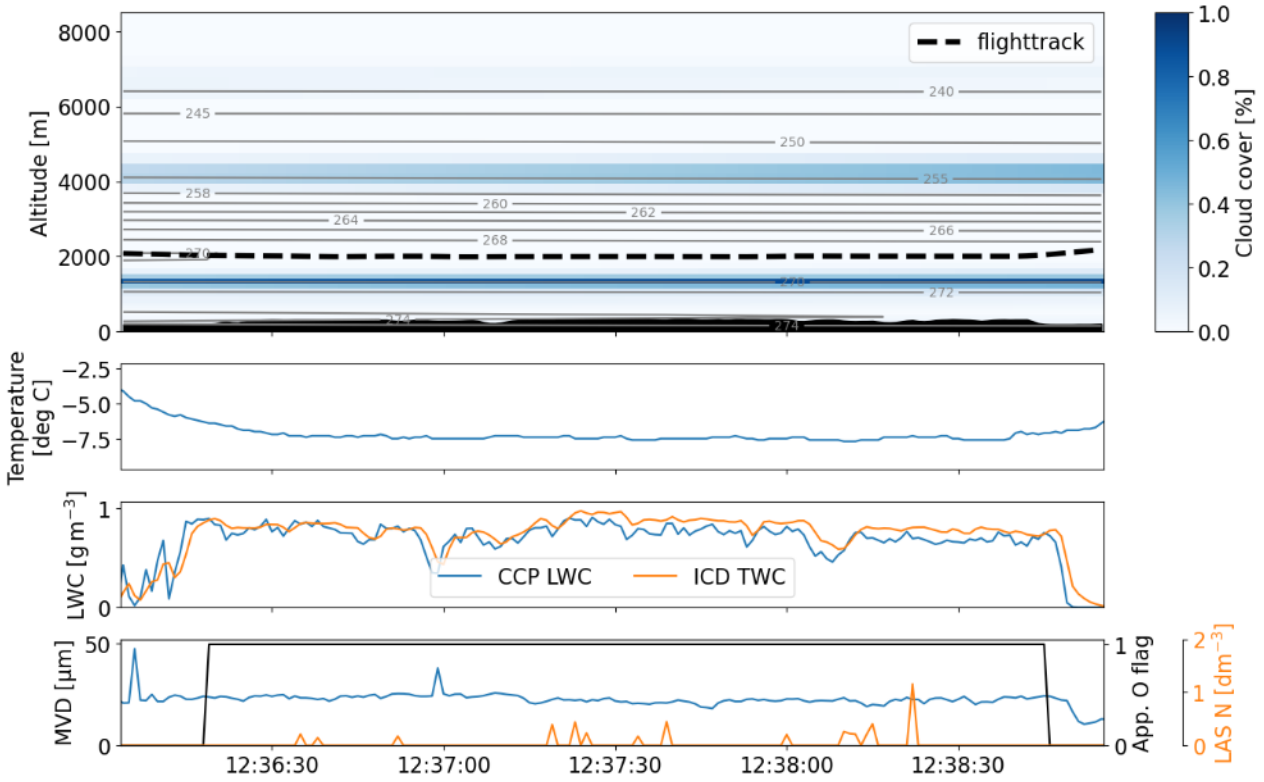

Figure 18: Appendix O encounter with high LWC during F1477-1. The cloud cover data from ERA5 does not show the clouds that were sampled.

5.1.5 F1477-2 – 1 March 2023

After refueling at Des Moines, Iowa (KDSM), the aircraft returned northward for Flight F1477-2, sampling clouds that immediately trailed the main cold front. This feature and the attendant clouds sampled were moving eastward across southern Minnesota and northern Iowa over the course of the day (Figure 19, Figure 20). By 18 UTC, the cold front had passed Rochester, Minnesota (KRST) and the clouds of interest were just to the west of this location. These well-mixed clouds were somewhat cooler than those sampled during the first flight and their tops were near 850 mb (~1.5 km). They were not producing significant precipitation. The aircraft sampled the clouds between 1725 and 1755 UTC, before returning to the base at Alton, Illinois.

The sampled clouds were lower than those sampled during the previous flight, with the cloud tops between 1400 and 1800 m. Again, both Appendix C and Appendix O conditions were encountered. LWCs were lower than during the first flight, with maximum values around 0.6 g/m³ observed. Although MVDs were small (mostly 10-20 µm), Appendix O conditions were still present at times. Aircraft, ERA and NAM data all indicated the presence of an inversion near cloud top. This feature was not captured well by the HRRR model (not shown), though it did forecast stable lapse just above cloud top. The inversion was not as strong as during some of the previous flights. An example of an icing encounter can be seen in Figure 20. LWC varied more than during many of the previous icing encounters. MVDs were quite low at ~11 µm, even during the Appendix O encounter from 17:51 to 17:52. During one of the short encounters, large droplets contributed significantly to the LWC and thus increased the MVD to about 25 µm for a few seconds.

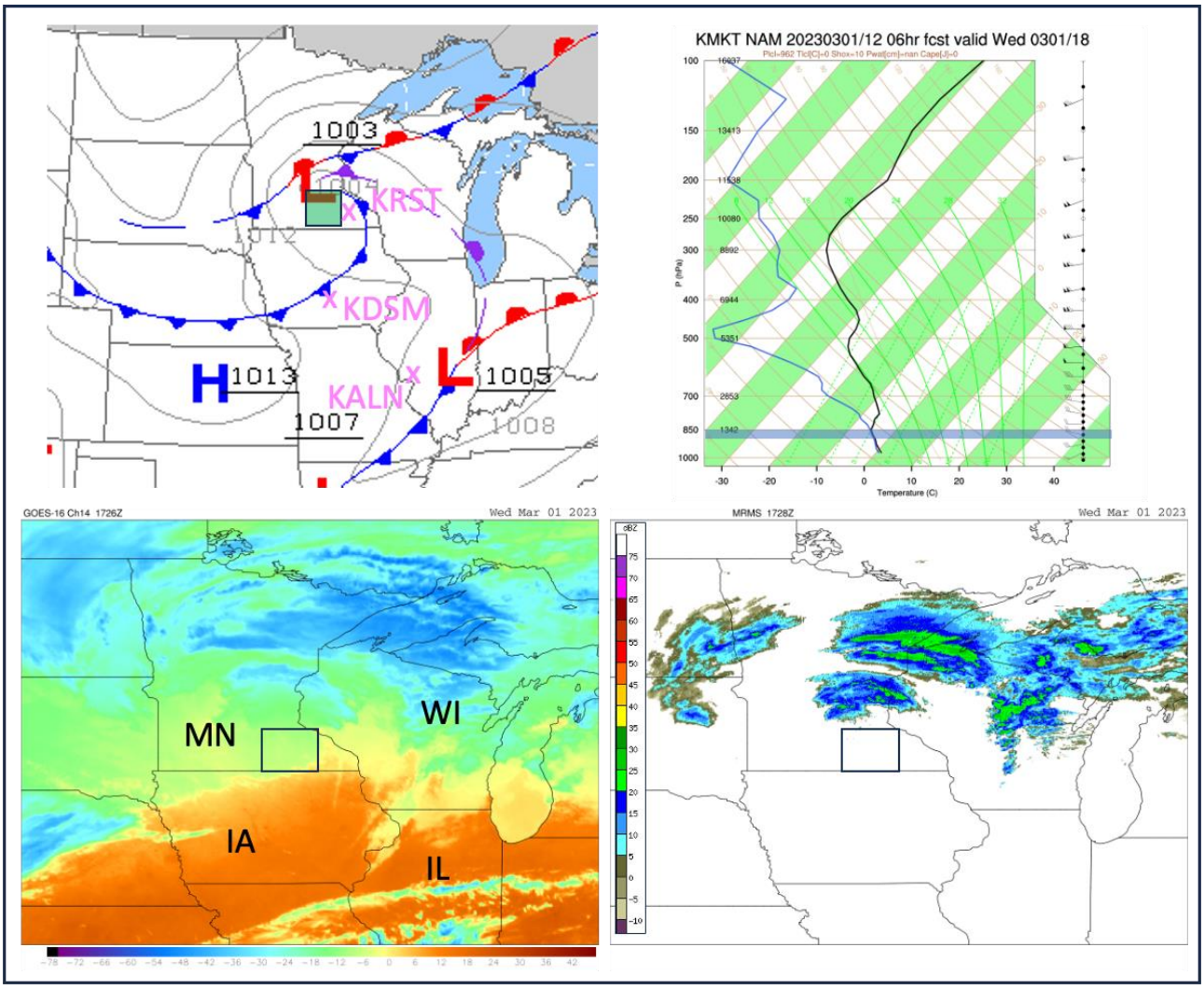

Figure 19: Same as Figure 9, but for Flight F1477-2, showing charts valid at ~18 UTC. MN=Minnesota, WI=Wisconsin, IA=Iowa, IL=Illinois. The NAM forecast sounding is for Mankato, Minnesota (KMKT), located to the west of Rochester (KRST).

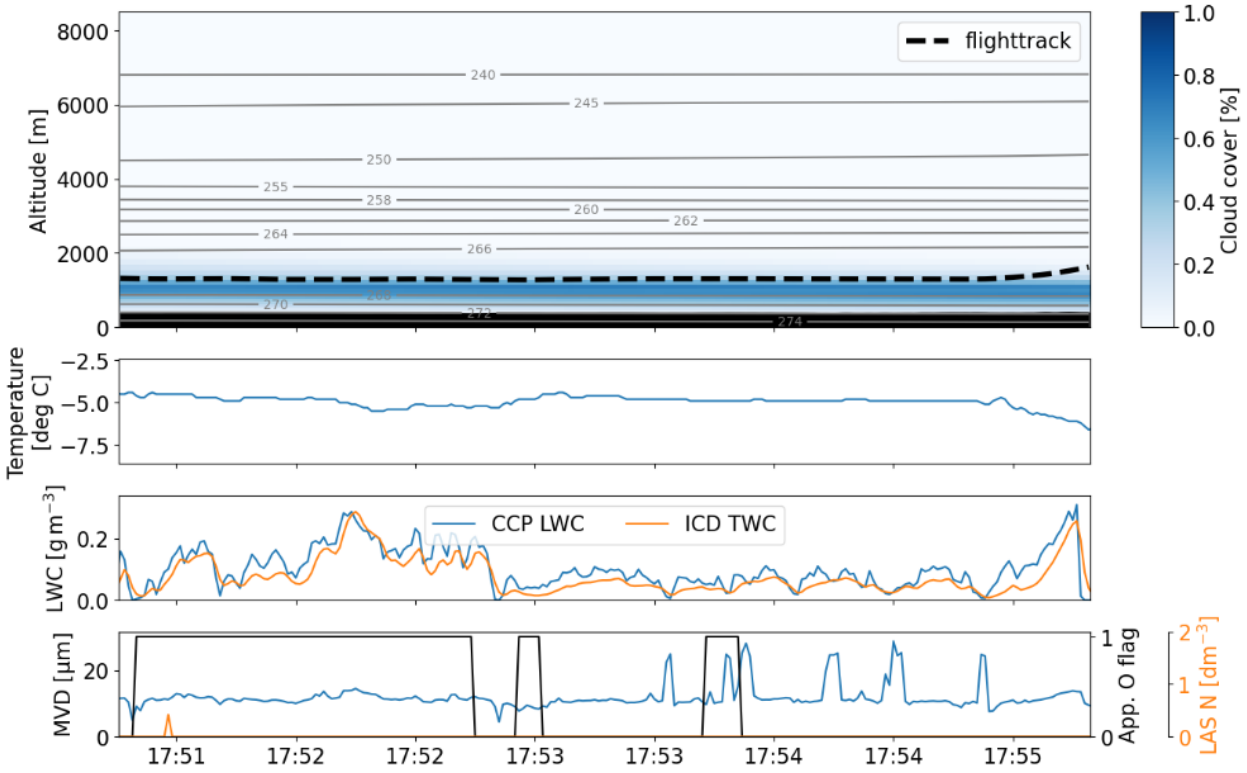

Figure 20: Several short Appendix O encounters that were observed during F1477-2.

5.1.6 F1478 – 6 March 2023

Flight 1478 was made within layered clouds to the north of a warm front that extended across northern Illinois, near Chicago, and southeast of an advancing cold front over Minnesota. The layer of interest was isothermal in nature, formed via gradual lift associated with overrunning. In the area of flight, the isothermal layer extended from ~1.3 km to ~2.1 km, and the unstable layer above it extended to ~3.0 km, based on forecast soundings and pilot reports. There was also a rather cold, ice-dominated cloud layer much further aloft, between ~7 and ~8 km (Figure 21, Figure 22). The presence of multiple layers was captured well by the HRRR model. The ERA5 re-analysis also had both layers, but the lower layer did not appear to extend high enough, with tops indicated to be closer to 2 km, rather than 3 km. During Flight F1478, the aircraft sampled the lower layer near Green Bay, Wisconsin (KGRB), focusing on altitudes between 1.5 and 2.1 km, within the isothermal layer.

Several long Appendix C encounters occurred, while Appendix O was only encountered very intermittently. LWCs were as large as 0.7 g/m³ and MVDs varied between 15 µm for the Appendix C encounters and up to 25 µm for the Appendix O encounters. An example of an icing encounter during the flight can be seen in Figure 22.

After sampling was complete, the aircraft landed at South Bend, Indiana (KSBN) for refueling, then returned to the operations base at Alton, Illinois. Some icing was encountered on this flight as well, but it is not discussed here.

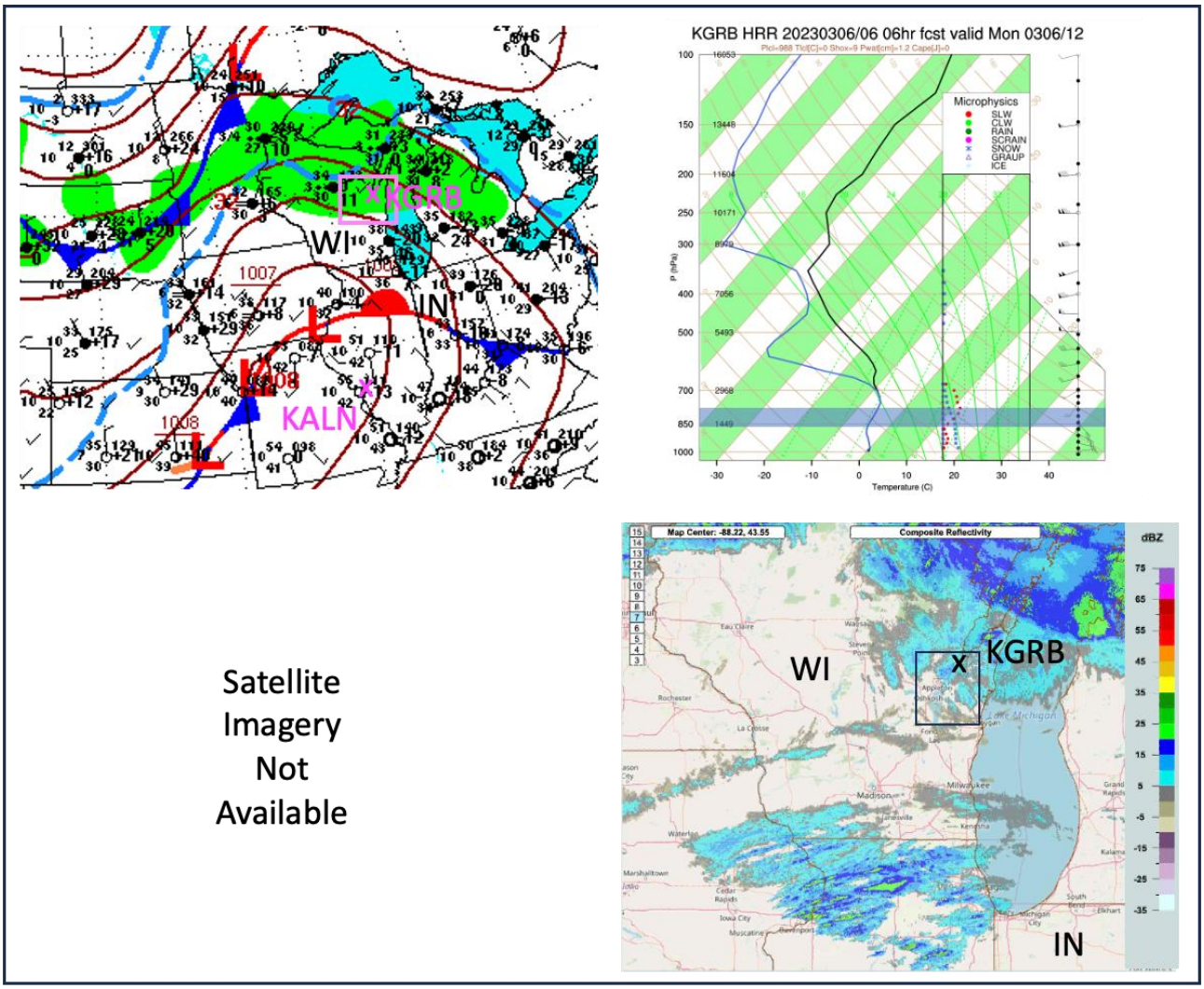

Figure 21: Same as Figure 9, but for Flight F1478, showing charts valid at ~12-13 UTC. WI=Wisconsin, IN=Indiana. The HRRR forecast sounding is for Green Bay, Wisconsin (KGRB). Satellite imagery was not available.

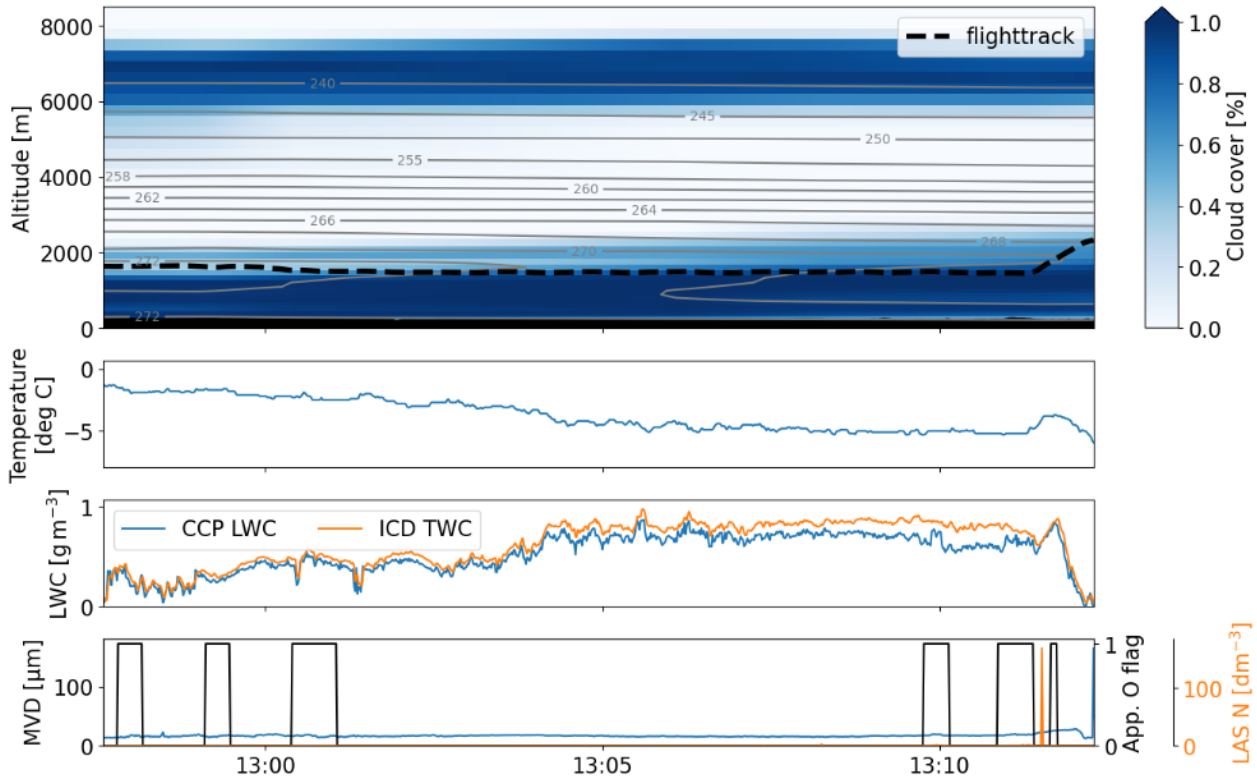

Figure 22: Icing encounter during F1478.

5.1.7 F1481 – 9 March 2023

F1481 was a brief attempt to capture some very warm icing in north-central Illinois, to the northeast of the KALN operations base. Though conditions were expected to be warm, there was a chance for drizzle to be present and they were near the base, so an attempt was made to sample the clouds. Synoptic-scale forcing was quite weak over Illinois and surrounding states, with numerous, weak low-pressure centers and troughing in multiple directions. There was some evidence that weak overrunning was forcing a shallow cloud layer that sloped upward from ~2 km near KALN to slightly higher altitudes and cooler temperatures over northern Illinois. There were also some higher-level, patchy ice clouds to the east and stronger, deeper ice clouds approaching from Iowa to the west (Figure 23). The variable, layered cloud situation was evident on the 13 UTC satellite imagery, while spotty, light patches of precipitation (drizzle/rain) evident in radar mosaic data over northern Illinois, near Galesburg and Peoria, Illinois (KGBG, KPIA). The HRRR model predicted a rather robust liquid layer around 2.0-2.2 km, with LWCs exceeding 0.5 gm^{-3} above KGBG with a small amount of SLD at temperatures between 0 and -3˚C. Cloud top height and depth appears to have been slightly overestimated. As was the case in many other events sampled during the North American campaign, the cloud layer of interest was isolated from the boundary layer, so drop concentrations were expected to be low, enhancing the chances of the cloud forming SLD via the collision-coalescence process. ERA5 re-analysis grids also indicated clouds between 2.0 and 2.4 km, and more robust clouds above ~6 km (Figure 24). In-flight photographs by the pilots (not shown) confirmed the presence of some broken, weak clouds just above the icing layer but the higher clouds were not evident where the photos were taken.

During the flight, clouds were sampled at an altitude of ~2 km. The conditions encountered during this flight were somewhat unusual, with relatively large SLD encountered several times (Figure 25).

The MVD for the encounter shown in this figure was 46 µm, with VD90 and VD99 reaching 282 and 397 µm, respectively. These values are much larger than those found during any of the other campaign flight. As expected, temperatures were quite warm at -1.6°C during the encounter shown in Figure 24 and Figure 25, and even higher (but still below the melting point) for other similar encounters. According to the ERA data and the HRRR forecast sounding, there was no warm air above the levels sampled, which supports collision coalescence as the formation process, rather than melting. Unlike the approach used in previous flights, the aircraft entered this cloud layer from below. The thickness of the cloud layer is estimated to have been 300 m (see Figure 24).

Most of the icing conditions encountered during F1481 were Appendix C conditions, with temperatures just slightly colder than 0°C and having LWCs between 0.5 and 0.8 g/m³.

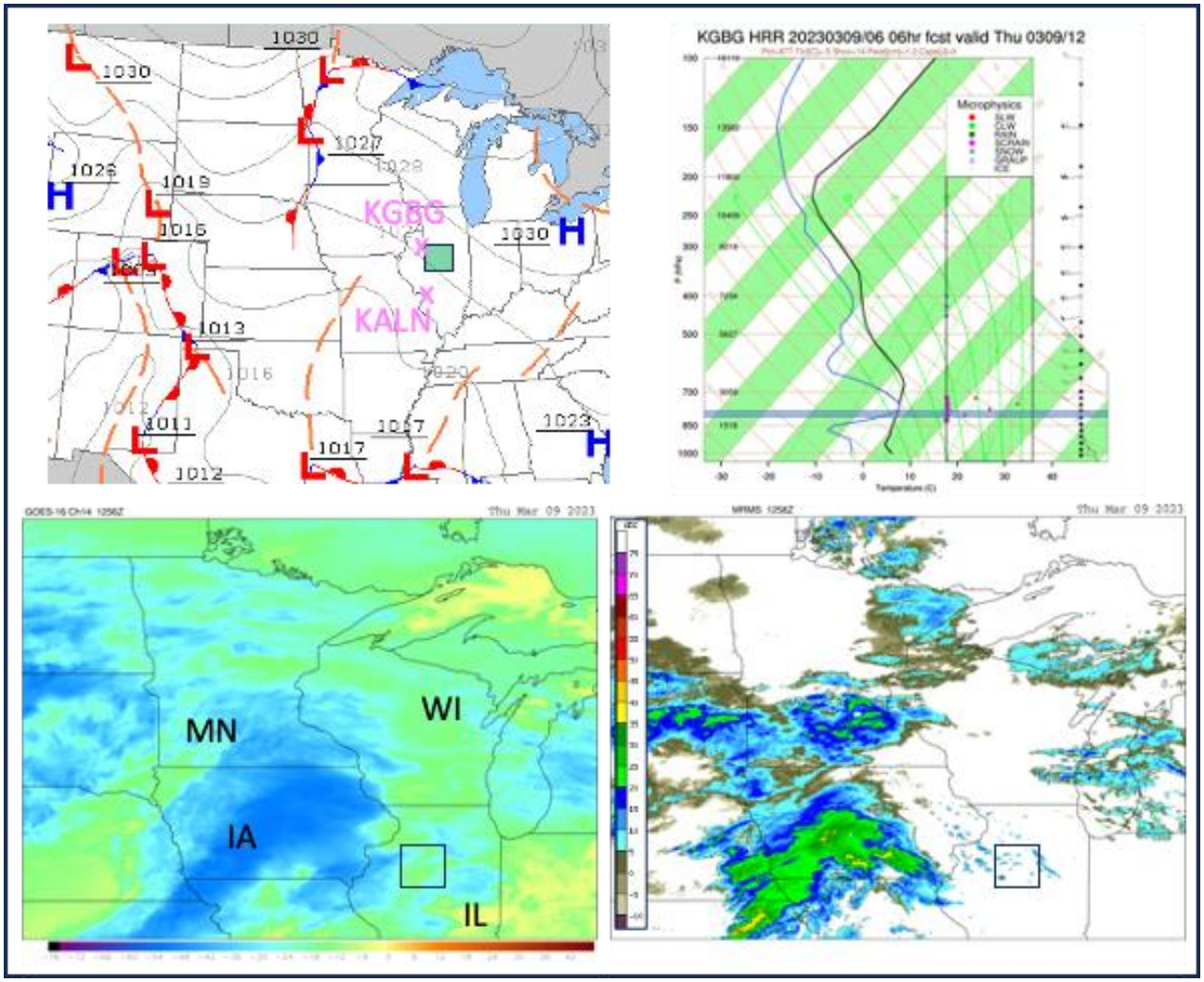

Figure 23: Same as Figure 9, but for Flight F1481, showing charts valid at ~12-13 UTC. MN=Minnesota, WI=Wisconsin, IA=Iowa, IL=Illinois. The HRRR forecast sounding is for Galesburg, Illinois (KGBG), just northwest of the area of flight.

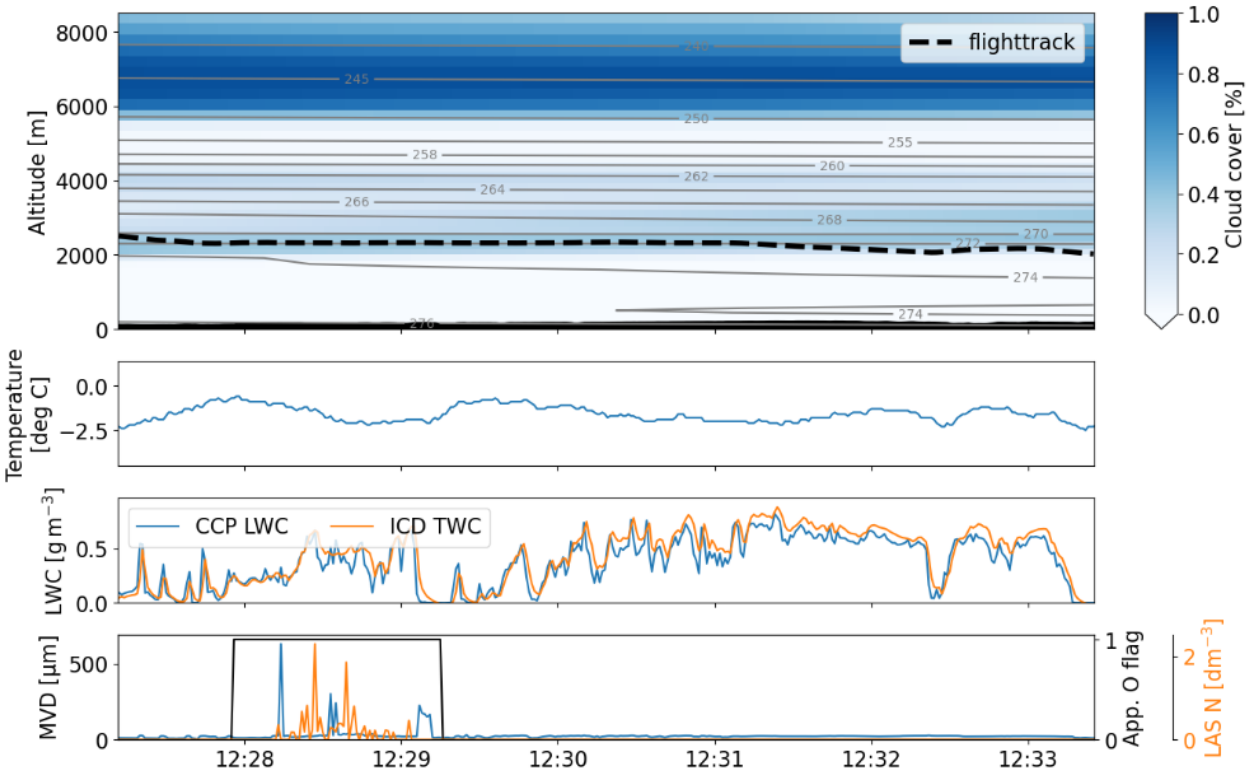

Figure 24: Icing encounter during F1481. The particles shown in Figure 25 are those encountered during the Appendix O segment shown in this Figure.

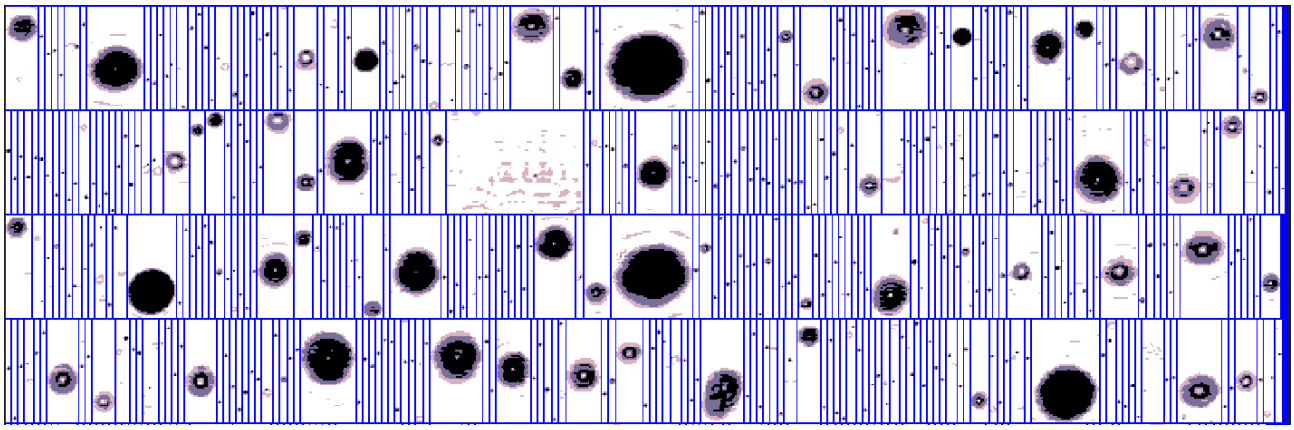

Figure 25: Images of particles encountered during F1481.

5.1.8 F1482 – 10 March 2023

Flight 1482 was made to sample widespread stratocumulus clouds over eastern Illinois and western Indiana in the early morning. These clouds existed to the southwest of a fairly vigorous low-pressure area centered along the Indiana-Ohio border at 12 UTC, behind an occluded front and cold front, that extended across Ohio and Kentucky. They were also located ahead of a surface trough that extended west-northwest from the low to Chicago and Iowa. This complex system caused widespread light and moderate precipitation to its north, and only spotty, very light precipitation to its south and west. The latter includes the area of flight, where cloud tops were on the order of -10˚C

and nighttime satellite imagery hinted at the presence of some drops bordering on SLD sizes. This was supported by the presence of light, patchy drizzle/rain echoes along the southern part of the Illinois-Indiana border, and some sporadic surface reports of those precipitation types in surface observations (Figure 26, Figure 27). The clouds were located at the top of a well-mixed boundary layer, with a deep isothermal layer at its top and dry air up to the tropopause. While such boundary layer-rooted clouds tend to produce small drop icing, as predicted by the HRRR, the clouds had arrived from Iowa, which had significant snow cover. This can sometimes limit the influence of ground sources of CCN and IN, helping to allow clouds to remain mostly water and for drop sizes to be larger than what would typically be expected in boundary-layer clouds when formed in CCN-rich air over exposed ground.

The clouds were sampled just to the southwest and south of Terre Haute, Indiana (KHUF). Cloud base was located at between 0.4 and 0.6 km, and cloud top was at ~1.6 km. Only Appendix C conditions were encountered on this day. Cloud LWC increased from top to bottom, as is often observed for stratocumulus clouds. LWCs reached up to 1 g/m³ on several occasions (see Figure 28). MVDs were about 15 µm most of the time and were always less than or equal to 20 µm.

After refueling at KHUF, the aircraft sampled Appendix C conditions on the return flight through essentially the same area, between ~1640 and 1735 UTC.

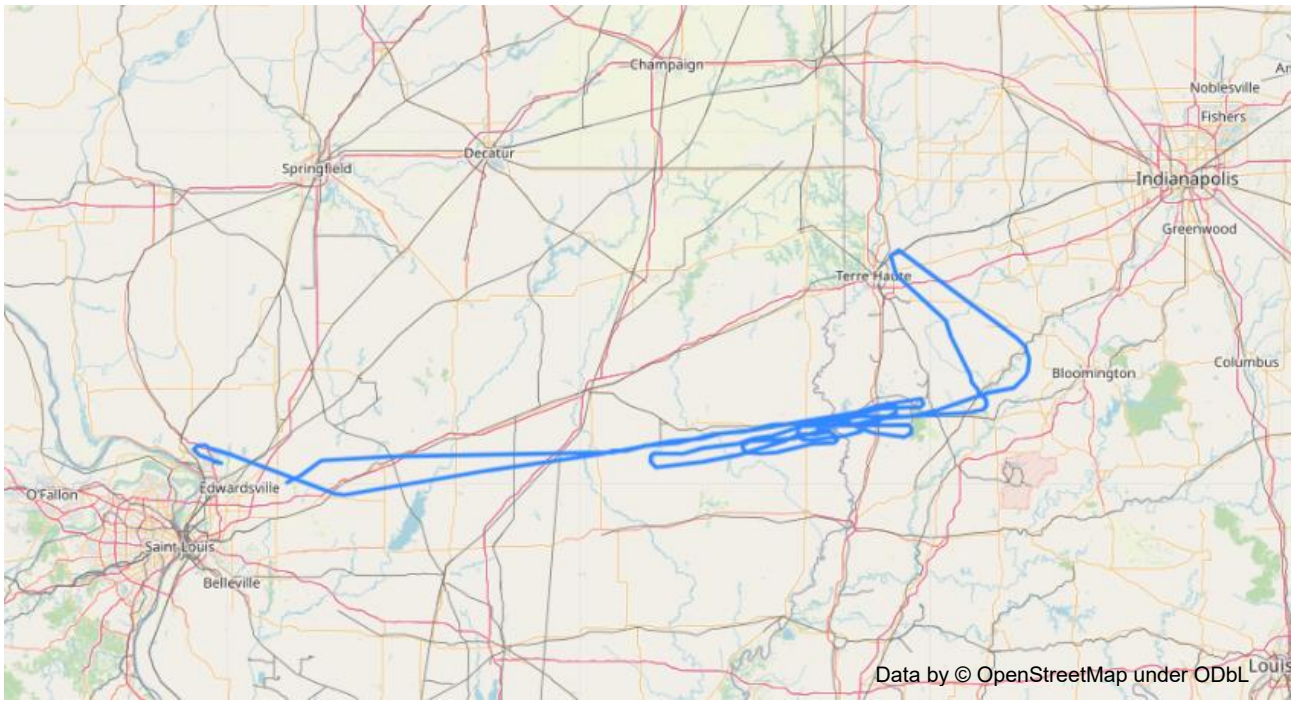

Figure 26: Flight track of F1482.

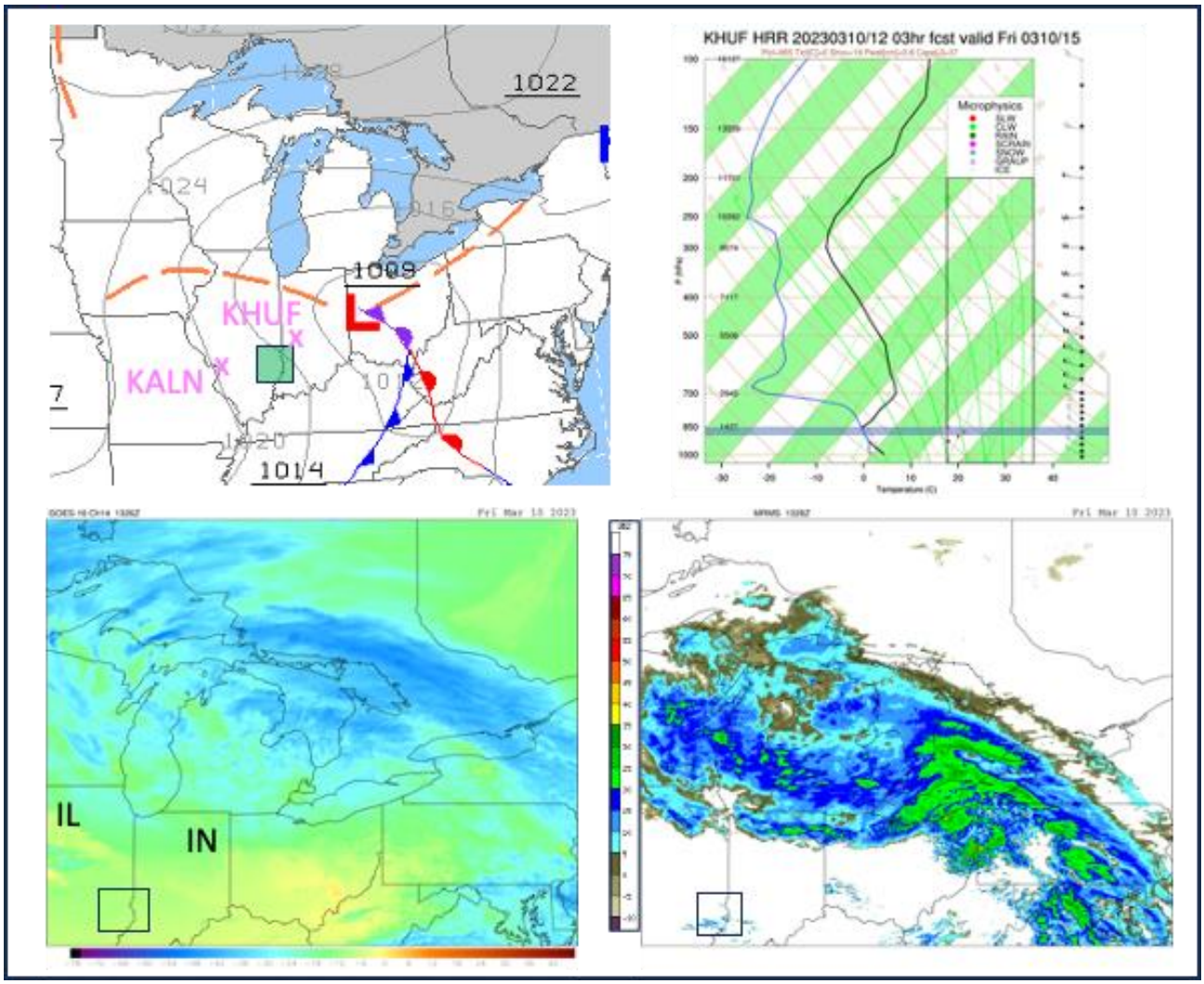

Figure 27: Same as Figure 9, but for Flight F1482, showing charts valid at 1200 UTC (prog chart), 1330 UTC (satellite, radar) and 1500 UTC (HRRR forecast sounding). IL=Illinois, IN=Indiana. The HRRR forecast sounding is for Terra Haute, Indiana (KHUF).

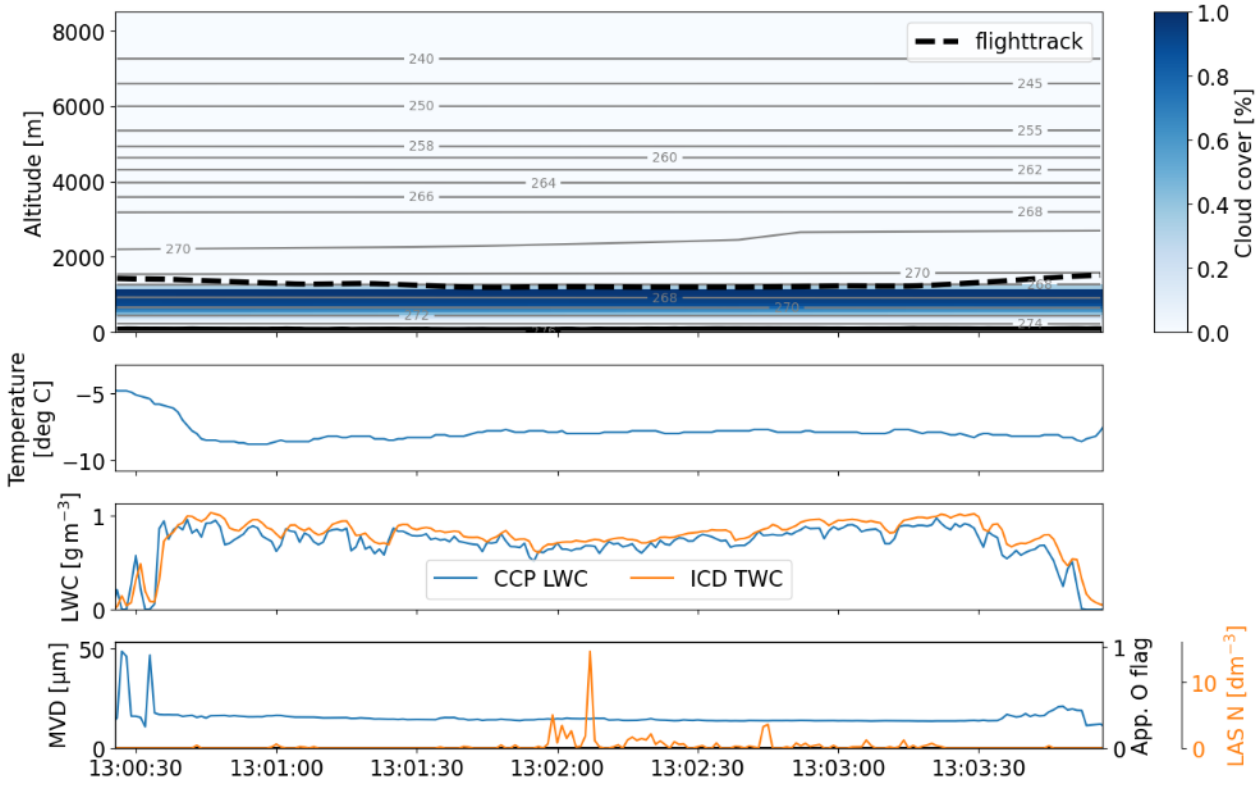

Figure 28: Icing encounter during F1482.

5.2 Atmosphere characterization for the North American flight test campaign

This chapter summarizes observations on the atmospheric parameters observed during the North American flight test campaign based on the full flight data set. Figure 29 shows a histogram of the LWCs encountered in Appendix C (a) and O (b) conditions in all flights. Appendix C conditions being defined as data points where the icing flag equals one but the Appendix O flag equals zero.

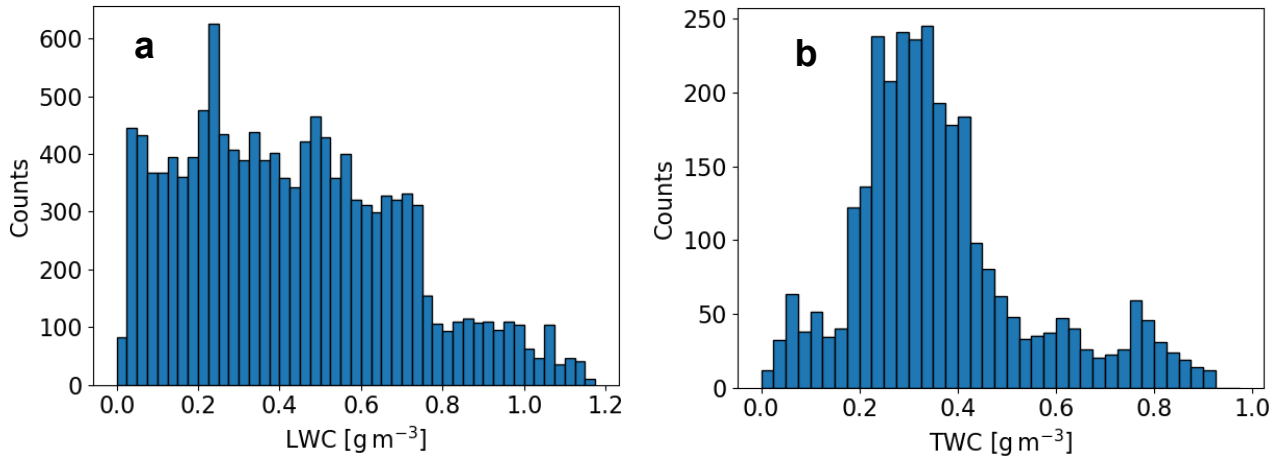

Figure 29: Distribution of ICD LWC measurements in Appendix C conditions (a) and ICD TWC measurements in Appendix O conditions (b) for the North American flight test campaign. The counts are based on rolling 15-seconds-averages which were computed for each second. Because Appendix O conditions are only defined if very few ice crystals are present, the TWC is generally equivalent to LWC in these cases.

The LWC of Appendix C encounters is relatively equally distributed between 0 and 0.8 g/m³. The LWC is below 0.77 g/m³ in 90% of the cases. For Appendix O, the majority of TWCs fall between 0.2 and 0.5 g/m³, with 10% of TWCs exceeding 0.65 g/m³. It should be noticed, that these are instantaneous LWCs based on 1Hz data, which have not been averaged over a specific exposure distance, as is the case in [17]. Of relevance for Appendix O conditions is especially the LWC that is contained in SLD, as it causes the critical ice accretion. Therefore, Figure 30 shows a histogram of the LWC that was contained in SLD during the American flight test campaign. In the majority of cases, the LWC contained in SLDs is below 0.05 g/m³. But isolated cases exist, where SLD LWCs were larger than 0.075 g/m³. These measurements stem mostly from F1475-1 and F1481.

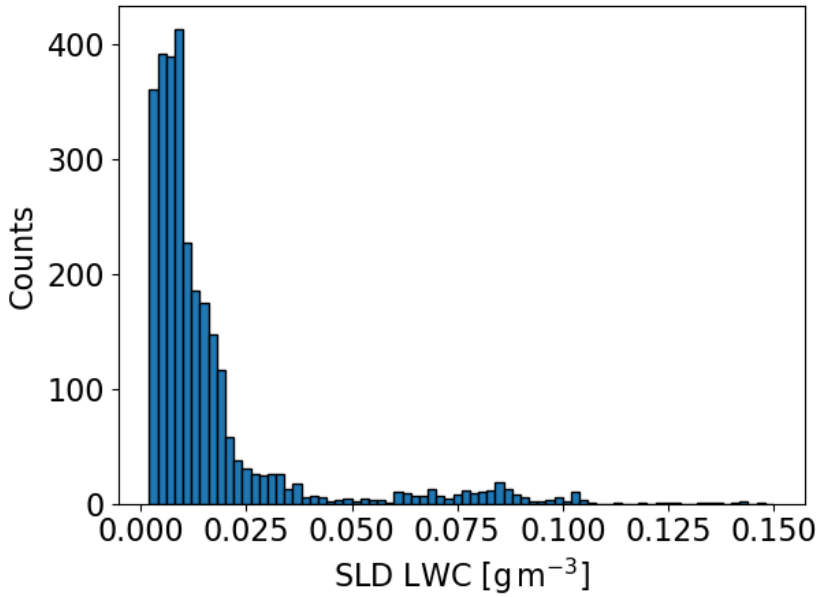

Figure 30: LWC contained in SLDs (i.e. all droplets with diameters larger than 100 µm) during the North American flight campaign. The data are based on rolling 15 second averages.

Figure 31 provides a map of the LWC content measurements along the flight track as observed during the American flight test campaign. Blueish to black colors denote enhanced LWC while white shading symbolizes cloud free air. The grey colors give flight segments without any data (e.g. transfer flights).

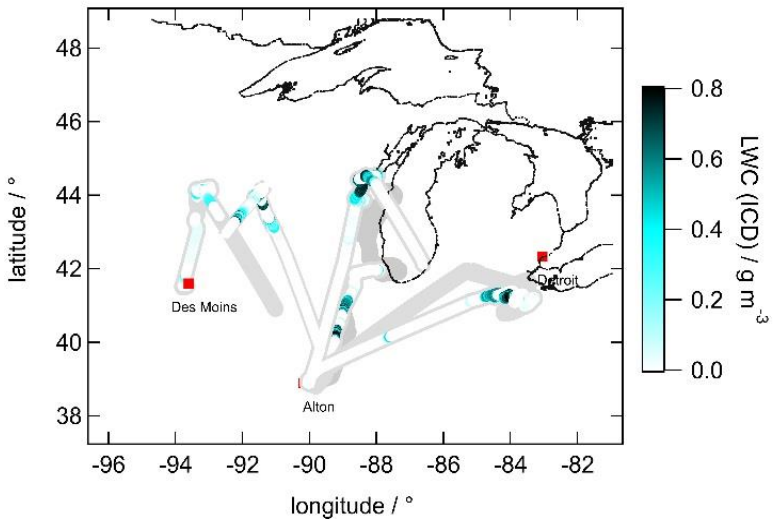

Figure 31: Map of selected flight paths from the North American campaign color coded with the LWC measured by the ICD. Enhanced LWD shows region of icing encounters. Only flights F1475-1, F1475-2, F1476, F1477-1, F1477-2 are included in the plot. Plot taken from [1] © SAE/ SENS4ICE project.

The time spent in Appendix C and Appendix O conditions for all flight data is provided in an altitude profile in Figure 32. The LWC data for this analysis are based on 15 second averages, i.e. they are not directly comparable to the data used for the Appendix O certification envelopes described by Cober and Isaac [17]. Icing conditions during the North American flight test campaign were mostly encountered between 500 and 3000 m, with a maximum around 1500 m. Appendix O conditions were encountered at a lower rate than Appendix C conditions, and they were found between 1000 and 3000 m. Altitudes above 3000 m were mostly used for transfer and to deice. Therefore, the number of icing encounters is very small at higher altitudes.

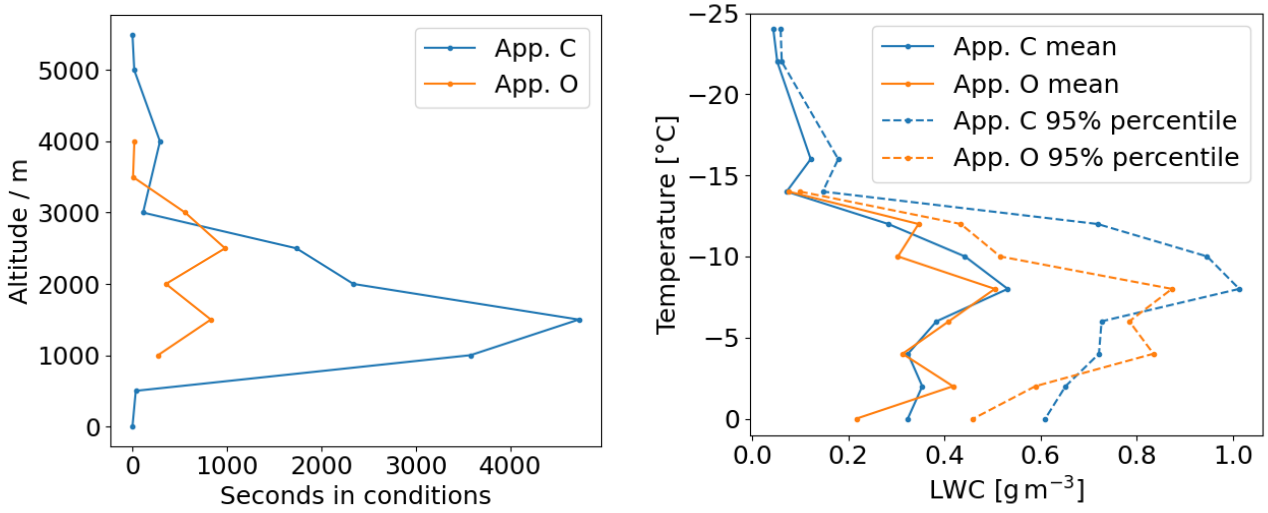

Figure 32: Altitude (left) and temperature (right) profile of the all icing encounters of the North American flight test campaign divided into Appendix C and Appendix O conditions as defined above. Shown are medians and 95 percentiles of the LWC contained in Appendix C and Appendix O classified clouds. LWC data are based on 15 second averages.

The mean LWC values of Appendix C and Appendix O conditions are mostly between 0.2 and 0.5 g/m³ and the maxima are encountered around -8°C. For colder temperatures, the mean LWC decreases for both Appendix C and Appendix O conditions up to -14°C, below which no Appendix O conditions were encountered and also Appendix C conditions have only minimal LWCs. The 95 percentiles of the Appendix O LWC peaks around values of 0.8 g/m³ for temperatures between -4 and -8°C. Appendix C conditions reach higher LWCs, which can exceed 1 g/m³.

The cumulative mass distributions of the SLD conditions that were encountered are shown in Figure 33. All but one of these distributions have more than 80% of LWC at diameters smaller than 100 µm. Median volume diameters were on average at 23 µm. Thus, mostly freezing drizzle conditions with MVD < 40 µm were sampled. Freezing rain conditions were not targeted and not encountered.

Due to sampling strategies designed to maximize safety, it was necessary to conduct most of the Appendix O sampling near cloud top, where the small drop contribution to Appendix O clouds tends to be quite significant, frequently resulting in MVD < 40 µm. Appendix O clouds with MVD > 40 µm tend to occur well below cloud top, often near or below cloud base, where the small drop contribution to the drop size spectrum is much smaller and drizzle has grown to larger sizes through collision coalescence.

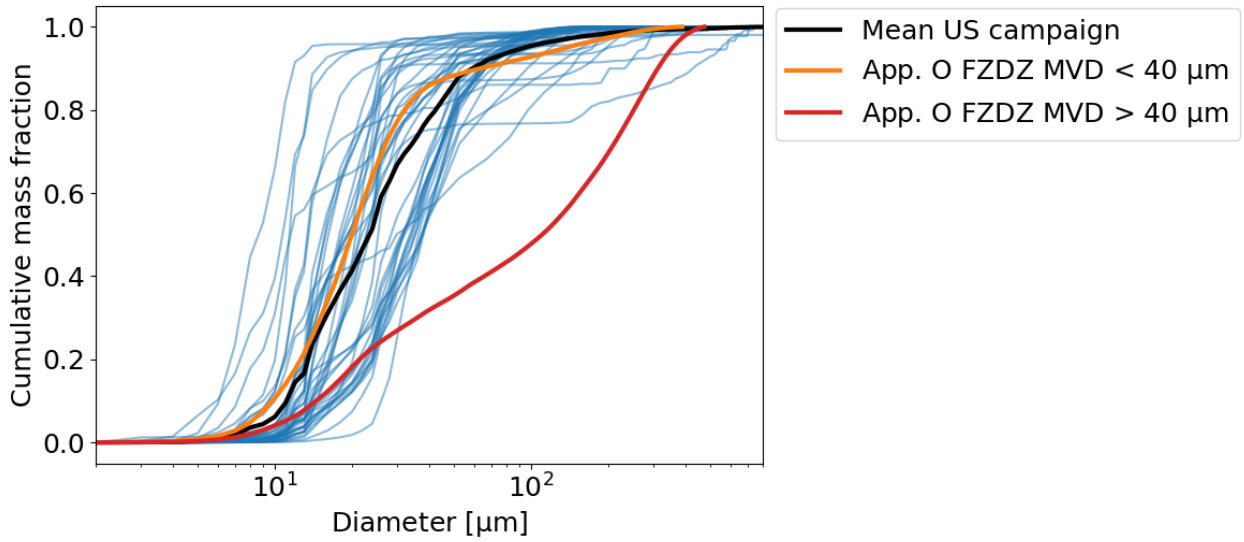

Figure 33: Cumulative mass distributions for each Appendix O encounter observed during the American flight test campaign. The mean curve is plotted in black, the MVD of the mean curve is 23 µm. The cumulative mass curves for freezing drizzle MVD < 40 µm and MVD > 40 µm from Cober and Isaac [17] are plotted in orange and red, respectively.

In Figure 29b the TWC encountered in Appendix O conditions (which is assumed to be equivalent to the LWC, due to the criterion that an Appendix O encounter contains at most one ice crystal per liter, see Section 3.3) was plotted as a histogram. It is apparent that occasionally TWC values occur which exceed the maximum specified in the Appendix O envelopes [17]. However, it needs to be considered that the values that were used to create the envelopes were averages over 17.4 nautical miles. According to Cober and Isaac [17], if data with different encounter lengths are considered, a scaling factor needs to be applied to the LWC. For instance, the average LWC measured during an encounter with a horizontal extent of 3000 m needs to be multiplied by 0.82 before it is compared to the LWC envelopes of Appendix O. This scaling reflects the decreasing probability to encounter high LWC over long distances. The comparison of the LWC of the Appendix O encounters of the American flight test campaign and the certification envelopes can be seen in Figure 34. The appropriate scaling factors were applied to all encounters. Most of the encounters fall within the envelopes and, as

mentioned earlier, there are no measurements in the portion of Appendix O which is at temperatures lower than -15°C. Two points clearly fall outside the envelope of FZDZ MVD < 40 µm, despite the scaling factor that has been applied. Also, of the just two encounters with MVDs > 40 µm, one falls outside the envelope. The highest LWC for Freezing Drizzle MVD < 40 µm occurred during Flight 1477-1, it is the same encounter that was already pictured in Figure 18. The meteorological conditions of this encounter would be a suitable subject for further study in order to assess the likelihood that the LWC exceeds the envelope limits. The highest LWC in the FZDZ MVD > 40 µm regime occurred during Flight 1481, it is the encounter also pictured in Figure 24. The temperature during the encounter was relatively high and it did not result in ice accretion.

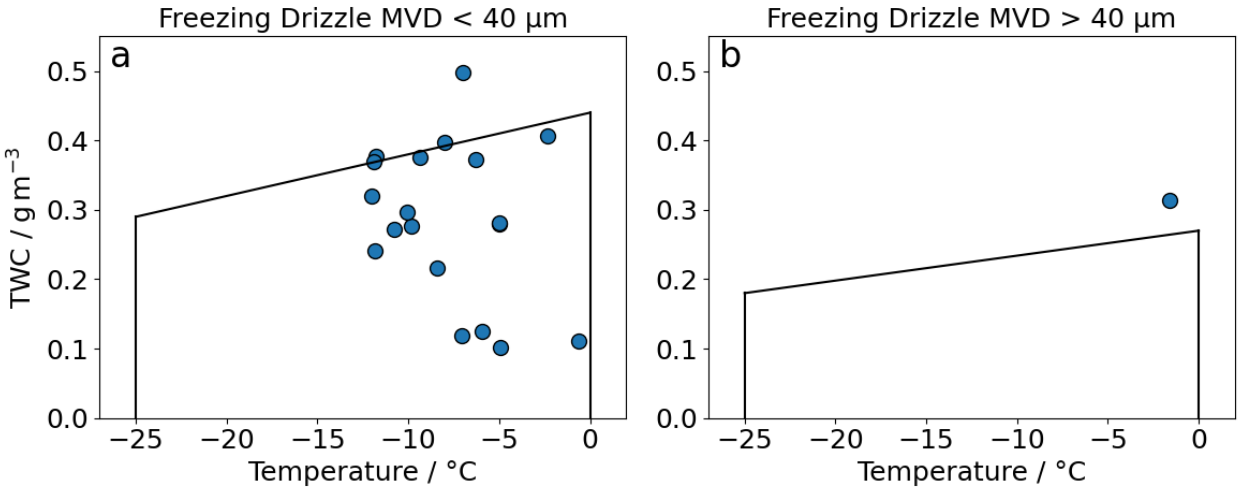

Figure 34: Nevzorov TWC of the Appendix O encounters during the North American flight test campaign in comparison to the envelopes of Freezing Drizzle MVD < 40 µm (a) and Freezing Drizzle MVD > 40 µm (b). The Nevzorov TWC is assumed to be equivalent to the LWC in Appendix O conditions because Appendix O encounters were required to contain few ice crystals. Due to ambiguities that may exist in the detection of particles (see Section 3.3) and due to the chance of intermittent mixed-phase clouds the TWC measurement of the Nevzorov may be contaminated by ice and thus too high for some of the encounters shown. Only encounters longer than 30 seconds were used for this plot.

Appendix O also defines a temperature and altitude envelope in which freezing drizzle conditions occur. This is shown, in comparison to the data from the North American SENS4ICE campaign, in Figure 35. It is apparent that all test points lie well within the envelope. Regarding altitude and temperature, the Appendix O conditions were therefore normal.

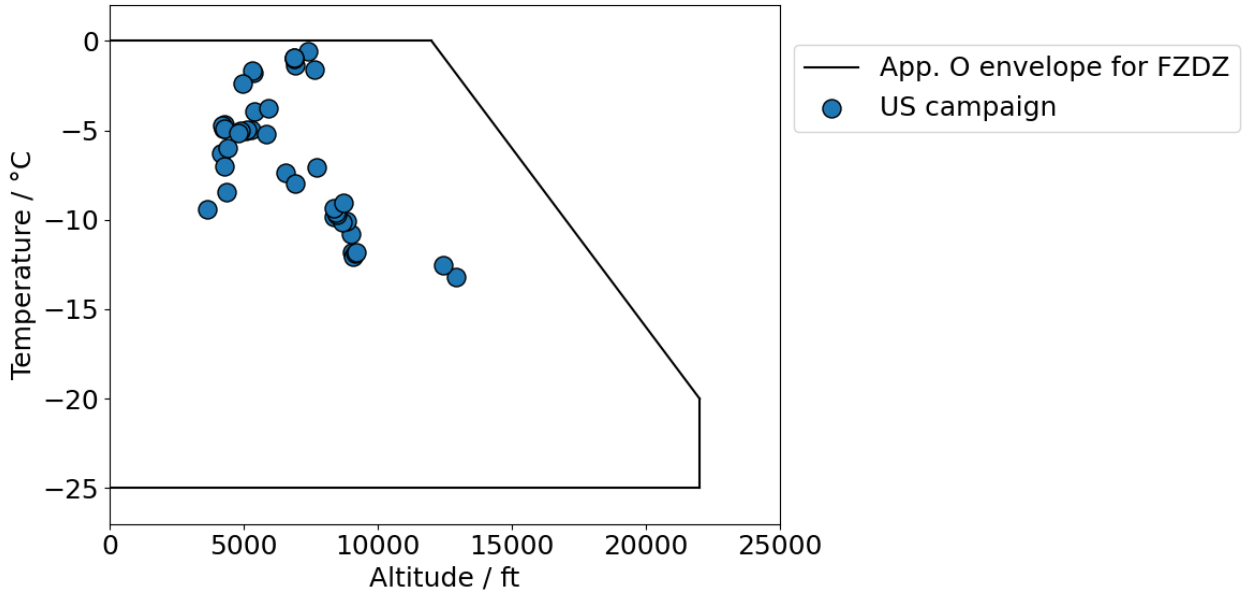

Figure 35: Pressure and altitude of Appendix O conditions encountered during the North American flight test campaign in comparison to the envelope for FZDZ from Appendix O.

Lastly, a short overview of the overall occurrence of different cloud conditions is given. We differentiate between small droplet icing (i.e. Appendix C conditions which contain almost no ice crystals), mixed-phase clouds (also Appendix C conditions, but with a significant number of ice crystals) and Appendix O conditions. Glaciated conditions were not encountered. A plot of the frequency of occurrence of each of these conditions in each flight is shown in Figure 36.

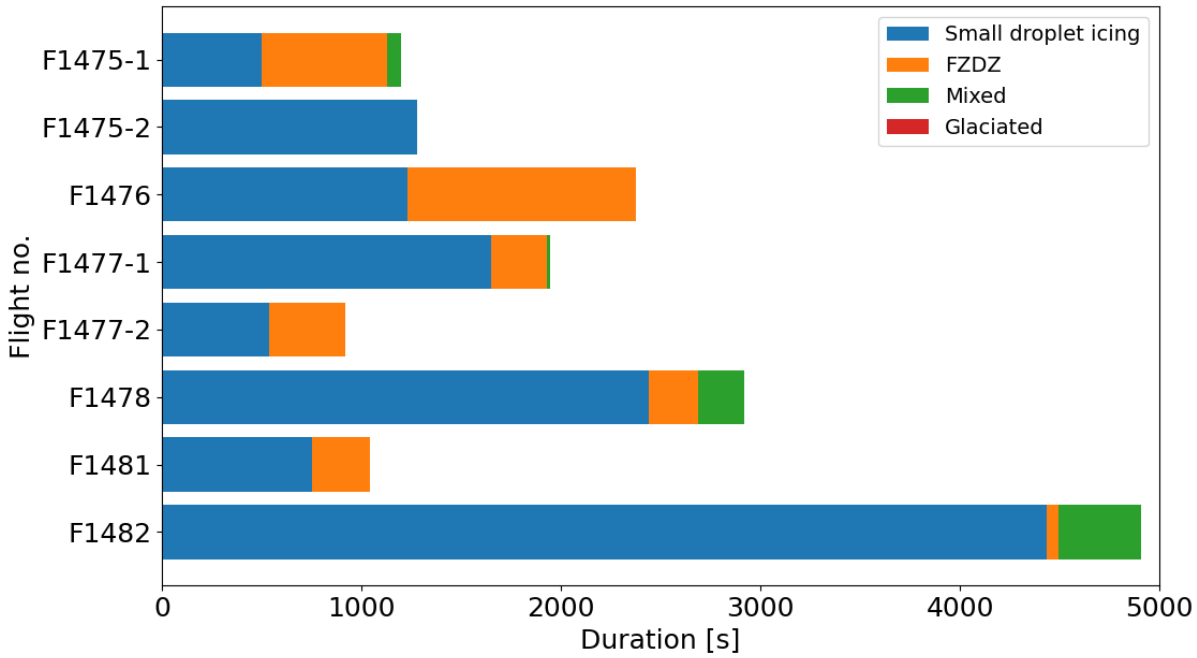

Figure 36: Frequency of occurrence of different cloud conditions during the North American flight test campaign.

Table 4 already listed the times in Appendix C and Appendix O conditions. From Figure 36 it is now apparent that most of the Appendix C conditions contained hardly any ice crystals, just during few flights several minutes in mixed-phase conditions were encountered. During the campaign an effort was made to avoid conditions that are conducive to the formation of ice crystals, such as cloud top temperatures below -15°C and situations where ice clouds above could have seeded the cloud of interest. Furthermore, Appendix O conditions are often found above a significant stable layer that limits the potential for ice nucleating particles and cloud condensation nuclei from ascending into the cloud from the boundary layer.

6. European flight test campaign

This chapter details the individual flights of the European flight test campaign and summarizes the atmospheric conditions that were encountered. The flights of the European flight test campaign were either performed as CER flights or as Airways flights. CER refers to specifically designated areas that were reserved for the test aircraft. Flights in these areas were controlled by a dedicated controller, hence there was a lot of flexibility for adjusting the flight plan. However, CER zones only existed in the vicinity of Toulouse and towards the Atlantic coast near Bordeaux. If no suitable conditions were predicted for these regions, airways flights were performed. In contrast to CER flights, airways flights had essentially no flexibility to make changes in the flight path or even in altitude.

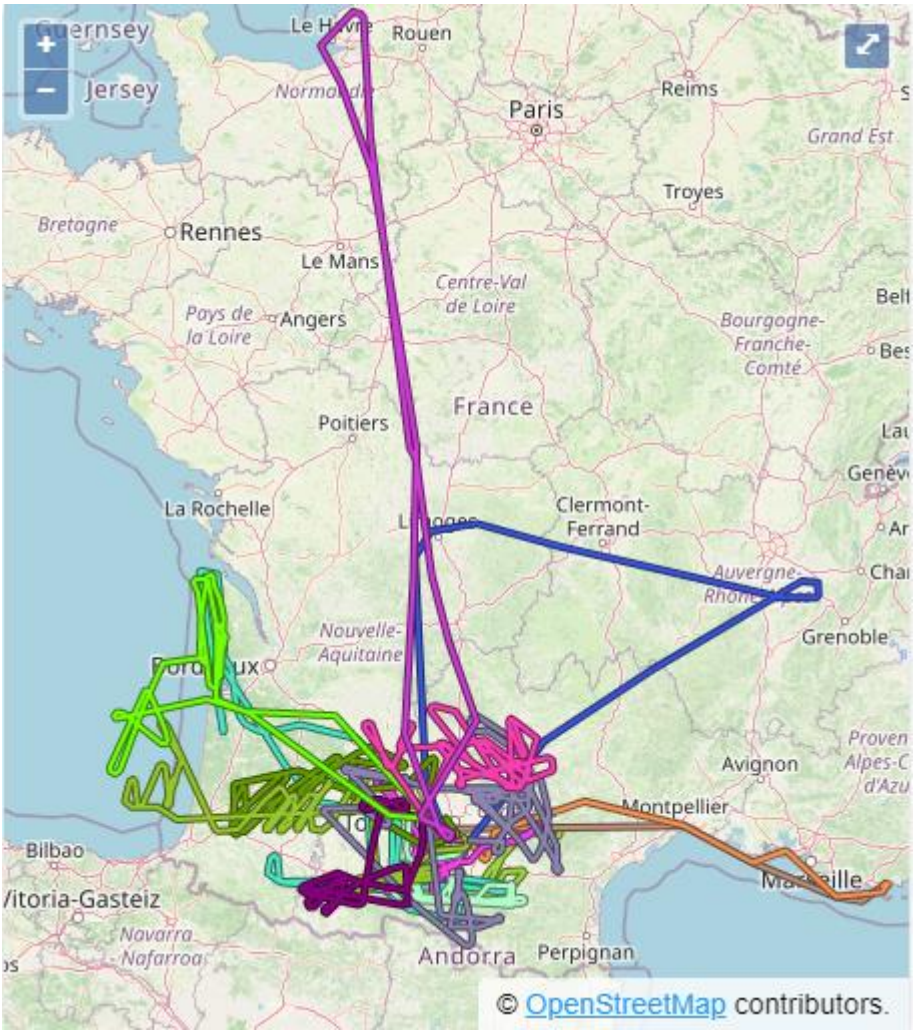

Figure 37: Flight tracks of the European test campaign. Most flights were conducted over land while some flights were conducted above the Atlantic Ocean and the Mediterranean Sea.

6.1 Description of measurement flights

Fifteen scientific flights were performed within the European flight test campaign. A map with the most relevant flights can be seen in Figure 37. Additionally, one EMI flight and two test flights have been performed, which were not evaluated. Furthermore, aircraft and instrument issues were encountered during observational flights (OFs) 3 and 4, respectively so these flights were subsequently not evaluated. On flight OF1 to OF8 the Nevzorov data was considered unreliable and is hence not used. The LWC and derived parameters, such as icing flags, stem from the CCP for these flights. An overview of selected flights of the European flight test campaign is given in the following.

Table 5: Overview of flights performed during the European flight test campaign.

Flight	SAFIRE flight number	Day	Flight time (UTC)	Time in Icing conditions [mm:ss]	Time in Appendix O conditions [mm:ss]	Comments
OF1	as230009	03/04/2023	05 :47-09 :35	90:13	1:28	LWC from CCP
OF2 pt1	as230010	04/04/2023	11:12-12:52	10:42	0:11	LWC from CCP
OF2 pt2	as230011	04/04/2023	13:05-14:29	12:14	1:48	LWC from CCP
OF3	as230012	06/04/2023	n/a	n/a	n/a	Aircraft problem
OF4	as230013	14/04/2023	n/a	n/a	n/a	Instrument failure
OF5	as230014	15/04/2023	05:24-08:11	40:37	12:40	LWC from CCP
OF6	as230015	18/04/2023	13:04-17:01	72:01	0:00	LWC from CCP
OF7	as230016	20/04/2023	09:43-13:17	2:38	0:00	LWC from CCP
OF8	as230017	22/04/2023	05:16-08:47	34:07	0:00	LWC from CCP
OF9	as230018	24/04/2023	12:24-16:47	90:57	59:48	
OF10	as230019	25/04/2023	10:06-15:51	90:14	43:01	
OF11	as230020	26/04/2023	05:56-08:52	13:42	0:00	
OF12	as230021	26/04/2023	12:37-17:04	52:20	14:01	
OF13	as230022	27/04/2023	05:50-09:57	62:42	6:14	
OF14	as230023	27/04/2023	11:28-15:43	42:09	13:39	

6.1.1 OF1 – 3 April 2023

The first observational flight of the campaign was made within to the CER south of Toulouse (Figure 38). There, clouds were blocked by the Pyrenees and reached altitudes of about 2500 m. The cloud top temperature was between -7 and -8°C. Cloud tops were partially glaciated and partially supercooled (observed from satellite imagery, not shown here). Predominantly Appendix C conditions were encountered. MVDs and LWCs varied widely. MVDs were between 10 and 25 µm and LWCs were mostly around 0.2 g/m³, but values exceeding 1 g/m³ were intermittently encountered. Regions with a significant number of ice crystals were sampled frequently. One intense icing encounter, where also Appendix O was intermittently present, occurred around 09:22 UTC. This can be seen in Figure 40. During this encounter, the aircraft appeared to have entered a cloud section of especially high LWC.

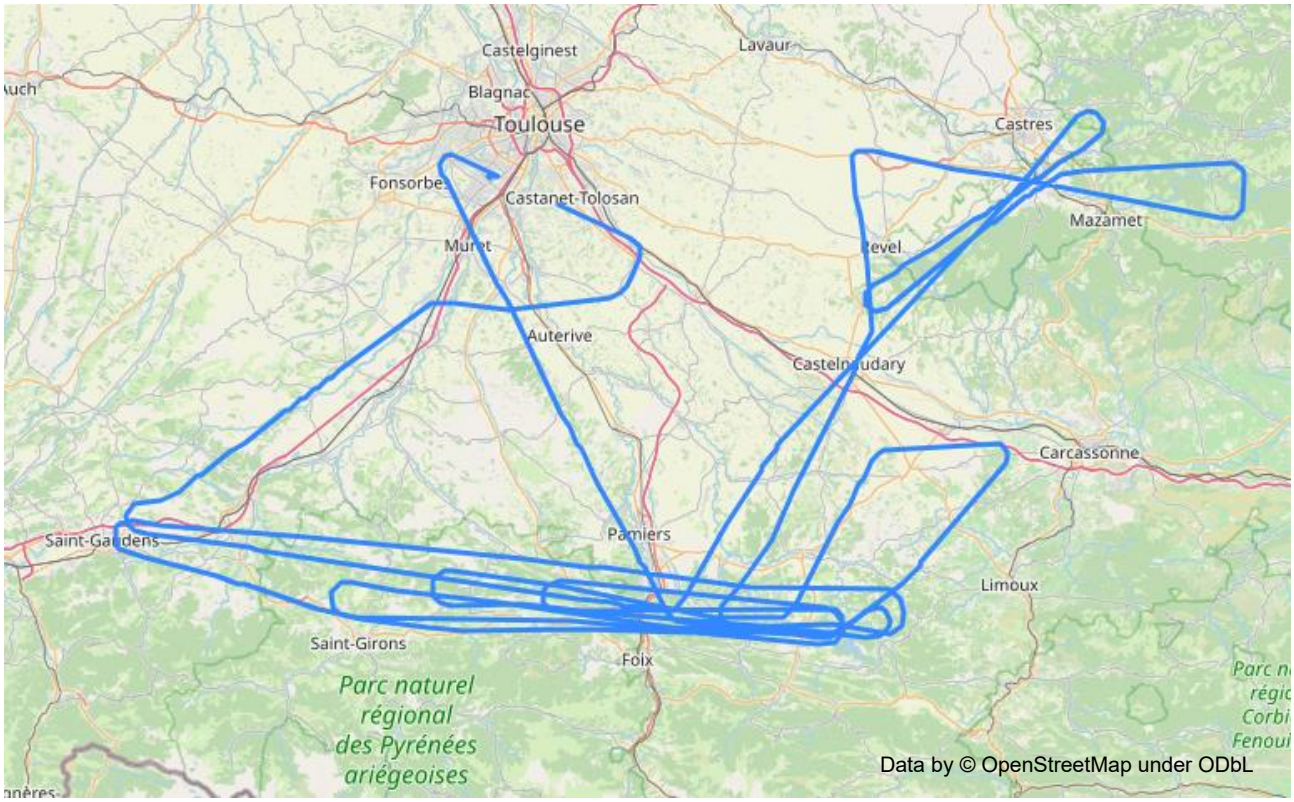

Figure 38: Flight track of OF1.

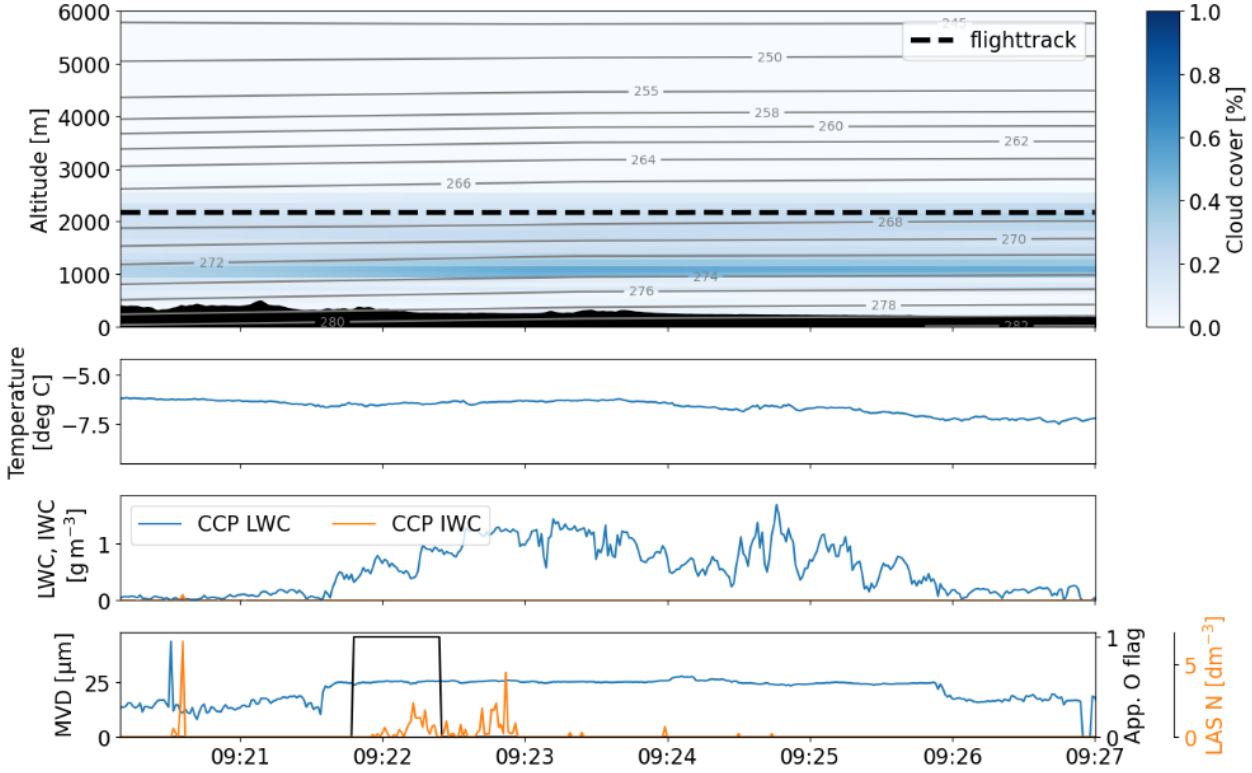

Figure 39: Appendix O encounter during OF1.

6.1.2 OF5 – 15 April 2023

The fifth observational flight of the European flight test campaign took place on 15th April 2023, with a flight track in the vicinity of Toulouse. Cloud top heights varied on that day between 2200 m and 2800 m and cloud top temperatures were between -6 and -4°C, which is also the reason why only cloud tops were measured. Mixed phase clouds with a large number of ice crystals prevailed on this day, hence mostly Appendix C icing conditions were encountered. However, also a few short instances of Appendix O encounters were identified in the data analysis, especially towards the end of the flight. These encounters occurred in a layer with a relatively low lapse rate (apparent from the large altitude between the iso-lines of 270 K and 268 K) (Figure 40).

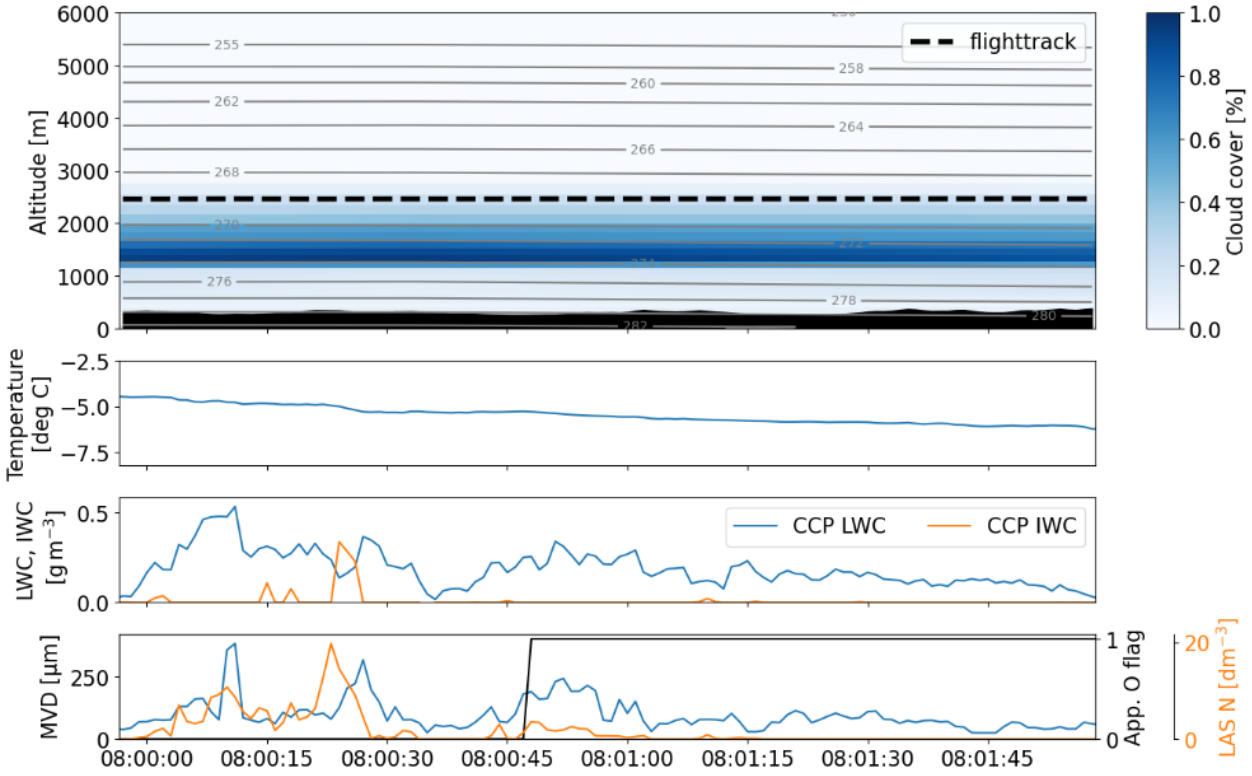

Figure 40: Appendix O encounter during OF5.

6.1.3 OF9 - 24 April 2023

The ninth observational flight sampled a front that was coming from the West over the Atlantic Ocean. The flight targeted the front over the Atlantic, south of Bordeaux and then followed it inland in a Lagrangian manner. The cloud system was followed for several hours. Over the ocean SLD conditions existed at altitudes between 4200 and 4700 m and later at lower altitudes of 3800 m. After icing conditions weakened over land, the aircraft headed towards the Pyrenees, where icing conditions were encountered once again (see Figure 41). Appendix O conditions were first encountered at an altitude of approximately 4600 m, a temperature of -12°C, LWCs around 0.2 g/m³ and MVDs between 30 µm and 40 µm. The clouds were relatively patchy and multiple encounters with durations of about 1 minute were observed. Even within the encounters, the SLD occurred in localized pockets. A relatively long Appendix O encounter occurred over land from 14:19 to 14:23 (see Figure 42). The average LWC during the encounter was low, only about 0.15 g/m³, but the peak MVD was high, about 190 µm. It can be seen from Figure 42, that at times ice crystals were present during the encounter, which may distort the drop size distribution towards higher diameters. The

MVD is therefore likely an overestimate. The images of particles however confirmed, that SLD were present.

Very large MVDs were found during an Appendix O encounter at 16:17 UTC. Interestingly, the Dmax was smaller than during previous encounters, only 107 µm, hence a relatively narrow size distribution existed.

Figure 41: Flight track of OF9.

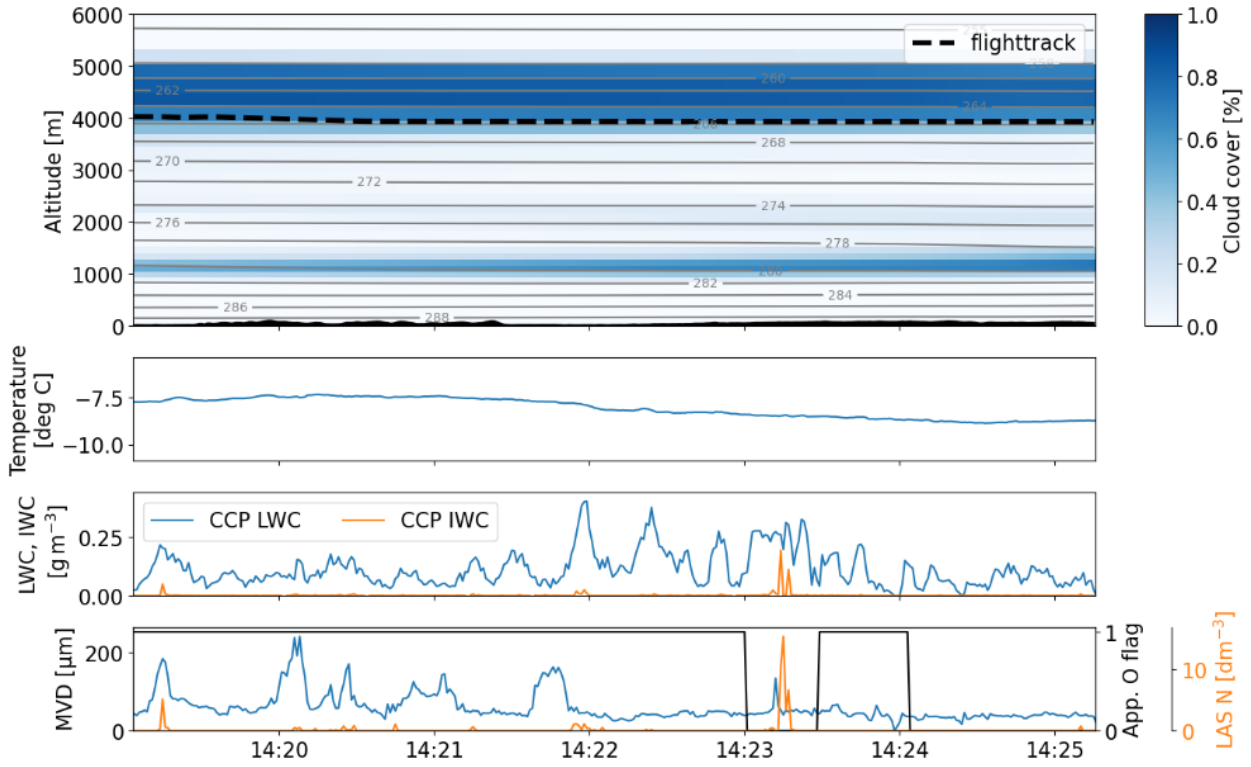

Figure 42: Appendix O encounter during OF9.

6.1.4 OF10 – 25 April 2023

OF10 took place in the vicinity of Toulouse, in the North, West and South of the city (see Figure 43). Appendix O conditions were at first encountered over the Pyrenees, at remarkably low LWCs of just 0.05 g/m³, an altitude of 4400 m and a temperature of -9°C (see Figure 44). When suitable conditions dissolved over the Pyrenees, the aircraft headed towards the North-West, where Appendix O conditions were again encountered, this time with higher MVDs (around 40 µm) than over the Pyrenees and at lower altitude and higher temperatures. Later during the flight, ice crystals became more prevalent, but Appendix O conditions were still encountered intermittently. LWCs during the flight hardly ever exceeded 0.2 g/m³.

Figure 43: Flight track of OF10.

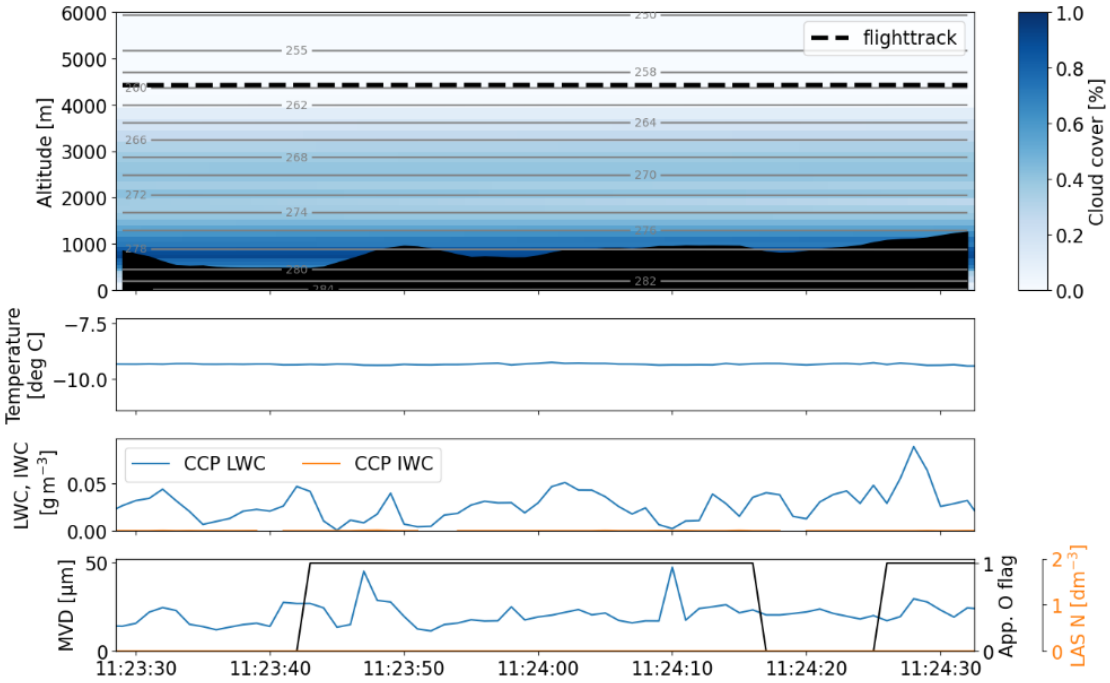

Figure 44: Appendix O conditions over the Pyrenees during OF10.

6.1.5 OF12 – 26 April 2023

OF12 sampled clouds in the CER area west of Bordeaux over the Atlantic Ocean. The flight track can be seen in Figure 45. During this flight, icing conditions at an altitude higher than 6000 m were encountered, the highest of all flights (see Figure 46). The LWC throughout the flight was low however, usually less than 0.2 g/m³. A few Appendix O encounters existed, with MVDs around 35 µm. A weak inversion existed at some locations at an altitude of about 500 m, but in the preliminary analysis no link between that inversion and the occurrence of Appendix O conditions could be established.

It is interesting to note, that as for OF10, the layer where icing was encountered contains only little humidity in the ERA5 data (see Figure 46).

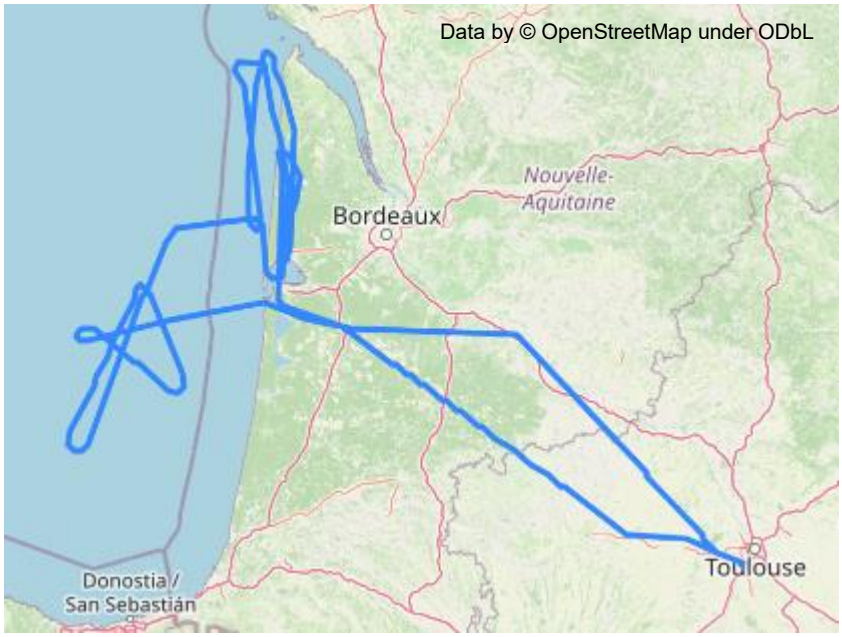

Figure 45: Flight track of OF12.

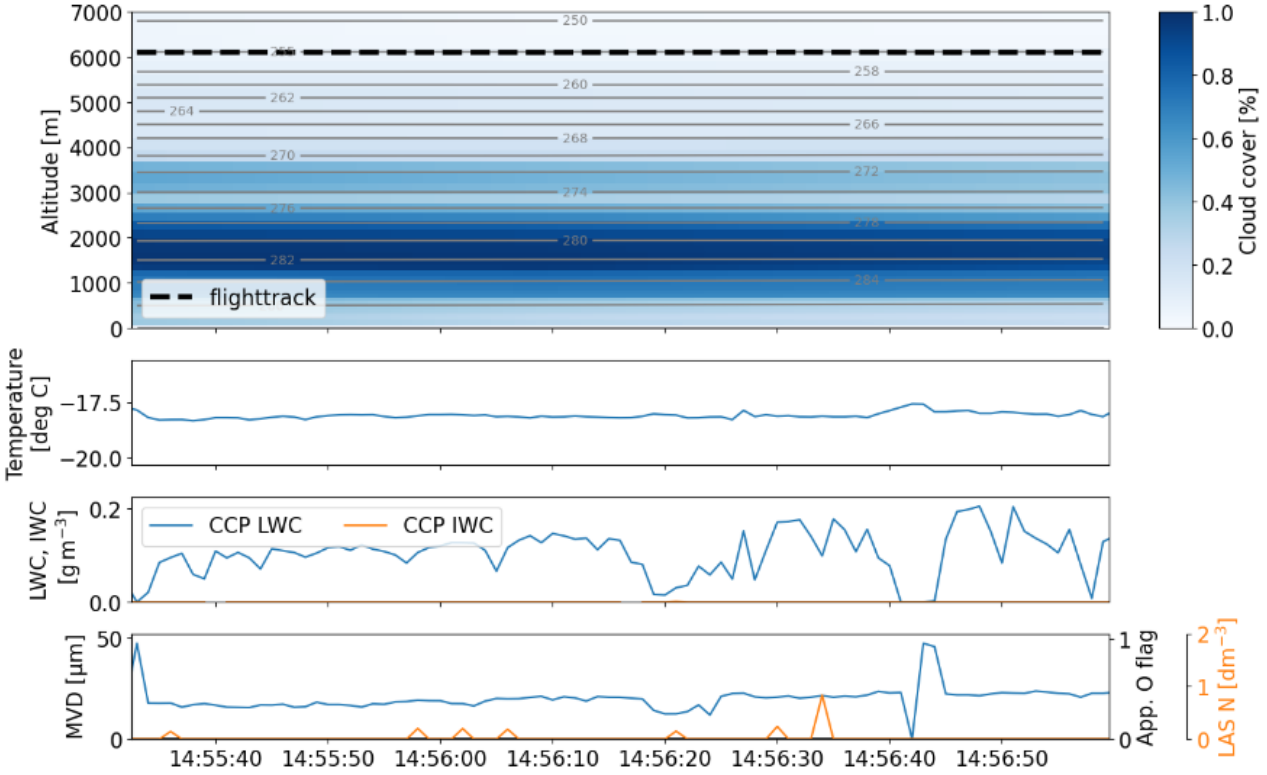

Figure 46: Icing encounter during OF12 at an altitude of 6000 m, at a temperature of approximately -18°C, an average LWC of around 0.1 g/m³ and MVD of 20 µm.

6.1.6 OF13 – 27 April 2023

The penultimate flight of the campaign sampled clouds north of Toulouse. At first, cloud tops were at altitudes between 4000 and 5000 m, where temperatures were about -6°C. Predominantly Appendix C conditions were encountered, with MVDs between 10 and 20 µm. Later cloud tops reached altitudes of 5000 m where temperatures were about -12°C. LWCs at these altitudes reached approximately 0.4 g/m³. Intermittently also Appendix O conditions were encountered, but these encounters were never longer than 1 minute.

6.1.7 OF14 – 27 April 2023

The last flight of the European campaign was an airways flight to Le Havre, where a front was predicted to pass. Since it was an airways flight, the flight altitude was nearly constant throughout all of the flight at 4000 m. Icing conditions varied between Appendix C conditions with a large number of ice crystals to short intervals of Appendix O conditions, with MVDs around 40 µm. LWCs during the Appendix O conditions varied between 0.1 and 0.4 g/m³. In Figure 47 the different conditions are clearly apparent. The Appendix O conditions between 14:08 and 14:10 occurred after the low approach at Le Havre and did not cause any ice accretion due to temperatures being too warm. Large concentrations of ice crystals were present at around 14:13. Appendix O conditions were encountered from 14:14 to 14:15 when almost no ice crystals were present.

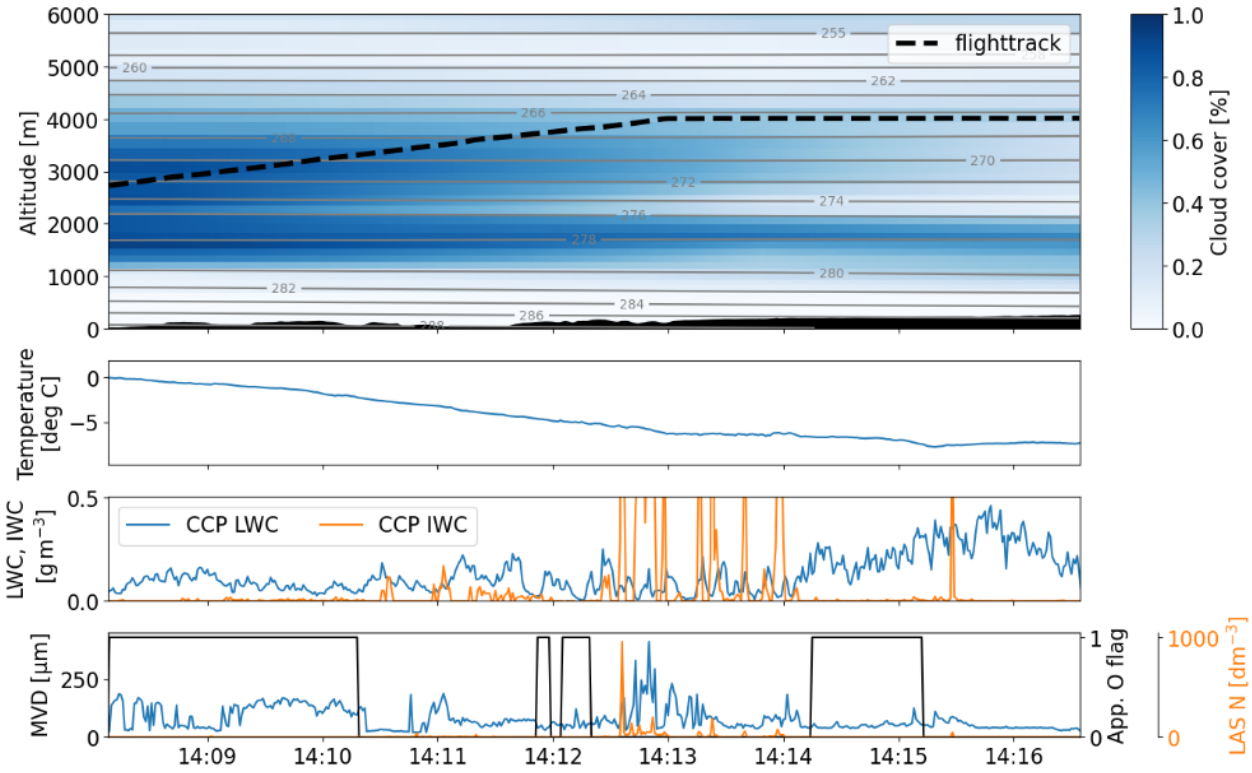

Figure 47: Example of icing conditions encountered during OF14.

6.2 Atmosphere Characterization of the European flight test campaign

This chapter summarizes the atmospheric conditions in terms of microphysical cloud properties, temperature and altitudes observed during the European flight test campaign. The statistical analysis is based on 13 flights (all flights listed in Table 5 except for OF3 and OF4) or, in the case that

Nevzorov data is used, only on the five flights during which the Nevzorov probe worked. We note, that the uncertainties in LWC and TWC here are higher than during the North American flight test campaign, due to the discrepancies between optical and hotwire sensors that were discussed in Section 3.2.

The temperature profile in Figure 48 shows median and 95 percentile LWC encountered during the SENS4ICE-Europe mission for Appendix C and Appendix O conditions. The highest frequency of measurements was obtained in the temperature range between -5 and -10°C. Mean LWCs were mostly between 0.05 and 0.10 g/m³ for Appendix C conditions and between 0.10 and 0.35 g/m³ for Appendix O conditions. The 95th percentiles reach values of nearly 0.3 g/m³ in Appendix C and more than 0.5 g/m³ in Appendix O conditions. The data is based on the Nevzorov LWC sensor for Appendix C and on the Nevzorov TWC sensor for Appendix O. Median values and 95 percentiles were lower than during the North American flight campaign. As in the North American flight test campaign, few icing conditions were sampled at temperatures less than -15°C, where they tend to occur less frequently in general. LWCs observed during flight in Appendix O conditions were slightly higher than those observed during flight in Appendix C conditions. That might be related to the presence of mixed-phase clouds, which were more dominant during the European campaign than during the North American campaign. The ice crystals in mixed-phase clouds tend to deplete the available water vapor and thus decrease the overall LWC.

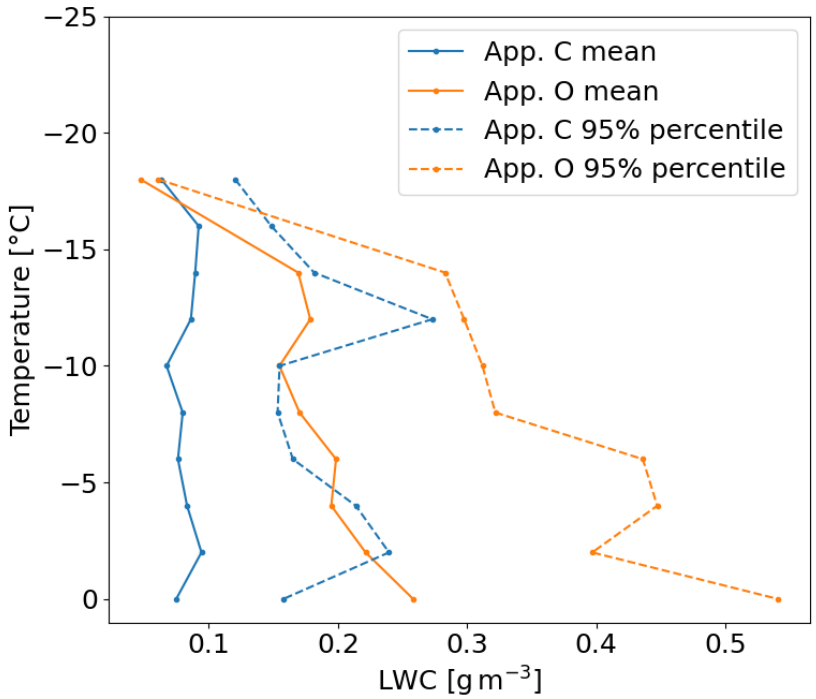

Figure 48: Mean and 95th percentile of the LWC in Appendix. C and Appendix O conditions plotted against the temperature for the data of the European flight test campaign. The Appendix C values are based on the Nevzorov LWC sensor, the Appendix O values on the Nevzorov TWC sensor as previously explained. Only flights where the Nevzorov worked are used for this plot. The data are based on 30 second averages.

Figure 49 shows the TWC that was observed in Appendix C and Appendix O conditions for the European flight test campaign. In Appendix O conditions, which are defined such that hardly any ice crystals are present, the TWC can be considered to be equivalent to the LWC. Maximum LWC values observed during Appendix O encounters reached 0.6 g/m³, everything above that value is rare.

Maximum TWC values (as opposed to the LWC values that were shown in Figure 48) observed during Appendix C encounters were as large as 1.2 g/m³.

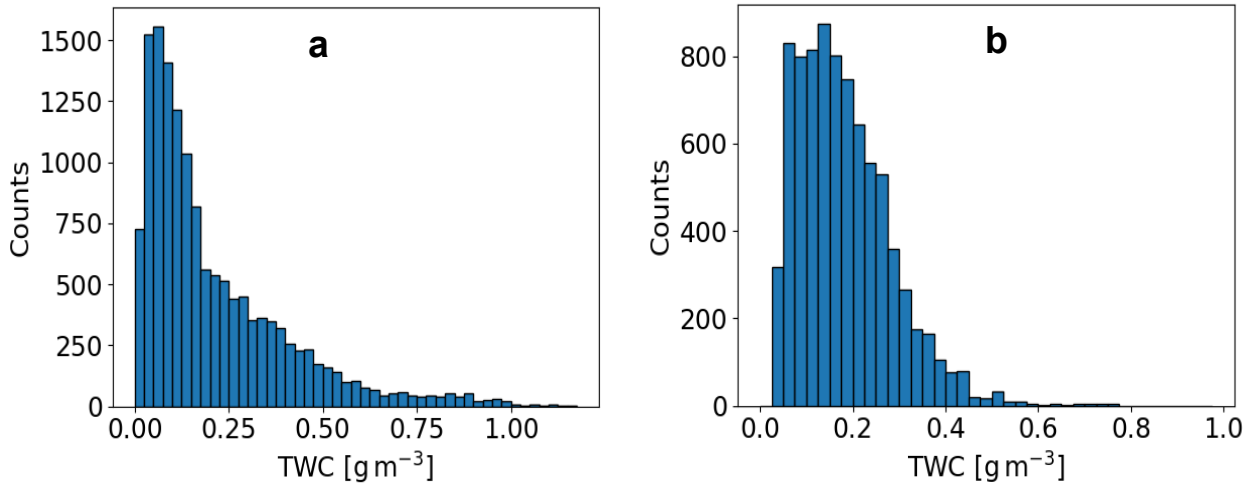

Figure 49: Distribution of Nevzorov TWC in Appendix C (a) and Appendix O (b) condition during the European SENS4ICE campaign. Only flights where the Nevzorov worked are used for this plot. The data are based on 30 second averages

As for the North American campaign, also for the European flight test campaign the LWC contained in SLD conditions is of great interest. A plot of the LWC contained in SLD can be seen in Figure 50. In comparison to the North American flight test campaign, we find a significant amount of clouds to have SLD LWC values close to or even larger than 0.05 g/m³ during the European flight test campaign. Also, the extreme values are larger, though these are very few and might be related to precipitation, which was very close, or, if slight inaccuracies exist in the temperature measurement, even above the melting point.

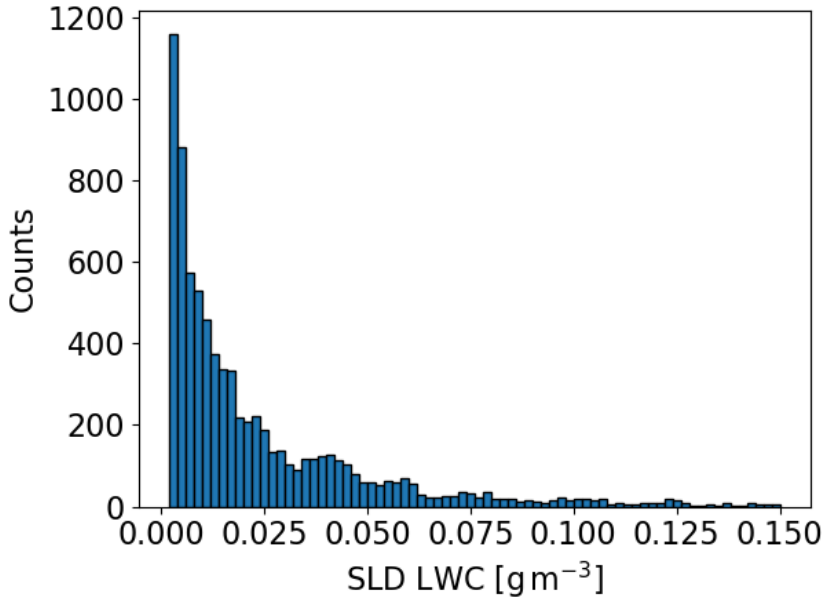

Figure 50: Histogram of LWC contained in SLDs (i.e. all droplets with diameters larger than 100 µm) during the European flight test campaign. The data are based on 30 second averages.

Furthermore, we present the cumulative mass distributions observed during the European flight test campaign. These can be seen in Figure 51. Many more Appendix O encounters were observed during the European flight test campaign than during the North American campaign, in part due to the number of missions, but also because the Appendix O encounters during the European campaign were often of short duration (frequently well below one minute). The clouds were in general patchier. A comparison of the cumulative mass distributions of North American and European campaign reveals, that the case of a cloud with an MVD around 23 µm, with few SLD embedded into the conditions, was hardly observed during the European campaign, while it was relatively common during the North American flight test campaign. The European flight test campaign data contains a lot of cumulative mass distribution curves with MVDs around 45 µm. The majority of MVDs observed during the North American flight test campaign was smaller. Once again, differences in sampling strategy and the meteorological environments present (e.g. continental vs. maritime, month of the year, altitude, consistency) may have contributed significantly to the contrasting conditions of the two campaigns.

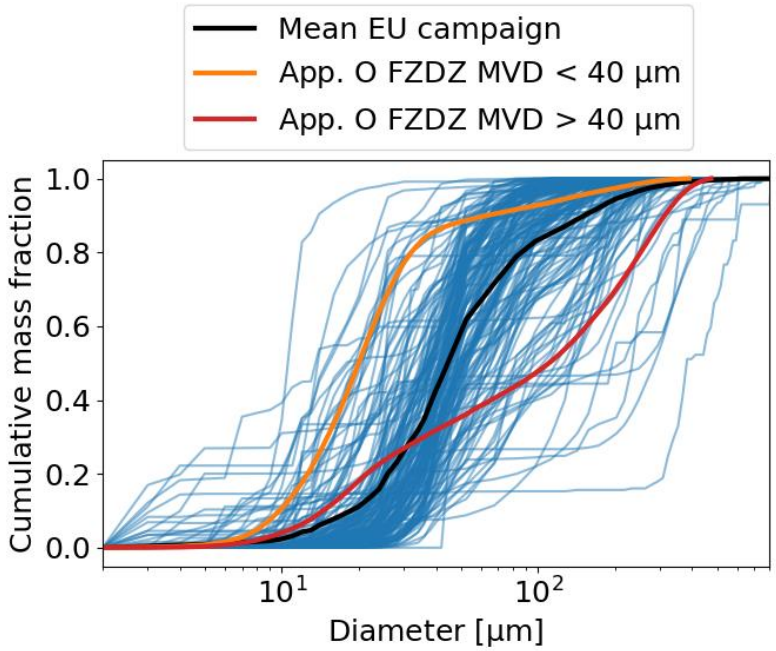

Figure 51: Cumulative mass distributions for each Appendix O encounter observed during the European flight campaign. The mean curve is plotted in black, the MVD of the mean curve is 45 µm. The cumulative mass curves for freezing drizzle MVD < 40 µm and MVD > 40 µm from Cober and Isaac [17] are plotted in orange and red, respectively.

Also for the European flight test campaign, the liquid water content encountered in Appendix O conditions in comparison to the certification envelopes is of interest. The respective plot can be seen in Figure 52. Similar as in Section 5.2, the LWC was scaled to account for varying encounter lengths. It is apparent that especially for the regime FZDZ MVD > 40 µm several encounters exceed the maximum LWC specified in the envelopes. The encounters that exceeded the maximum LWCs originated from OF9, OF10 and OF14. All of these flights predominantly sampled mid-level clouds. Further studies should therefore be performed to assess if mid-level clouds frequently contain drizzle drops and have LWCs that exceed the Appendix O maxima.

The Nevzorov TWC is assumed to be equivalent to the LWC in Appendix O conditions because Appendix O encounters were required to contain few ice crystals. Due to ambiguities that may exist

in the detection of particles (see Section 3.3) and due to the chance of intermittent mixed-phase pockets the TWC measurement of the Nevzorov may be contaminated by ice and thus too high for some of the encounters shown.

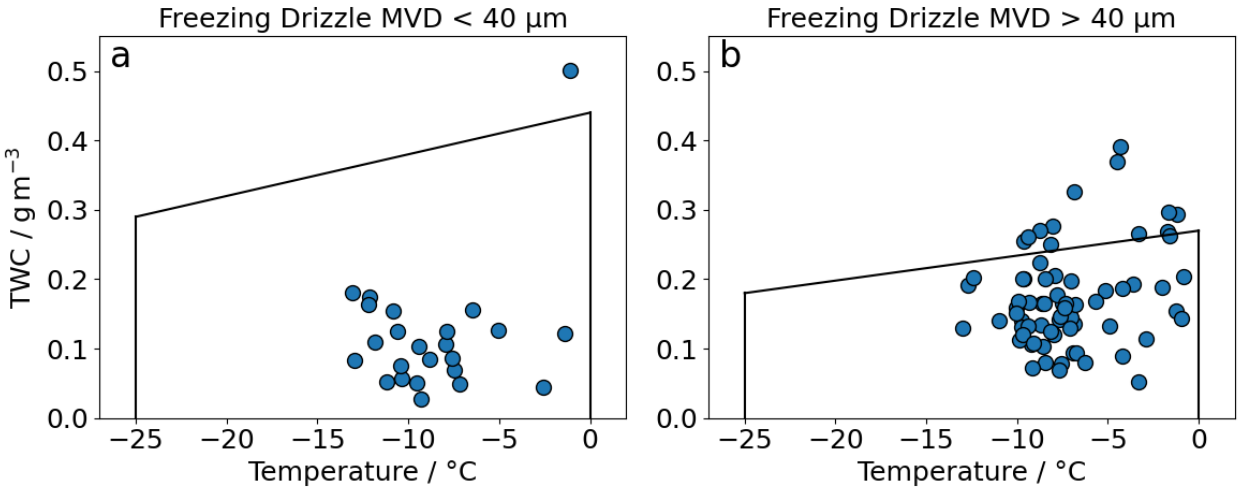

Figure 52: Nevzorov TWC of the Appendix O encounters during the European SENS4ICE campaign in comparison to the envelopes of Freezing Drizzle MVD < 40 µm (a) and Freezing Drizzle MVD > 40 µm (b). The Nevzorov TWC is assumed to be equivalent to the LWC in Appendix O conditions because Appendix O encounters were required to contain few ice crystals. Due to ambiguities that may exist in the detection of particles (see Section 3.3) and due to the chance of intermittent mixed-phase pockets the TWC measurement of the Nevzorov may be contaminated by ice and thus too high for some of the encounters shown. Only encounters longer than 30 seconds were used for this plot.

As for the North American campaign also for the European campaign a comparison of the temperature and altitude range between the encountered conditions and the Appendix O certification envelopes was performed. This can be seen in Figure 53. As is to be expected for a flight campaign in spring, most of the points lie in the upper right portion of the envelope. We observe that the temperature decrease with increasing altitude follows very well the decrease in the envelope. No point exceeds the envelope. The temperature and altitude range were therefore characteristic for high altitude Appendix O conditions in spring.

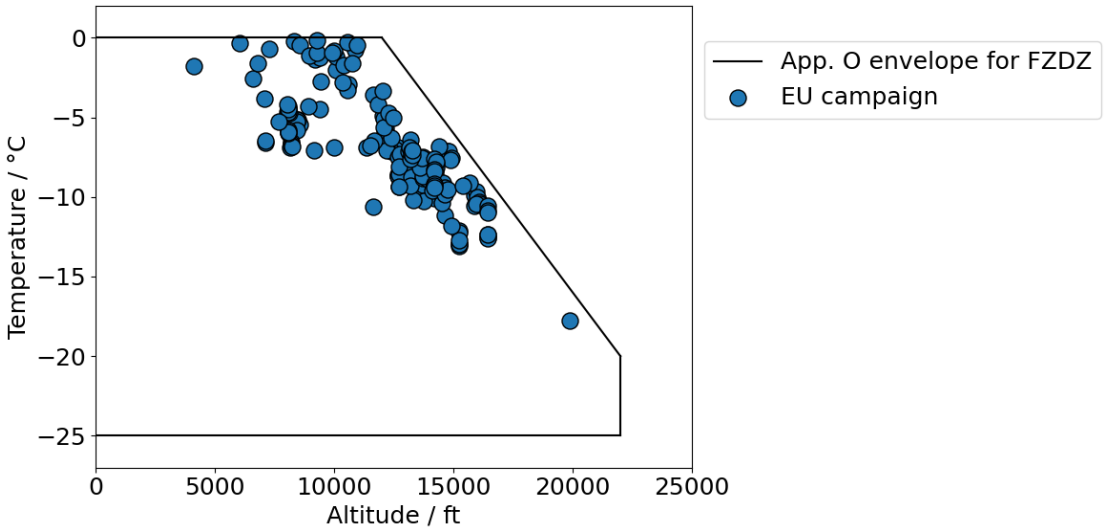

Figure 53: Pressure and altitude of Appendix O conditions encountered during the European SENS4ICE campaign in comparison to the envelope for FZDZ from Appendix O.

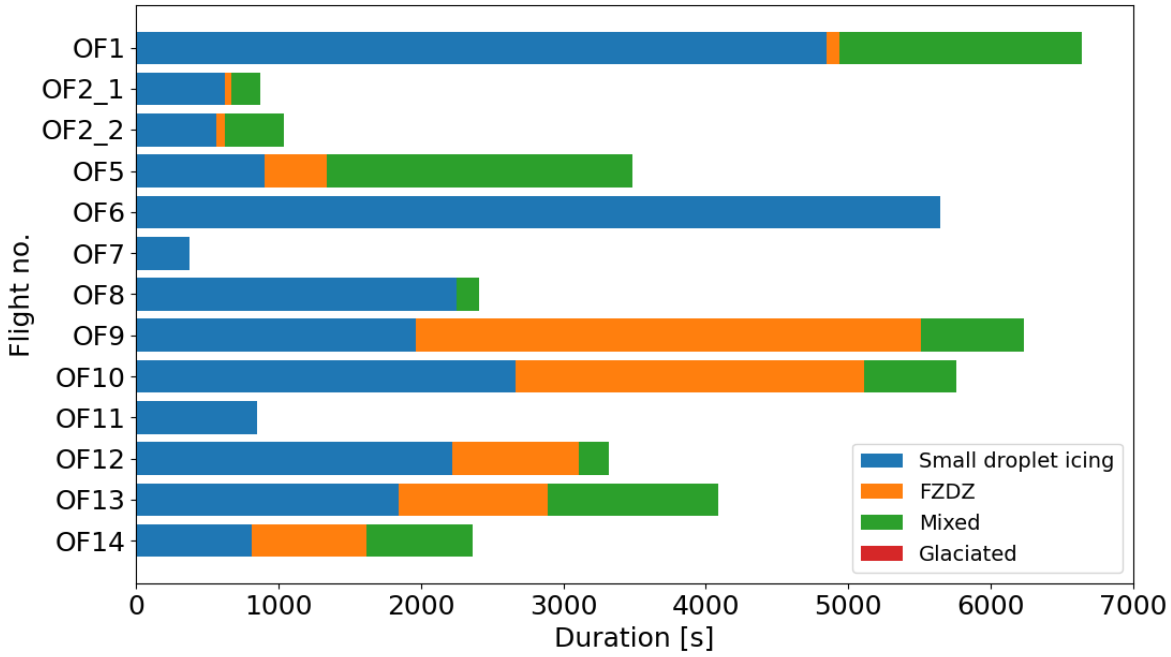

Figure 54: Overview of sampled time in different cloud conditions for all flights during the European campaign (except OF3). The definitions of the atmospheric conditions are provided in the text.

Lastly, similar as for the North American campaign, Figure 54 gives an overview over the absolute time spent in different atmospheric conditions (definitions similar as described in section 5.2). The rate of mixed-phase conditions observed during the European flight test campaign is much higher than what was observed during the American flight test campaign. This could be because there was in many cases no or only a weak inversion present below the clouds that were sampled or because seeding with ice crystals occurred from higher level clouds. The numerous Appendix O encounters

in the last flights were related to the passage of several frontal systems, which created mid-level clouds with high MVDs.

7. Evaluation of CIRA satellite remote detection technology for icing condition with regard to the flight test results

The satellite-based tools for detection and nowcasting of icing conditions, developed by CIRA in the first phase of the SENS4ICE project, have been tested during the European flight campaign. During the campaign, information on monitoring and nowcasting of icing conditions relying on the developed tools have been provided via a Teamsite platform in pre-flight phase and updated in near-real time, i.e., with a delay of a few tens of minutes due to the time of receiving and processing satellite data.

In Figure 55 an example of the output of the icing detection tool is reported: it shows the areas potentially affected by in-flight icing hazard, giving an estimate of the severity of the phenomenon (light, moderate, severe) with indication of possible SLD conditions. An estimate of the minimum and maximum altitudes affected by the icing hazard is also available for each pixel of the map. The spatial and temporal resolutions of the product are respectively of about 3 km and 15 minutes, as the satellite data used as input. The implemented nowcasting tool is based on the extrapolation in time of the current weather condition, provided by the detection tool, to perform a forecast over a short period ahead. It provides in output the same kind of information of the detection tool on a reduced domain and at four different lead times: 15 minutes, 30 minutes, 45 minutes and 1 hour. Figure 56 shows an example of the nowcasting tool output. A complete description of the detection and nowcasting tools developed by CIRA is reported in [20].

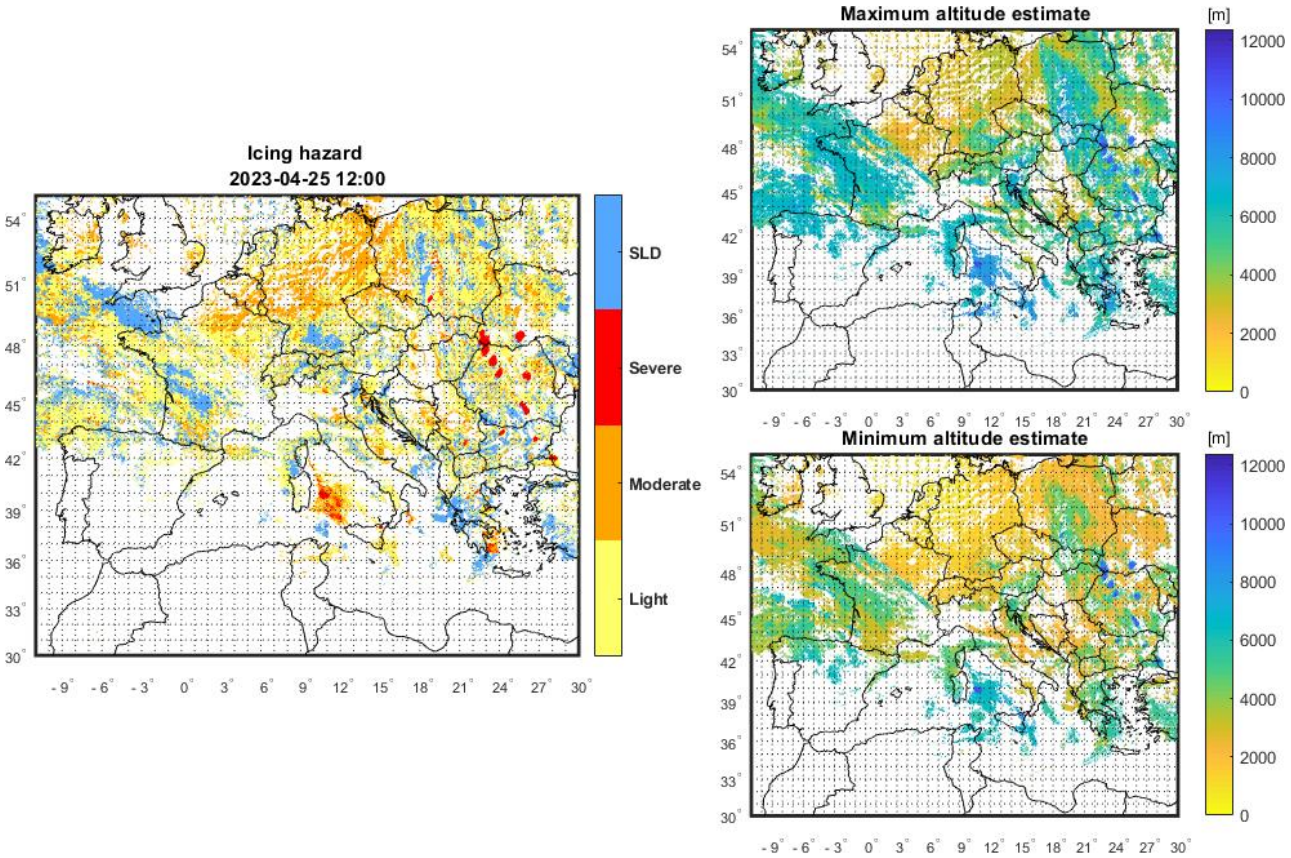

Figure 55: Example of the graphical output of the icing detection algorithm referred to 25 April 2023 at 12:00 UTC. The map on the left shows the icing hazard classified in light, moderate and severe plus an additional flag indicating possible SLD conditions. The two maps on the right reports the corresponding minimum and maximum altitudes estimated by the algorithm.

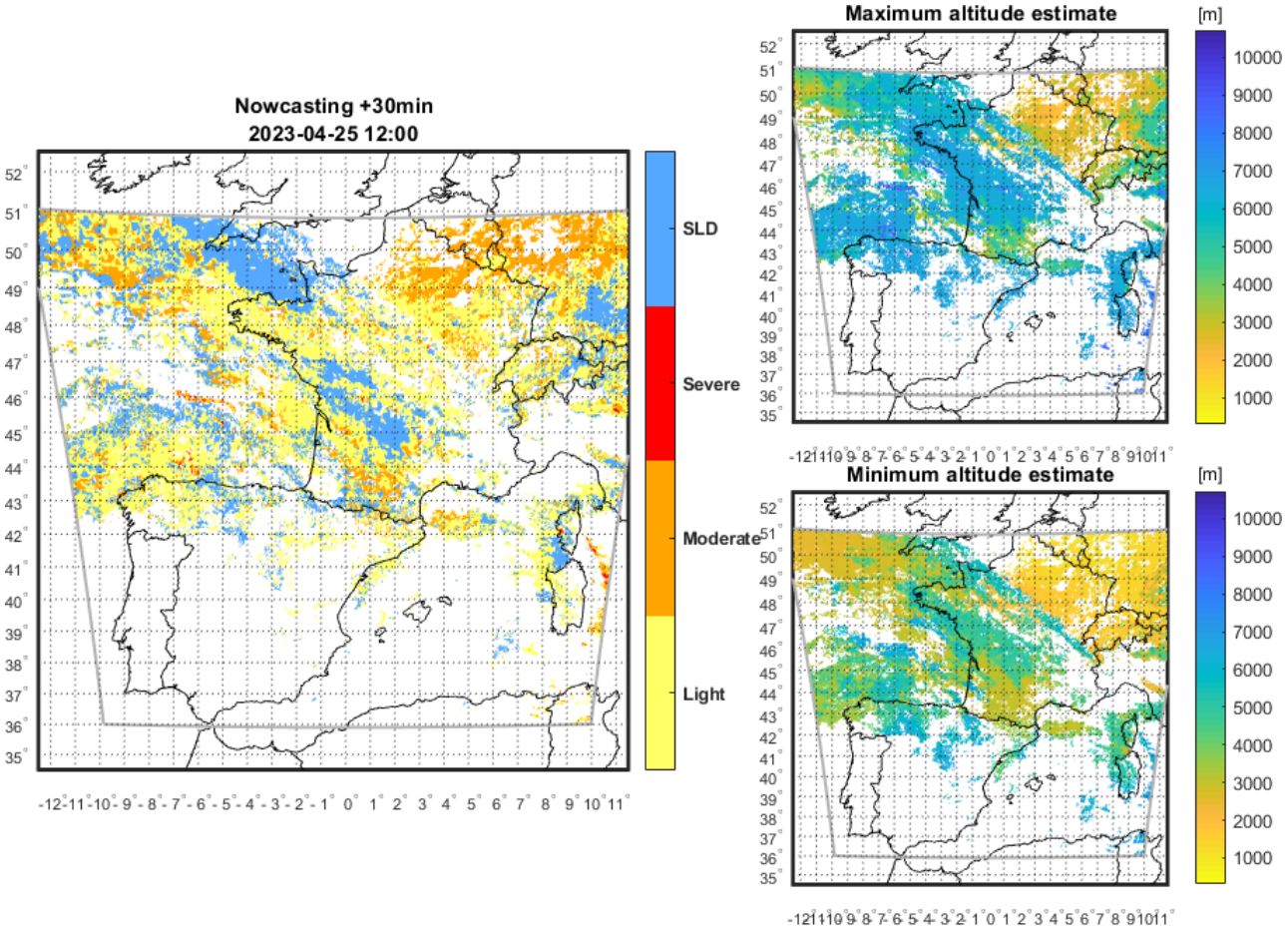

Figure 56: Example of the graphical output of the nowcasting algorithm. The maps are obtained starting from the detection product of 25 April 2023 at 12:00 UTC and applying a 30-minute forecast. The reported information is similar to Figure 55.

Considering the challenge of validating such kind of a product, the SENS4ICE flight test campaign represents an important chance to evaluate the performance of the tool in known environmental icing conditions.

It is worth noting that data coming from the satellite detection tool have very different characteristics in terms of spatial and temporal resolution with respect to flight data. Concerning the spatial comparison, the nearest point to the position of the aircraft has been considered from the satellite data. As for the temporal comparison, an updated satellite product has been considered every 15 minutes (satellite data refresh rate) and each one has been considered as representative of the time range of 15 minutes centered around its reference time.

An example of the methodology used to compare flight data and satellite data is shown in Figure 57; the details of the considered flight are reported in Table 6.

SENS4ICE Flight No	Safire Flight ID	Date	Takeoff (UTC)	Landing (UTC)
OF2	as230010	2023-04-04	11:38:45 in Francazal	12:53:28 in Hyeres

Table 6: Details of the SENS4ICE flight OF2 considered for the example of Figure 57.

The panels in Figure 57 represent the progress of the aircraft along its route every 15 minutes. Specifically, each panel shows, on the left side, the map of the CIRA detection tool with the

corresponding flight leg highlighted in blue, and, on the right side, the time series of the variables recorded during the flight. In particular, the time series of the top plot reports the flight altitude of the aircraft along with the minimum and maximum altitude estimated by the satellite detection tool for the icing field (if present). The second plot reports the reference icing flags evaluated by DLR relying on the microphysical cloud parameters measured in-situ and, finally, the third one reports the icing flags detected by the CIRA tool. In the first phase of the flight (Figure 57 (a)), no icing conditions were encountered by the aircraft, and this has been correctly detected by the CIRA satellite tool. Then the aircraft entered an area affected by icing hazard (Figure 57 (b)), where the icing is indicated according to the icing flag from the DLR reference measurements. It is interesting to note the good timing of the satellite detection tool which correctly starts to indicate icing conditions. These conditions are detected also in the following leg of the flight (Figure 57 (c)), when the comparison is not possible as the aircraft was descending for landing and was outside the range of altitudes identified by the satellite tool (which refers to the cloud layer).

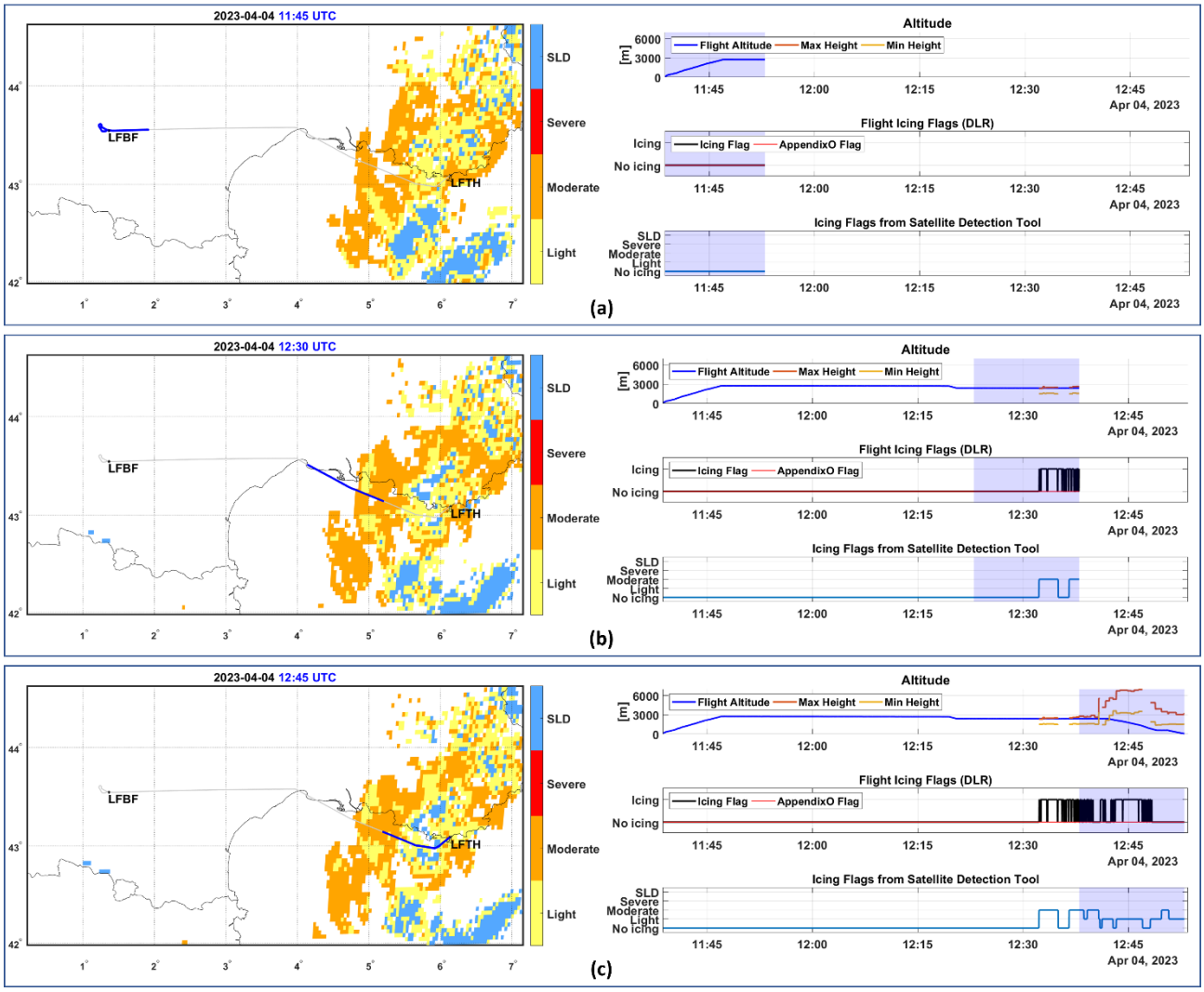

Figure 57: Example of the methodology used to compare flight data and satellite data. Each panel shows, on the left side, the map of the CIRA detection tool and, on the right side, the time series of the flight variables.

Another example of comparison between the time series of the CIRA tool output and the variables observed during the flight is shown in Figure 58; the details of the considered flight are reported in

Table 7 and Figure 59 depicts the complete path of the aircraft overlapped on the map of the CIRA detection tool (referring to the staring time of the flight).

SENS4ICE Flight No	Safire Flight ID	Date	Takeoff (UTC)	Landing (UTC)
OF9	as230018	2023-04-24	12:22:37 in Francazal	16:52:22 in Francazal

Table 7: Details of the SENS4ICE flight OF9 considered for the example of Figure 58.

In Figure 58 the parts of the time series highlighted with a shaded blue area represent the flight legs characterized by static air temperature below 0°C and are the parts for which the comparison with satellite tool output can be made. Indeed, the remaining parts (with white background) are not comparable since they correspond to times in which the aircraft was descending in altitude for de-icing, but clearly the satellite tool always refers to the cloud layer above. From the comparison between cloud drop diameters it seems that the two curves are very different, but it is worth noting that greater differences occur inside or near the areas of the plot with white background, corresponding to the descent in altitude of the aircraft. These differences are due to the big droplet measured when the aircraft descended because it was raining below the clouds (as reported in the SAFIRE flight report). Excluding these parts of the time series, the order of magnitude of the two variables is similar, and this is a good result as the estimation of MED (Median Effective Diameter) from satellite is a difficult task. The two bottom plots of Figure 58 report the icing flag from the in-situ reference measurements of DLR and the icing flag remotely detected from satellite by CIRA. In particular, for this last one, the three severity levels (light, moderate and severe) have been collapsed in a single icing flag (yes/no) in order to facilitate the comparison with observed conditions. The plots reveal that almost all the flight was conducted in icing conditions, and the satellite tool correctly detected icing. Furthermore, several encounters of Appendix O conditions occurred and they have been detected also from the satellite tool. The matching is not punctual, but this is partly due to the different nature of the data compared, characterized by very different spatial and temporal resolutions.

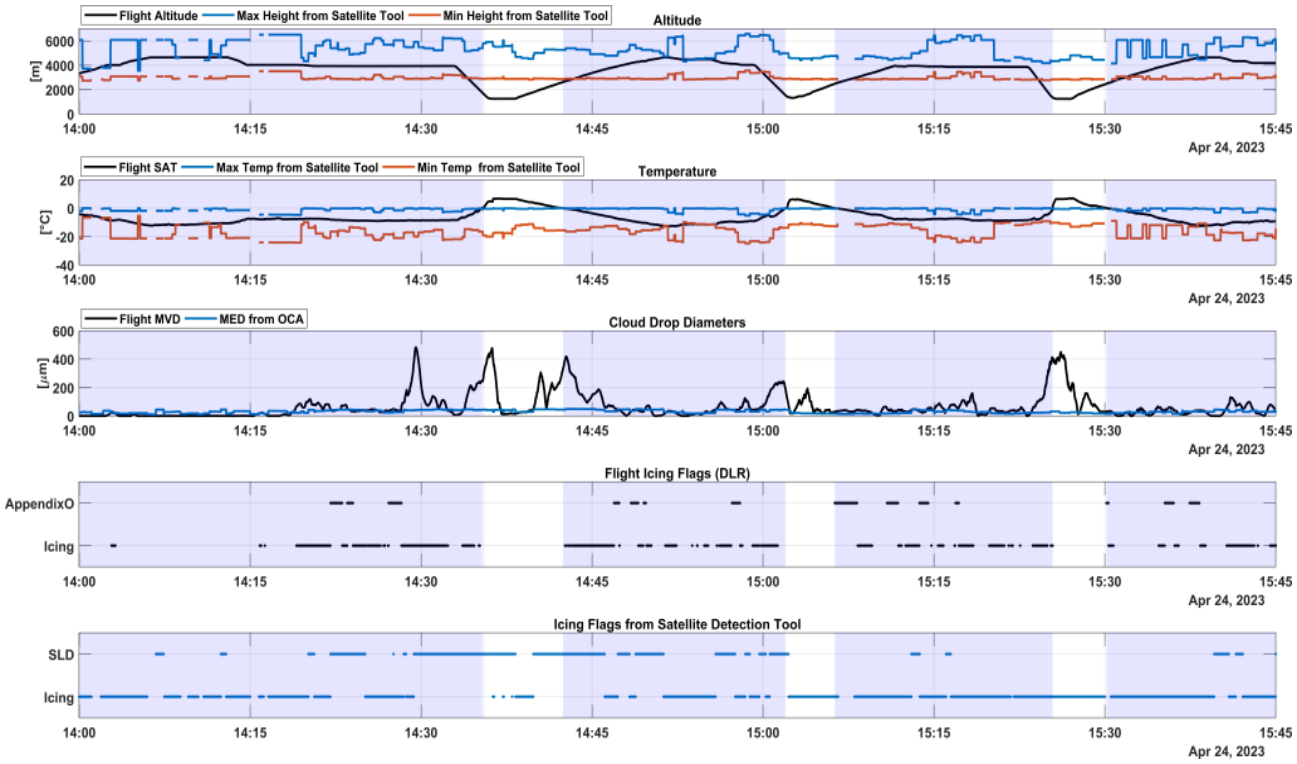

Figure 58: Comparison between the time series of the variables observed during the flight and the output of CIRA detection tool.

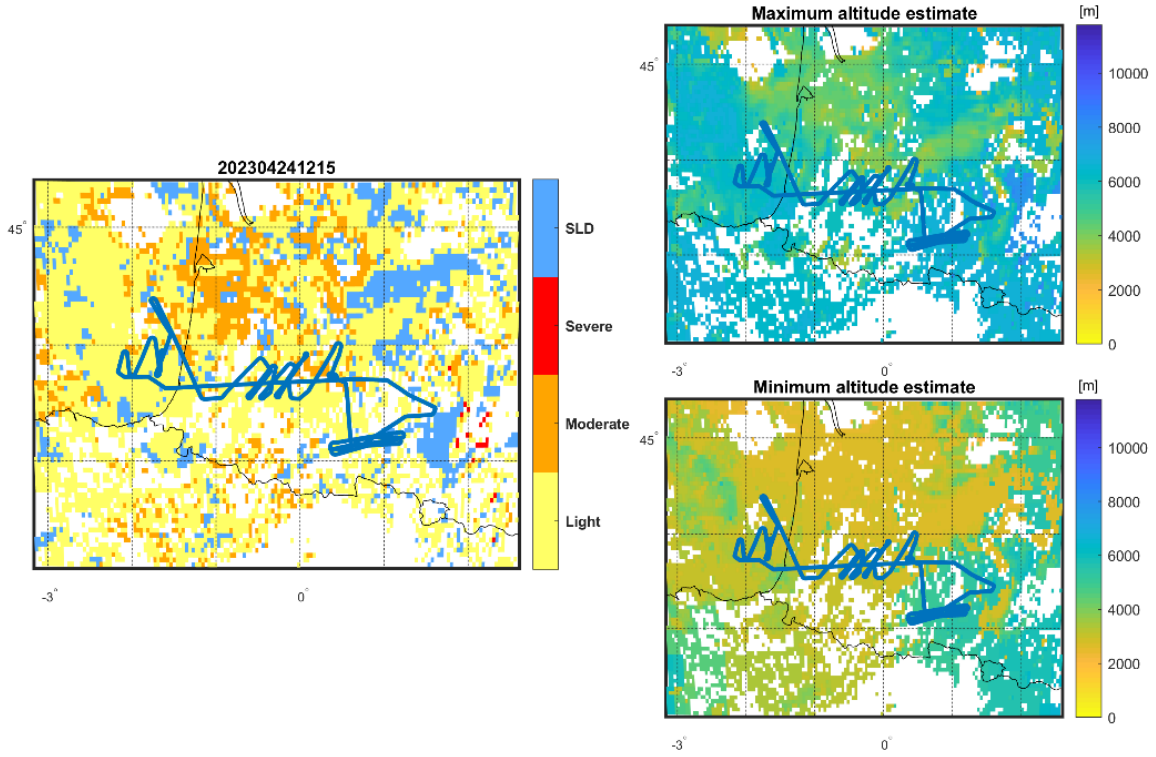

Figure 59: Complete path of the SENS4ICE flight OF9 overlapped on the map of the CIRA detection tool referring to the staring time of the flight.

The described preliminary results regarding the evaluation of the detection tool in relevant icing conditions are promising, suggesting that this satellite-based approach may be useful for applications supporting aviation meteorology after further maturation. Indeed, additional investigations are ongoing with the aim of performing a more detailed validation to identify the strengths and weaknesses of the tool and the needed steps for its future exploitation.

8. Summary

The main observations of atmospheric conditions during the SENS4ICE flight campaigns are summarized in the following:

- Two successful flight campaigns in relevant icing conditions were performed with a significant number of Appendix O and C encounters and time spent in clouds with enhanced supercooled LWC.
- The current data evaluation represents a lower limit of the Appendix O encounters and exceptionally those encounters with pure liquid clouds. Appendix O encounters due to mixed-phase clouds have been largely excluded from the data set.
- All reference sensors performed in general well during the campaign. LWC measurement of optical probes and hotwire type sensors agreed well during the North American flight test campaign. More uncertainties remain for the European flight test campaign where additional analysis is necessary. The data evaluation will continue in the coming 6 months.
- Temperatures of icing encounters reached down to -17°C during both campaigns.
- Appendix O conditions solely comprised FZDZ in both campaigns. FZDZ conditions encountered during the North American flight test campaign tended to be bimodal and had mostly MVDs < 40 µm. FZDZ conditions during the European flight test campaign were often unimodal (atypical for Appendix O conditions) and had MVDs which mostly ranged between 25 and 60 µm. For the North American flight test campaign two Appendix O encounters exceeded Appendix O envelopes while for the European campaign several of Appendix O conditions exceeded the LWC specified in the envelopes (Figure 60 and Figure 61). One reason may be the strategic sampling of mid-level clouds at higher altitudes during the European flight test campaign. It is still to be investigated in how far incorrect classification of particles (liquid/ice) may have contributed to the data lying outside of the envelope.
- MVDs of Appendix O conditions during the North American flight test campaign were on average around 23 µm and for the European flight test campaign larger with an average 45 µm.
- The altitude of icing conditions for the European flight test campaign (3.5 to 5 km) are higher than for the American flight campaign (1 to 3 km). While the latitude of both measurements is similar, the altitude shift is mainly an effect of the season of the measurement. The higher temperatures in April shift the cloud layers with icing conditions to higher altitudes. It is yet to be noted that unexpectedly a significant number of Appendix O conditions was measured above 3 km during the European flight test campaign.
- Higher LWCs in the range up to 1 g/m³ were observed in the North American flight test campaign. Yet higher LWC contained in the SLD mode was observed in the European campaign.
- For the North American flight test campaign, more than 4 hours and 23 minutes were spent in icing conditions, 42 minutes in Appendix O conditions was achieved.
- For the European flight test campaign, in total more than 10 hours were spent in icing conditions, and more than 2 hours in Appendix O conditions was achieved.
- A first evaluation of the CIRA satellite detection mechanism was achieved using SENS4ICE data from the European test campaign and promising results with a qualitative good agreement between the satellite detection algorithm and the in-situ data was observed.

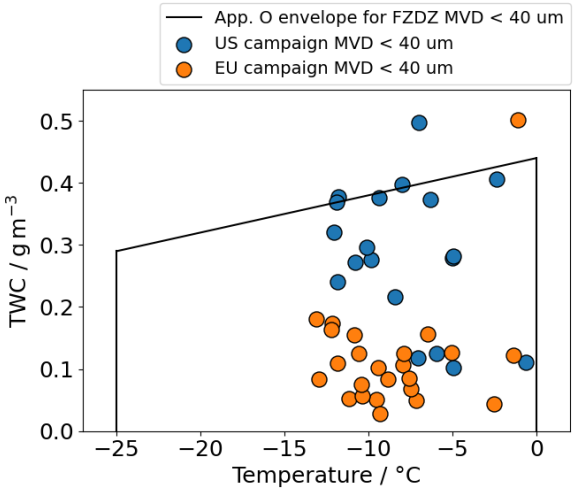

Figure 60: Comparison of the Nevzorov TWC measured during freezing drizzle encounters with MVD < 40 µm during both flight campaigns with the Appendix O envelope for freezing drizzle MVD < 40 µm. The Nevzorov TWC is assumed to be equivalent to the LWC in Appendix O conditions because Appendix O encounters were required to contain few ice crystals. Due to ambiguities that may exist in the detection of particles (see Section 3.3) and due to the chance of intermittent mixed-phase cloud pockets the Nevzorov probe may have sampled ice crystals and thus the TWC is too high for some of the SLD encounters shown. Only encounters longer than 30 seconds were used for this plot.

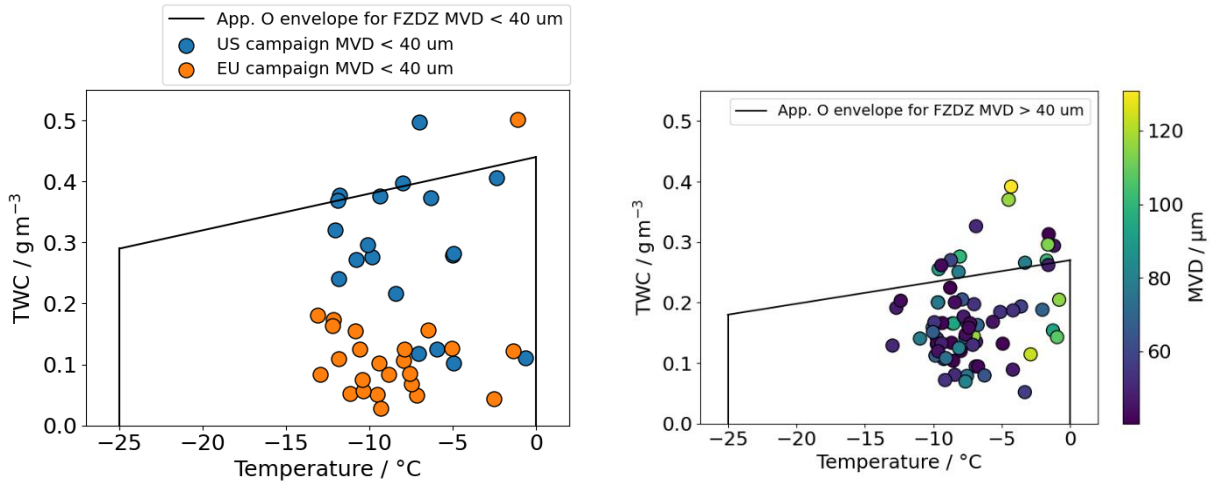

Figure 61: Comparison of the Nevzorov TWC measured during freezing drizzle encounters with MVD > 40 µm during both flight campaigns with the Appendix O envelope for freezing drizzle MVD > 40 µm (left: two different flight campaigns colour coded, right MVD colour coded). The Nevzorov TWC is assumed to be equivalent to the LWC in Appendix O conditions because Appendix O encounters were required to contain few ice crystals. Due to ambiguities that may exist in the detection of particles (see Section 3.3) and due to the chance of intermittent mixed-phase cloud pockets the Nevzorov may have sampled ice and thus the TWC is too high for some of the encounters shown. Only encounters longer than 30 seconds were used for this plot.

References

[1] T. Jurkat-Witschas, J. Lucke, C. Schwarz, C. Deiler, F. Sachs, S. Kirschler, D. Menekay, C. Voigt, B. Bernstein, O. Jaron, F. Kalinka, A. Zollo, L. Lilie, J. Mayer, C. Page, B. Vié, A. Bourdon, R. P. Lima and L. Vieira, "Overview of Cloud Microphysical Measurements during the SENS4ICE Airborne Test Campaigns: Contrasting Icing Frequencies from Climatological Data to First Results from Airborne Observations," in *SAE Technical Paper Series*, 2023.

[2] R. C. Braga, D. Rosenfeld, R. Weigel, T. Jurkat, M. O. Andreae, M. Wendisch, M. L. Pöhlker, T. Klimach, U. Pöschl, C. Pöhlker, C. Voigt, C. Mahnke, S. Borrmann, R. I. Albrecht, S. Molleker, D. A. Vila, L. A. T. Machado and P. Artaxo, "Comparing parameterized versus measured microphysical properties of tropical convective cloud bases during the ACRIDICON–CHUVA campaign," *Atmospheric Chemistry and Physics,* vol. 17, p. 7365–7386, June 2017.

[3] S. Lance, "Coincidence Errors in a Cloud Droplet Probe (CDP) and a Cloud and Aerosol Spectrometer (CAS), and the Improved Performance of a Modified CDP," *Journal of Atmospheric and Oceanic Technology,* vol. 29, p. 1532–1541, October 2012.

[4] S. Faber, J. R. French and R. Jackson, "Laboratory and in-flight evaluation of measurement uncertainties from a commercial Cloud Droplet Probe (CDP)," *Atmospheric Measurement Techniques,* vol. 11, p. 3645–3659, June 2018.

[5] L. E. Lilie, D. Bouley, C. P. Sivo and T. P. Ratvasky, "Test Results for the SEA Ice Crystal Detector (ICD) under SLD Conditions at the NASA IRT," 2021.

[6] J. R. Lucke, T. Jurkat-Witschas, D. Baumgardner, F. Kalinka, M. Moser, E. D. L. T. Castro and C. Voigt, "Characterization of Atmospheric Icing Conditions during the HALO-(AC)³ Campaign with the Nevzorov Probe and the Backscatter Cloud Probe with Polarization Detection," in *SAE Technical Paper Series*, 2023.

[7] A. V. Korolev, J. W. Strapp, G. A. Isaac and A. N. Nevzorov, "The Nevzorov Airborne Hot-Wire LWC–TWC Probe: Principle of Operation and Performance Characteristics," *Journal of Atmospheric and Oceanic Technology,* vol. 15, p. 1495–1510, December 1998.

[8] J. Lucke, T. Jurkat-Witschas, R. Heller, V. Hahn, M. Hamman, W. Breitfuss, V. R. Bora, M. Moser and C. Voigt, "Icing wind tunnel measurements of supercooled large droplets using the 12 mm total water content cone of the Nevzorov probe," *Atmospheric Measurement Techniques,* vol. 15, p. 7375–7394, December 2022.

[9] S. Lance, C. A. Brock, D. Rogers and J. A. Gordon, "Water droplet calibration of the Cloud Droplet Probe (CDP) and in-flight performance in liquid, ice and mixed-phase clouds during ARCPAC," *Atmospheric Measurement Techniques,* vol. 3, p. 1683–1706, December 2010.

[10] R. G. Knollenberg, "The optical array: An alternative to scattering or extinction for airborne particle size determination," *Journal of Applied Meteorology (1962-1982),* p. 86–103, 1970.

[11] A. V. Korolev, J. W. Strapp and G. A. Isaac, "Evaluation of the Accuracy of PMS Optical Array Probes," *Journal of Atmospheric and Oceanic Technology,* vol. 15, pp. 708-720, 1998.

[12] E. De La Torre Castro, T. Jurkat-Witschas, A. Afchine, V. Grewe, V. Hahn, S. Kirschler, M. Krämer, J. Lucke, N. Spelten, H. Wernli and others, "Differences in microphysical properties of cirrus at high and mid-latitudes," *EGUsphere,* vol. 2023, p. 1–34, 2023.

[13] S. Kirschler, "Effekte von Aerosol und Dynamik auf die Eigenschaften ozeanischer Wolken im Nordwestatlantik," 2023.

[14] D. Menekay, "Comparative analysis of optical in-situ probes and the MSG satellite for improved detection of aircraft icingconditions," 2023.

[15] J. Lucke, "Detection and differentiation of supercooled large drop icing conditions," 2024.

[16] A. Schwarzenboeck, G. Mioche, A. Armetta, A. Herber and J.-F. Gayet, "Response of the Nevzorov hot wire probe in clouds dominated by droplet conditions in the drizzle size range," *Atmospheric Measurement Techniques,* vol. 2, p. 779–788, 2009.

[17] S. G. Cober and G. A. Isaac, "Characterization of Aircraft Icing Environments with Supercooled Large Drops for Application to Commercial Aircraft Certification," *Journal of Applied Meteorology and Climatology,* vol. 51, p. 265–284, February 2012.

[18] J. Lucke, T. Jurkat-Witschas, R. Heller, V. Hahn, M. Hamman, W. Breitfuss, V. R. Bora, M. Moser and C. Voigt, *Icing Wind Tunnel Measurements of Supercooled Large Droplets Using the 12 mm Total Water Content Cone of the Nevzorov Probe: Measurement Data,* 2022.

[19] Copernicus Climate Change Service, *Complete ERA5 global atmospheric reanalyis,* ECMWF, 2023.

[20] A. Zollo and E. Bucchignani, "A Tool for Remote Detection and Nowcasting of In-Flight Icing Using Satellite Data," *SAE Technical Paper2023-01-1489, https://doi.org/10.4271/2023-01-1489,* 2023.

ACKNOWLEDGEMENTS

North America flight campaign data was obtained with the Embraer Phenom 300 operated by Embraer.

Airborne data for the European flight campaign was obtained using the aircraft managed by Safire, the French facility for airborne research, an infrastructure of the French National Center for Scientific Research (CNRS), Météo-France and the French National Center for Space Studies (CNES). Distributed data are processed by SAFIRE.